First-Principle Approach to Electronic States and Metal–Insulator Transition in Selected Correlated Model Systems

Andrzej P. Kądzielawa

Ph.D. Thesis
Promotor: **Prof. dr hab. Józef Spałek**
Promotor pomocniczy: **dr Andrzej Biborski**

Uniwersytet Jagielloński
Instytut Fizyki im. Mariana Smoluchowskiego
Zakład Teorii Materii Skondensowanej i Nanofizyki

Kraków 2015

Wydział Fizyki, Astronomii i Informatyki Stosowanej
Uniwersytet Jagielloński

Oświadczenie

Ja niżej podpisany Andrzej P. Kądzielawa (nr indeksu: 1014332) doktorant Wydziału Fizyki, Astronomii i Informatyki Stosowanej Uniwersytetu Jagiellońskiego oświadczam, że przedłożona przeze mnie rozprawa doktorska pt. "First-Principle Approach to Electronic States and Metal–Insulator Transition in Selected Correlated Model Systems" jest oryginalna i przedstawia wyniki badań wykonanych przeze mnie osobiście, pod kierunkiem prof. dr hab. Józefa Spałka. napisałem samodzielnie.

Oświadczam, że moja rozprawa doktorska została opracowana zgodnie z Ustawą o prawie autorskim i prawach pokrewnych z dnia 4 lutego 1994 r. (Dziennik Ustaw 1994 nr 24 poz. 83 wraz z późniejszymi zmianami).

Jestem świadom, że niezgodność niniejszego oświadczenia z prawdą ujawniona w dowolnym czasie, niezależnie od skutków prawnych wynikających z ww. ustawy, może spowodować unieważnienie stopnia nabytego na podstawie tej rozprawy.

Kraków, dnia 7 VIII 2015

.....
podpis doktoranta

Abstract

In this Thesis we present a fully microscopic, first-principle approach to describe the systems of molecular and atomic hydrogen. We apply the **E**xact **D**iagonalization **Ab I**nitio approach (EDABI) both with the employment of the exact Hamiltonian diagonalization procedures and the so-called **S**tatistically-Consistent **G**utzwiller **A**pproximation (SGA), to model the system described by the so-called extended Hubbard model. We analyze the selected hydrogenic systems, and study their stability under high pressure, observing the insulator-to-metal transition of the Mott-Hubbard type and molecular-to-atomic transition, as well as assessing the zero-point motion amplitude and energy and electron–lattice coupling constants. These all are important steps in description of superconductivity in the hydrogenic systems with both the inclusion of interelectronic correlations and the electron–lattice interaction. From the last point of view, the present work represents the first step towards this goal.

The EDABI method provides a realistic depiction of many-electron states, starting from the renormalization of the single-particle wave-function basis. This allows us to obtain quality results while using rather small number of basis functions. Also, we are able to characterize the many-body wavefunction in the resultant correlated state.

We study metallization of solid atomic hydrogen by applying the EDABI method combined with SGA to the simple-cubic lattice with half-filled $1s$ Slater-type orbitals. This allows us to describe the insulator–metal transition of the weakly first-order Mott-Hubbard type, at the external pressure $\sim 100GPa$. We also examine the effect of applied magnetic field and the critical scaling of the ground-state energy and the inverse wave-function size (one of the variational parameters in EDABI). We have also made a first assessment of the zero-point motion energy in the correlated state.

Next, we take steps to include the vast spectrum of the solid molecular-hydrogen phases. We start from the complex description of the H_2 molecule, taking into account all electronic interactions, electron–proton coupling, and estimating the zero-point energy with the ground-state energy contribution up to the ninth order. The zero-point motion energy is assessed to be $\sim 1\%$ of the molecular binding energy, as is observed experimentally. We also create the first model of molecular crystal - a one-dimensional molecular chain in the extended Hubbard model with long-range interactions and periodic boundary conditions. We find that, when nonzero force is applied, there exist two phases - one of the molecular and one of the quasiatomic nature, leading, at some point, to the molecular–quasiatomic transition. The relation of this transition to the Mott-Hubbard insulator–metal transition is proposed. We also test the software and proposed computational solutions used to obtain the results presented in this Thesis.

This Thesis is supplemented with the computer animation on CD of the molecular– to quasiatomic-hydrogen transition, carried out on the example of linear chain (cf. `http://th-www.if.uj.edu.pl/ztms/download/supplementary_material/molecular_to_quasiatomic_transition-hydrogen_chain.avi`). Additionally, both the cited and the original works have been linked to the original sources of the publications.

Keywords: *solid hydrogen, metal–insulator transition, molecular–atomic transition, ab-initio quantum computations, correlated electron systems, extended Hubbard model, long-range interaction, molecular crystals, Exact Diagonalization Ab Initio approach (EDABI), Statistically-Consistent Gutzwiller Approximation (SGA)*

Streszczenie

W rozprawie zaprezentowano w pełni mikroskopowe podejście z pierwszych zasad do opisu układów molekularnego i atomowego wodoru. Zastosowano metodę EDABI (ang. ***E**xact **D**iagonalization **Ab I**nitio approach*) do modelowania układów opisywanych rozszerzonym modelem Hubbarda, stosując zarówno dokładne procedury diagonalizacji hamiltonianu, jak i tak zwane statystycznie konsystentne przybliżenie Gutzwillera (ang. ***S**tatistically-Consistent **G**utzwiller **A**pproximation* - SGA). W rozważanych układach wodorowych, przy uwzględnieniu wysokich ciśnień, obserwowano przejście izolator–metal typu Motta-Hubbarda i przejście z układu molekularnego do atomowego. Oszacowano również energię drgań punktu zerowego, jak i stałe sprzężenia elektron–sieć. Są to niezbędne komponenty spójnego opisu nadprzewodnictwa takich układach, uwzględniając zarówno korelacje międzyelektronowe, jak i oddziaływanie elektron-sieć. Ta rozprawa jest pierwszym krokiem do osiągnięcia tego celu.

Metoda EDABI zapewnia realistyczny opis stanów wieloelektronowych, wychodząc z renormalizacji bazy jednocząstkowych funkcji falowych, co pozwala na otrzymanie dobrych jakościowo wyników przy dosyć małej liczbie funkcji bazowych. Dzięki temu możemy scharakteryzować właściwości wielocząstkowej funkcji falowej w stanie skorelowanym.

Przebadano metalizację stałego, atomowego wodoru, stosując metodę EDABI jednocześnie z SGA do opisu sieci prostej kubicznej z w połowie wypełnionymi orbitalami Slatera $1s$. Doprowadziło to do modelu przejścia pierwszego rodzaju z fazy izolatora to fazy metalicznej przy ciśnieniu zewnętrznym $\sim 100GPa$. Przeanalizowano też wpływ pola magnetycznego na stan podstawowy układu i przedstawiono skalowanie krytyczne energii stanu podstawowego i odwrotności rozmiaru funkcji falowej (jednego z parametrów wariacyjnych w metodzie EDABI). Wyprowadzono też pierwsze przybliżenie na energię drgań punktu zerowego.

Następnym krokiem było uwzględnienie szerokiego spektrum molekularnych faz stałego wodoru. W tym celu opracowano kompleksowy opis molekuły H_2 jak układu dwuwęzłowego z uwzględnieniem wszystkich oddziaływań międzyelektronowych i sprzężenia elektron–proton. Wyliczono energię drgań punktu zerowego z uwzględnieniem wkładu energii stanu podstawowego do wyrazów stopnia dziewiątego i stanowi ona $\sim 1\%$ energii wiązania cząsteczki H_2, co jest w pełnej zgodności z eksperymentem. Stworzono też pierwszy model molekularnego kryształu - jednowymiarowy łańcuch molekuł H_2 opisany rozszerzonym modelem Hubbarda z periodycznymi warunkami brzegowymi z uwzględnieniem oddziaływań długozasięgowych. Pokazano, że przy niezerowej sile zewnętrznej działającej na łańcuch układ ma dwie fazy - molekularną i kwaziatomową, co prowadzi do przejścia od fazy molekularnej do kwaziatomowej dla dostatecznie wysokiej wartości zewnętrznej siły. Zaproponowano odniesienie pomiędzy tą przemianą, a przejściem izolator–metal typu Motta-Hubbarda. Przeanalizowano i przetestowano oprogramowanie i metody obliczeniowe użyte do otrzymania wyników prezentowanych w pracy.

Do ninejszej rozprawy dołączono dysk CD z animacją komputerową przejścia stałego wodoru molekularnego do fazy kwaziatomowej, zamodelowaną na przykładzie takiego przejścia dla łańcucha liniowego (zobacz `http://th-www.if.uj.edu.pl/ztms/download/supplementary_material/molecular_to_quasiatomic_transition-hydrogen_chain.avi`). Dodatkowo dołączono linki do cytowanych oraz oryginalnych prac wchodzących w skład pracy.

Słowa kluczowe: *stały wodór, przejście metal–izolator, przejście kryształ molekularny–atomowy, obliczenia z pierwszych zasad, skorelowane układy elektronowe, rozszerzony model Hubbarda, oddziaływania długozasięgowe, kryształy molekularne, metoda EDABI, statystycznie konsystentne przybliżenie Gutzwillera (SGA)*

Contents

Acknowledgements

I would like to express my gratitude to my supervisor, Prof. Józef Spałek, for suggesting the subject of the Thesis, all the discussions, inspiration to do research, help and good word, as well as for the critical reading of this Thesis and the multitude of his corrections.

I would also like to thank Dr. Andrzej Biborski, for all the time we spent programming, his support and openness towards me.

I am thankful to Marcin Abram, Agata Bielas, Dr. Danuta Goc-Jagło, Dr. Jan Kaczmarczyk, Ewa Kądzielawa-Major, Dr. Jan Kurzyk, Prof. Maciej Maśka, Grzegorz Rut, Dr. hab. Adam Rycerz, Dr. Leszek Spałek, Prof. Włodzimierz Wójcik, Marcin Wysokiński, and Dr. Michał Zegrodnik, for all the discussions we had.

I would like to thank Dr. Marcello Acquarone for his hospitality and help during my visit at the University of Parma.

I also would like to show my appreciation for my family for their unconditional support, especially Kasia and Kostek without whom this Thesis would be finished earlier.

The work was supported by the Project TEAM awarded by the Foundation for Polish Science (FNP) for the years 2011-2015 and by the project MAESTRO from the National Science Centre, Grant No. DEC-2012/04/A/ST3/00342.

The principal part of the computations in this Thesis has been carried out on TERA–ACMIN supercomputer located at Academic Centre for Materials and Nanotechnology, AGH University of Science and Technology.

Frequently used abbreviations

DFT	Density Functional Theorem
DMFT	Dynamical Mean-field Theory
EDABI	Exact Diagonalization Ab Initio Approach
GA	Gutzwiller Approximation
LDA	Local-Density Approximation
MIT	Metal–Insulator Transition
QMT	Quantum Metallization Tools
SGA	Statistically-consistent Gutzwiller Approximation
STO	Slater-type Orbital
ZPM	Zero-point Motion

Frequently used symbols

E_G	ground-state energy
$\hat{c}^\dagger_{i\sigma}(\hat{c}_{i\sigma})$	creation (annihilation) operator of a fermion with spin σ on site i
$\mathcal{H}$	Hamiltonian
$w_i(\mathbf{r})$	single-particle basis wave function
t_{ij}	one-body microscopic parameter of Hamiltonian
V_{ijkl}	interaction microscopic parameter of Hamiltonian
U	on-site Hubbard interaction (V_{iiii})
K_{ij}	Coulomb interaction between sites i and j (V_{ijij})
J_{ij}	exchange interaction between sites i and j (V_{ijji})
W	bandwidth
$\|\psi_G\rangle$	Gutzwiller wave function
$\|\psi_0\rangle$	uncorrelated wave function
$\mathcal{P}(\mathcal{P}_i)$	(local) Gutzwiller correlator
q_σ	band-narrowing factor
d^2	average double occupancy
n_σ	average number of particles with spin σ per site
n	band filling (average number of particles per site)
m	magnetic moment (spin polarization)
λ_n	Lagrange multiplier (molecular field) coupled with n
λ_m	Lagrange multiplier (molecular field) coupled with m
$\mathcal{F}^{GA}$	Landau functional in Gutzwiller Approximation

Chapter 1

Introduction and Motivation

In this Chapter we introduce a general notion of fermionic localization as induced by the repulsive interactions among particles, here shown on the example of the Coulomb interactions among electrons. In particular, we discuss how the competition between the kinetic (band) and the Coulomb energies leads to the metal–insulator transition which at temperature $T = 0$ represents a quantum phase transition.

1.1 Mott-Hubbard Systems and their Phase Transitions

Defining *an insulator* as a material with a vanishing electrical conductivity at $T = 0$ in the electrical field is not precise. If investigated carefully, the microscopic behavior of electrons in the ionic lattice, brings several mechanisms of the evanescence of the metallicity. Namely, the Coulomb interaction between system elements will contribute to its macroscopic behavior in a different way. We can separate insulators into two groups [1], in which the leading role will be played by

1. electron–ion interactions,

2. electron–electron interactions.

Within the first group we can distinguish: *the band insulator* [2–4] (also called the Bloch-Wilson insulator), where the conductance is suppressed by interaction between electrons and the lattice periodic potential, *the Peierls insulator* [5, 6], with the interaction between electron and static lattice deformation, and *the Anderson insulator* [7], were the main contribution comes from electron–impurity interaction. A new kind of physics emerge from collective electron behavior in 2 – *the Mott insulator* [8–12]. This phenomenon can be observed in a variety of system, including perovskites [13–17], $NiS_{2-x}Se_x$ [18–21], as well as VO_2 and V_2O_3 [22–25].

1.1.1 Mott-Hubbard Criterion of Metal–Insulator Transition

One can consider a Mott insulator as a system, where an intriguing competition takes place: the kinetic (band) energy of the electrons in the lattice (much alike in the free-electron case), experience mutual repulsive Coulomb interactions. Even a rather crude approximation of locality of the electronic interaction allows us to model a system with metallic or insulating features. Namely, to asses the interaction, we take the so-called *Hubbard U*

$$U \equiv E(-) + E(\updownarrow) - (E(\uparrow) + E(\downarrow)), \tag{1.1}$$

where $E(-)$, $E(\uparrow)$, $E(\downarrow)$, and $E(\updownarrow)$ are energies of one-site with zero, one, and two electron respectively. From the other side, we take the bandwidth W related to the dispersion relation $\epsilon(\mathbf{k})$

$$W \equiv \max(\epsilon(\mathbf{k})) - \min(\epsilon(\mathbf{k})). \tag{1.2}$$

As both these quantities depend on the system topology, we list some examples in Tab. 1.1.

Table 1.1: Dispersion relation in the tight-binding approximation [26] and the corresponding bandwidth for several exemplary systems with intersite distance a and nearest-neighbor hopping t.

lattice type	**dispersion relation** $\epsilon(\mathbf{k})$	**bandwidth** W
chain	$2t\cos(k_x a)$	$4\lvert t\rvert$
simple quadratic	$2t[\cos(k_x a) + \cos(k_y a)]$	$8\lvert t\rvert$
simple cubic	$2t[\cos(k_x a) + \cos(k_y a) + \cos(k_z a)]$	$16\lvert t\rvert$
hypercubic (d dimensions)	$2t\sum_{i=1}^{d}\cos(k_i a)$	$4d\lvert t\rvert$
triangular	$2t[\cos(k_x a) + 2\cos(\frac{1}{2}k_x a)\cos(\frac{\sqrt{3}}{2}k_y a)]$	$9\lvert t\rvert$
honeycomb	$\pm t\sqrt{3 + 2\cos(\sqrt{3}k_x a) + 4\cos(\frac{3}{2}k_y a)\cos(\frac{\sqrt{3}}{2}k_x a)}$	$3\lvert t\rvert$
face-centered cubic	$4t[\cos(\frac{1}{2}k_x a)\cos(\frac{1}{2}k_y a) + \cos(\frac{1}{2}k_y a)\cos(\frac{1}{2}k_z a) + \cos(\frac{1}{2}k_z a)\cos(\frac{1}{2}k_x a)]$	$16\lvert t\rvert$
body-centered cubic	$8t\cos(\frac{1}{2}k_x a)\cos(\frac{1}{2}k_y a)\cos(\frac{1}{2}k_z a)$	$16\lvert t\rvert$

Let us construct a criterion for metallicity. We take the half-filled (the number of electrons N_e equal to the number of sites Λ) lattice and define gap as

$$\Delta = \mu^+ - \mu^-, \tag{1.3}$$

where $\mu^\pm$ is the energy required to add/remove one electron to the system

$$\mu^+ = E_G(N_e + 1) - E_G(N_e), \tag{1.4a}$$
$$\mu^- = E_G(N_e) - E_G(N_e - 1), \tag{1.4b}$$

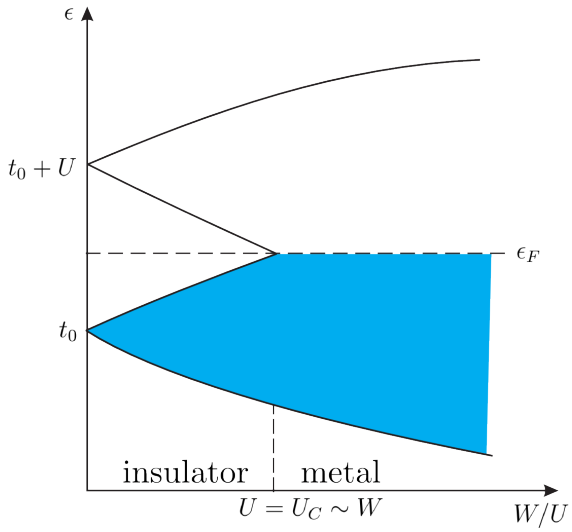

Figure 1.1: Schematic representation of repulsive interaction U splitting the single band into the two Hubbard bands (1.5). Visualization taken from Spałek [27]

where E_G is the ground-state energy. We can rewrite (1.4) in terms of U and bandwidth

$$\mu^+ = U - \frac{W_u}{2}, \tag{1.5a}$$

$$\mu^- = \frac{W_d}{2}, \tag{1.5b}$$

where W_u is so-called *upper Hubbard band* and W_d is so-called *lower Hubbard band* (cf. Fig. 1.1). W_u corresponds to the charge excitation in the system, whereas W_d with its charge removal. Combining (1.5) and (1.3) we get

$$\Delta = \mu^+ - \mu^- = U - \frac{W_u + W_d}{2} \approx U - W. \tag{1.6}$$

It is rather straightforward that for $W \ll U$ the system is insulating as the Hubbard interaction $U > 0$. Also, for $W \gg U$ the system is metallic as the system can be treated with the free-electron model (and the interaction consecutively included as perturbation). From the modeling point of view, the interesting physics happens when $W \approx U$ and the system approaches the metal–insulator transition (MIT) in the half-filled band case.

1.1.2 Original Mott Localization–Delocalization Criterion

One can look at the localization–delocalization phenomenon in a more general manner [27], as the competition between the kinetic energy of the electrons, dominating for the delocalized (metallic) state, and the electronic Coulomb repulsion, connected with the localized

(insulating) state. Let us consider a 3-dimensional, simple-cubic lattice. Average kinetic energy in such a system will be

$$\bar{E}_k = \frac{3}{5}\epsilon_F, \tag{1.7}$$

where ϵ_F is Fermi energy defined via dispersion relation

$$\epsilon_{\mathbf{k}} \equiv \frac{\hbar^2 \mathbf{k}^2}{2m}, \tag{1.8}$$

and Fermi momentum

$$k_F \equiv \left(\frac{2^3 \pi^{\frac{3}{2}} \Gamma\left(\frac{5}{2}\right)}{2S+1} \rho \right)^{\frac{1}{3}}. \tag{1.9}$$

$S = 1/2$ is the electron spin, $\Gamma(x)$ is the Euler Gamma function, and ρ is the particle density. Inserting (1.8) and (1.9) into (1.7) we have

$$\bar{E}_k = \frac{3}{5}\frac{\hbar^2}{2m}\left(3\pi^2\rho\right)^{\frac{2}{3}}. \tag{1.10}$$

On the other hand, the Coulomb repulsion will take form

$$E_{e-e} \approx \frac{e^2}{2\varepsilon \bar{r}}, \tag{1.11}$$

where e is the electron charge, ε is the absolute permittivity, and $\bar{r} \equiv \rho^{-1/3}$ is the average interelectronic distance.

We can now compare (1.10) with (1.11)

$$\frac{\bar{E}_k}{E_{e-e}} = \frac{\frac{3}{5}\frac{\hbar^2}{2m}\left(3\pi^2\right)^{\frac{2}{3}}\rho^{\frac{2}{3}}}{\frac{e^2}{2\varepsilon}\rho^{\frac{1}{3}}} = \frac{3}{5}\left(3\pi^2\right)^{\frac{2}{3}}\frac{\hbar^2\varepsilon}{me^2}\rho^{\frac{1}{3}}. \tag{1.12}$$

Both energies are comparable when (1.12) is equal to unity. Taking Bohr radius $a_B \equiv \hbar^2\varepsilon/me^2$ we obtain the so-called Mott (or Mott-Wigner) criterion for critical particle density ρ_C

$$a_B \rho_C^{\frac{1}{3}} = \frac{5}{3}\left(3\pi^2\right)^{-\frac{2}{3}} = 0.174 \approx 0.2. \tag{1.13}$$

One sees clearly that for $\rho < \rho_C$ the interaction energy is dominant, whereas for $\rho > \rho_C$ the kinetic energy is. In other words, for the low-density ($\rho < \rho_C$) the potential energy freezes the electrons in the hydrogenic-like orbits with the Bohr radius a_B, whereas for $\rho \gg \rho_C$ the particles are almost free, i.e. the metallic state is stable. Thus the Mott

criterion (1.13) defines in rough terms the limiting concentration on free-electron concept applicability to the description of metallic state.

At this point, one should mention that there exist other related criteria of metallicity (cf. Mott [10]); here we should mention only the original Mott criterion. This criterion addressed the discontinuous transition to the metallic phase in *ed* magnetic oxides. Namely, Mott argued that the transition from the (magnetic) insulating system to the metallic state as a function of e.g. pressure, should be discontinuous. This is because a small number of conduction electrons in the conduction band would increase largely the Coulomb repulsive energy (lack of mutual screening). Hence their number must be substantial so the emerging band energy overcomes the repulsive interaction. A reasoning of that kind leads to the criterion (1.13) which expresses the instability of the atomic bound state with respect to the free-particle (electron-gas) state.

1.2 Hydrogen systems: Principal Qualitative Features

The atomic hydrogen solid would present itself as an ideal system to model band-electron physics and the Mott-Hubbard type of metal–insulator transitions. This is because such system has only one valence electron, originally on $1s$-type orbital, as the distance of the first excited ($2s$, $2p$) state is located $3/4Ry \approx 10eV$ higher. So its admixture to the $1s$-type Wannier state should be rather small, particularly neat the metal-insulator transition, where according to (1.13) we have that the intersite distance $a \sim (4 \div 5)a_B$. It is quite amazing that studies of such hydrogenic-like solids has started only recently by incorporating the Mott-Hubbard physics into the first-principle electronic structure modeling [28–32]. These studies brought even some estimates for the critical pressure $p \sim 10^2 GPa$ for the atomic hydrogen metallization, as well as pointed out to the possibility of quantum critical behavior of the atomic orbit size at the metallization threshold. The zero point motion of the lightest ions (protons) in this case has been estimated and shown to be sizable, but without destroying the ionic lattice, what would amount to the transition from an atomic Mott insulating solid to the electron-proton plasma.

Having said that, one has to note one principal feature complicating any such atomic-hydrogen modeling. Namely, hydrogen as such is stable in the molecular state H_2 at ambient pressure and likewise, it forms a variety of molecular crystal structures at ambient and applied pressures [33, 34]. There are at least three known solid phases [33, 35–37], often referred to as phases I, II and III (cf. Fig. 1.2). Appearing for relatively small pressures closed-packed (hexagonal) molecular crystal ($P6_3/m$) constitutes what is known as phase I (cf. Fig 1.3.a). Phases II and III are not well recognized experimentally; nevertheless, there are DFT structural calculations [38, 39] recognizing phase II as monoclinic $C2/c$ molecular crystal (cf. Fig 1.3.b), and phase III as monoclinic $Cmca-12$ molecular crystal (cf. Fig 1.3.c). Whether or not the phase III is metallic, was carefully examined experimentally by Zha *et al.* [37] in the broad range of temperature and pressure (up to $300GPa$), but no

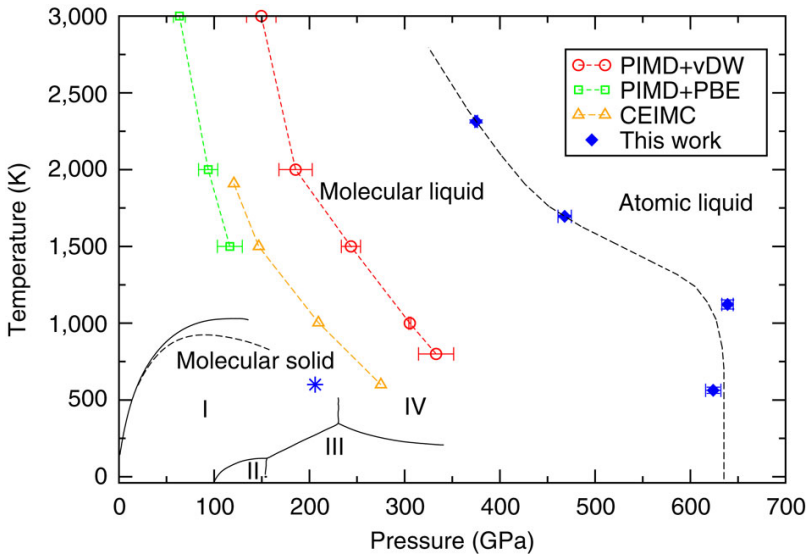

Figure 1.2: Phase diagram of hydrogen under pressure from Mazzola *et al.* [33]. Boundaries of hexagonal molecular crystal ($P6_3/m$ – phase I), monoclinic $C2/c$ molecular crystal (phase II), monoclinic $Cmca-12$ molecular crystal (phase III), and new phase IV with not yet determined structure are presented with the molecular and atomic liquids regimes marked. The points refer to different computational approaches to describe the system (cf. [33]).

metallic behavior had been observed. In 2011 a new phase IV was reported by Eremets and Troyan [40], claimed to be an atomic fluid. Both its atomic character and metallic properties were subsequently questioned [41–43]. The *ab initio* Molecular Dynamic approach by Goncharov *et al.* [41] suggests that phase IV could be a mixture of molecular liquid and the atomic, graphene-like two-dimensional layers. Additionally, Howie *et al.* [36] reported in an experiment (Raman spectroscopy under high pressure) a new phase transition at $255GPa$ and $480K$, which can be understood as a melting transition at surprisingly low temperature (given the magnitude of the pressure).

We can say that the natural starting situation is a dimerized hydrogen quantum solid which may metallize under applied pressure. The modeling of molecular phases at ambient and external pressures is one of the main purposes of the Thesis. To this aim, a specific combination of exact diagonalization and *ab initio* approach has been developed by us in recent years [44]. The method of approach is discussed in detail in the next Chapter. First, we characterized the aim and scope of the Thesis in general terms.

It is essential to say few words about the importance of hydrogen metallization. First, it is a model system for the correlated systems, albeit with the complications introduced by the molecular binding. Second, and most important, metallized by pressure hydrogen is regarded as a prospective room-temperature superconductor [45]. For that purpose, both

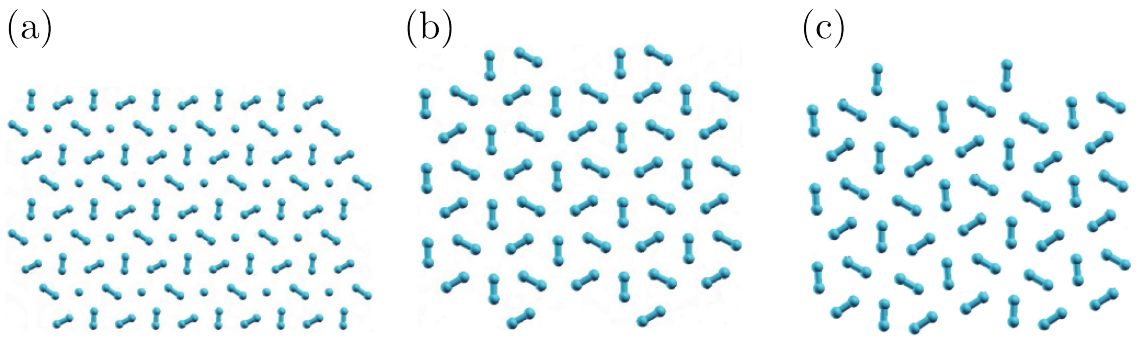

Figure 1.3: First three phases of solid molecular hydrogen. Hexagonal $P6_3/m$ phase I (a), monoclinic $C2/c$ phase II (b), and monoclinic $Cmca-12$ phase III (c). Visualization taken from Azadi and Foulkes [38].

the correlation effects and the local electron–lattice coupling constants must be considered concomitantly. The second task has been achieved already [46]. As for the first, there is still a road ahead, as we point it out explicitly in the Summary and Outlook section.

1.3 Aim and the Scope of the Thesis

As already said, the principal aim of this Thesis is to develop and implement a reliable method of calculating hydrogen or hydrogenic-like systems up to the metallization and characterization of resultant metallic state. In this Thesis we start from a precise approach to molecular systems regarded as the principal and necessary first step in that direction. We supplement the molecular considerations (cf. paper A-3) with rigorous treatment of molecular hydrogen chains (cf. papers A-4 and A-5).

One has to note that this is not a simple task as for example single-particle DFT calculations [39, 47–49] provide conflicting results [38]. Previously, promising results in this direction have been obtained within the Monte Carlo [33, 50–52], and other [53–56] techniques. In this respect, our approach may be regarded as systematic. This is because of few reasons. First of them, unlike the other approaches including the electronic correlations (LDA+U [57, 58], LDA+DMFT [59–63]) our approach does not have their drawback of counting twice the repulsive Coulomb interaction among the particles. Second, the method allows for determination of single-particle Wannier wave functions in the correlated state. Third, the microscopic parameters such as the intersite hopping integrals (t_{ij}) or magnitude of the Hubbard interaction (U) are evaluated also in the correlated state. In that manner, one can relate explicitly the ab initio electronic structure to the Mott-Hubbard criteria of localization.

As to the scope of the Thesis apart from two methodological papers setting the method

correctly both from the molecular [46] and the computational [64] sides, we have also demonstrated its effectiveness already on the nanoscopic (multi-molecular) level [65]. For infinite system, so far only the so-called *statistically consistent Gutzwiller approximation* (SGA) has been formulated [32]. The zero point motion problem has been tackled also successfully [46, 66]. In the near future, an extension of our results to the so-called diagrammatic expansion for the Gutzwiller wave function (DE-GWF), formulated in our group and successfully applied to a number of problems [67–72], is planned. The formal approach developed for the present problem of hydrogen metallization, allows utilizing both exact and approximated methods of diagonalization of the second-quantized Hamiltonians. Within this perspective, our results represent a first step towards the problem solution.

In general, the method is applicable to atoms, molecules, and correlated solids. Some of the examples of application to each type of the above systems are provided in the next Chapter.

Chapter 2

Methods of approach

In this Chapter we characterize in detail the methods used throughout the Thesis. Namely, the **E**xact **D**iagonalization – **Ab I**nitio Approach (EDABI) and the **S**tatistically-Consistent **G**utzwiller **A**pproximation (SGA). Both of these methods have been developed and used in our group in the context of electron localization in the correlated systems (EDABI) and in the context of unconventional superconductivity (SGA).

2.1 First-Principle Quantum-Mechanical Description of Matter

The starting many-electron Hamiltonian for calculating the stationary states has the following form within the first quantization scheme

$$\mathcal{H} = -\sum_i \nabla_i^2 \underbrace{-\sum_{ij} \frac{2Z_j}{|\mathbf{r}_i - \mathbf{R}_j|}}_{\text{electron–ion attraction}} + \overbrace{\frac{1}{2}\sum_{i\neq j} \frac{2}{|\mathbf{r}_i - \mathbf{r}_j|}}^{\text{electron–electron repulsion}} + \underbrace{\frac{1}{2}\sum_{i\neq j} \frac{2Z_i Z_j}{|\mathbf{R}_i - \mathbf{R}_j|}}_{\text{ion–ion repulsion}}, \tag{2.1}$$

where electronic coordinates are denoted by $\mathbf{r}_i$, whereas ions are statically at positions $\mathbf{R}_i$. The consecutive terms are represented schematically in Fig. 2.1. We utilize the Born-Oppenheimer approximation [73] and regard the ionic coordinates $\{\mathbf{R}_i\}$ as fixed and determine the ground-state energy E_G via the corresponding N-particle Schrödinger equation for the electronic part

$$\mathcal{H}\Psi(\mathbf{r}_1, \mathbf{r}_2, \mathbf{r}_3, \dots \mathbf{r}_N) = E_G \Psi(\mathbf{r}_1, \mathbf{r}_2, \mathbf{r}_3, \dots \mathbf{r}_N). \tag{2.2}$$

We call a method allowing to solve (2.2) the first-principle (of Quantum Mechanics) or *ab initio* method. It is today almost synonymic with use of modern-day Density Functional Theorem [74, 75] and its many variations (e.g., LDA+U [57, 58], LDA+DMFT [59–63]),

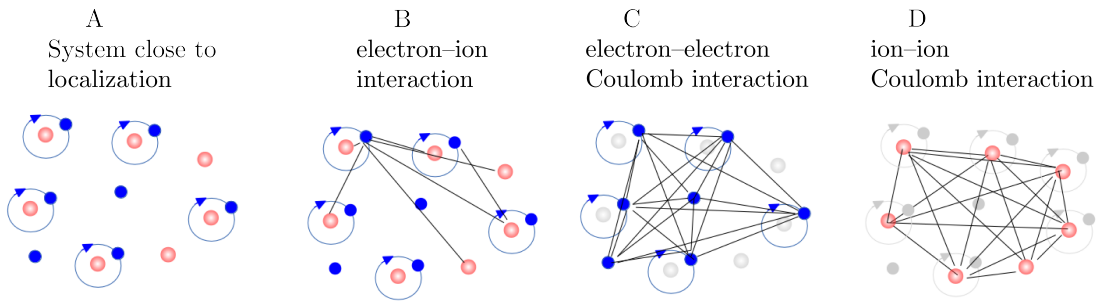

Figure 2.1: A schematic representation of system in a metallic state close to the first-order metal–insulator transition, as composed of frozen ions (in Born-Oppenheimer approximation), electron–ion (B), electron–electron (C), and Coulomb ion–ion (D) interactions.

which are not exact by any precise means. There is a vast number of tools in the first-quantization language dealing with Hamiltonian (2.1), worth mentioning is the Hartree-Fock method [76–78] and its many derivatives [79, 80], as well as the Møller–Plesset method [81], and the Configuration-Interaction methods [82]. In the next Section we present an original method, called **E**xact **D**iagonalization **Ab I**nitio approach (EDABI), which allows for first-principle description of the system, while employing both the second-quantization language and the renormalization of single-particle basis of wave functions. Instead of working with (2.1), we describe next our system in terms of second-quantized Hamiltonian.

2.2 Exact Diagonalization ab Initio Approach

As a method to tackle hydrogen systems we have selected the so-called **E**xact **D**iagonalization **Ab I**nitio approach (EDABI) [83–85], proved to be efficient to describe hydrogen systems both asymptotically (ionization energy of a free atom differs $< 0.1\%$ from experimental value, binding energy of a H_2 molecule is calculated with the accuracy of 2% [46, 83]) and as an atomic solid [30–32]. The method successfully combines first– and second-quantization pictures, and allows for employment vast number of algorithms of diagonalizing the parametrized Hamiltonian in its second-quantization form..

2.2.1 Principal points of Exact Diagonalization - Ab Initio Approach (EDABI)

To understand the method we start from the field operators in the form

$$\hat{\Psi}_\sigma(\mathbf{r}) = \sum_{i\nu} w_i^\nu(\mathbf{r})\chi_\sigma \hat{c}_{i\nu\sigma}, \tag{2.3}$$

where $w_i^\nu(\mathbf{r})$ is the set of single-particle ν-th band orthogonal and normalized wavefunctions centered on the lattice site i, $\hat{c}_{i\nu\sigma}$ is the corresponding annihilation operator, and χ_σ is the spin wavefunction ($\sigma = \pm 1$) with the single (global) spin quantization axis (z-axis). Band index ν can be dropped for clarity of formulas, and from now on we treat i as an arbitrary index (not necessarily connected only with the lattice site).

We can rewrite our many-particle Hamiltonian (2.1) in the second-quantized form

$$\begin{aligned}\hat{\mathcal{H}} = &\sum_\sigma \int d^3r \hat{\Psi}_\sigma^\dagger(\mathbf{r}) \left(-\nabla^2 - \sum_i \frac{2Z_i}{|\mathbf{r} - \mathbf{R}_i|} \right) \hat{\Psi}_\sigma(\mathbf{r}) \\ &+ \frac{1}{2} \sum_{\sigma\sigma'} \iint d^3r d^3r' \hat{\Psi}_\sigma^\dagger(\mathbf{r}) \hat{\Psi}_{\sigma'}^\dagger(\mathbf{r}') \frac{2}{|\mathbf{r} - \mathbf{r}'|} \hat{\Psi}_{\sigma'}(\mathbf{r}') \hat{\Psi}_\sigma(\mathbf{r}) + \frac{1}{2} \sum_{i \neq j} \frac{2Z_i Z_j}{|\mathbf{R}_i - \mathbf{R}_j|}.\end{aligned} \tag{2.4}$$

All terms are expressed in the atomic units ($\hbar = e^2/2 = 2m_e = 1$, where e is the charge of electron and m_e is its mass). The last term $1/2 \sum_{i \neq j} 2Z_i Z_j / |\mathbf{R}_i - \mathbf{R}_j|$ is the classical Coulomb repulsion between ions located respectively at the positions $\mathbf{R}_{i/j}$, and with the atomic numbers $Z_{i/j}$. Note that we assumed the classical behavior of the ions, i.e., the electrons interact with *frozen* ionic centers. If we proceed with including (2.3) into (2.4), we obtain the explicit second-quantized form of the Hamiltonian [86, 87] i.e.,

$$\mathcal{H} = \sum_{ij} \sum_\sigma t_{ij} \hat{c}_{i\sigma}^\dagger \hat{c}_{j\sigma} + \sum_{ijkl} \sum_{\sigma,\sigma'} V_{ijkl} \hat{c}_{i\sigma}^\dagger \hat{c}_{j\sigma'}^\dagger \hat{c}_{l\sigma'} \hat{c}_{k\sigma}, \tag{2.5}$$

where t_{ij} and V_{ijkl} are microscopic parameters represented by integrals

$$\begin{aligned} t_{ij} &\equiv \left\langle w_i(\mathbf{r}) \middle| \left(-\nabla^2 - \sum_i \frac{2Z_i}{|\mathbf{r} - \mathbf{R}_i|} \right) \middle| w_j(\mathbf{r}) \right\rangle \\ &\equiv \int d^3r \; w_i^*(\mathbf{r}) \left(-\nabla^2 - \sum_i \frac{2Z_i}{|\mathbf{r} - \mathbf{R}_i|} \right) w_j(\mathbf{r}), \end{aligned} \tag{2.6a}$$

$$\begin{aligned} V_{ijkl} &\equiv \left\langle w_i(\mathbf{r}) w_j(\mathbf{r}') \middle| \frac{2}{|\mathbf{r} - \mathbf{r}'|} \middle| w_k(\mathbf{r}) w_l(\mathbf{r}') \right\rangle \\ &\equiv \iint d^3r d^3r' \; w_i^*(\mathbf{r}) w_j^*(\mathbf{r}') \frac{2}{|\mathbf{r} - \mathbf{r}'|} w_k(\mathbf{r}) w_l(\mathbf{r}'). \end{aligned} \tag{2.6b}$$

Up to this point the discussion is general as long as the single-particle basis $\{w_i(\mathbf{r})\}$ is complete, i.e.,

$$\sum_i w_i^*(\mathbf{r}) w_i(\mathbf{r}') = \delta(\mathbf{r} - \mathbf{r}'). \tag{2.7}$$

As the basis is infinite, it is not possible to diagonalize (2.5) exactly. To do so, one must select *rich enough* finite basis to describe given system, which introduces an unknown error

to the calculations. The EDABI method offers a workaround to this problem: One assumes finite basis with a set of adjustable parameters $\{\alpha_i\}$ and minimizes the system energy to find the optimal values of these parameters. As we usually start from the single-particle basis being a solution of the one-electron situation, this approach allows us to obtain realistic results with relatively small bases. Please refer to Fig. 2.2 for the step-by-step essentials about the EDABI.

2.2.2 Many-particle wavefunction and the particle-density profile

In EDABI method we diagonalize the Hamiltonian (2.5) in the Fock space, obtaining the ground state defined as

$$|\Phi_0\rangle = \sum_{i_1,\ldots,i_N} C_{i_1,\ldots,i_N} \hat{c}^\dagger_{i_1} \ldots \hat{c}^\dagger_{i_N} |0\rangle . \tag{2.8}$$

We can reverse the procedure, and retrieve the first-quantization picture of resultant, physical state by employing field operators (2.3). The exact N-body wavefunction can be written in the following form

$$\Psi(\mathbf{r}_1, \ldots, \mathbf{r}_N) \equiv \frac{1}{\sqrt{N!}} \sum_{i_1,\ldots,i_N} \langle 0| \hat{c}_{i_N} \ldots \hat{c}_{i_1} |\Phi_0\rangle w_{i_1}(\mathbf{r_1}) \ldots w_{i_N}(\mathbf{r_N}). \tag{2.9}$$

Out of all features of many-body picture, the possibility of obtaining the particle density profiles is of particular significance. Namely, we can introduce the particle density operator

$$\hat{n}(\mathbf{r}) \equiv \sum_\sigma \hat{\Psi}^\dagger_\sigma(\mathbf{r}) \hat{\Psi}_\sigma(\mathbf{r}), \tag{2.10}$$

where $\hat{\Psi}_\sigma(\mathbf{r})$ is the field operator (2.3). (2.10) reduces to the particle density function

$$n(\mathbf{r}) \equiv \left\langle \Phi_0 \middle| \sum_\sigma \hat{\Psi}^\dagger_\sigma(\mathbf{r}) \hat{\Psi}_\sigma(\mathbf{r}) \middle| \Phi_0 \right\rangle = N \int d^3\mathbf{r}_1 \ldots d^3\mathbf{r}_{N-1} \left|\Psi(\mathbf{r}_1, \ldots, \mathbf{r}_{N-1}, \mathbf{r})\right|^2 . \tag{2.11}$$

By knowing the optimized basis $\{w_i(\mathbf{r})\}$ and correlation functions $\left\langle \hat{c}^\dagger_{i\uparrow} \hat{c}_{j\uparrow} \right\rangle$, one can draw the particle density profiles for the system at hand.

2.2.3 Testing case: Description of light atoms

The natural language to describe electrons in atoms is provided by the Slater-type orbitals (STO) [88], hence the choice of them as our basis. This causes an issue, as Slater functions

$$\psi_{nlm}(\mathbf{r}) \equiv \sqrt{\frac{(2\alpha_{nlm})^{2n+1}}{(2n)!}} r^{n-1} e^{-\alpha_{nlm} r} Y^m_l(\mathbf{r}), \tag{2.12}$$

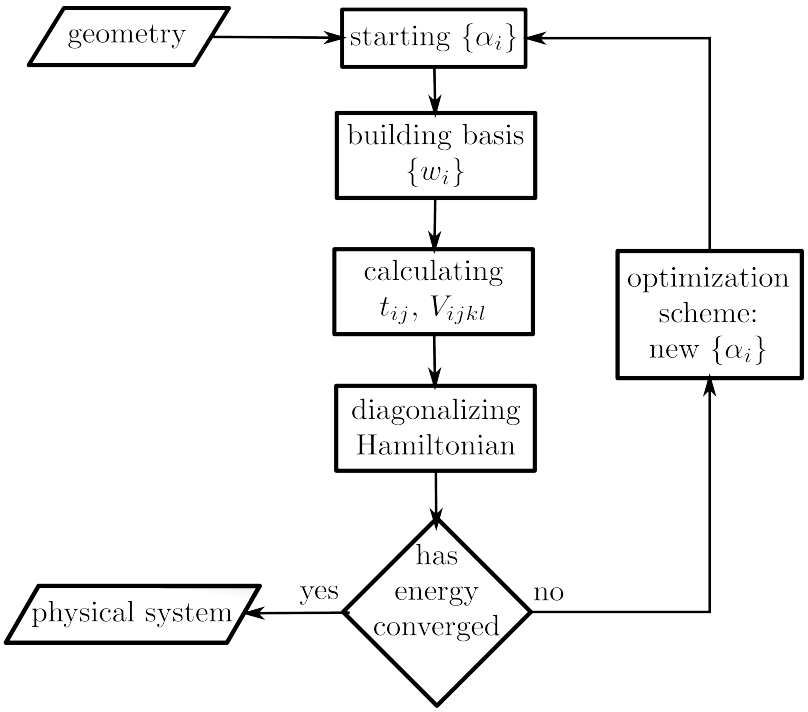

Figure 2.2: Flowchart of the EDABI method. The essence of the method is as follows: We start with setting the rules of the basis composition. This includes geometry of considered system and the single-particle wave-function renormalization parameters $\{\alpha_i\}$. We set the parameters, construct the basis with given rules (this usually consists of basis orthogonalization), then we calculate Hamiltonian parameters t_{ij} and V_{ijkl}. This is the most time-consuming part and usually requires some computational treatment (cf. paper A-4). Next, we must diagonalize the parametrized Hamiltonian (standard approach will include exact diagonalization, Lanczos algorithm, or statistically-consistent Gutzwiller approximation). Finally, the essential step in EDABI is invoked - basis is renormalized via (non-gradient) optimization scheme to obtain the physical ground-state energy E_G.

where $n = 1, 2, 3, \ldots$, $l = 0, 1, \ldots, n-1$, $m = -l, \ldots, -1, 0, 1, \ldots, l$ are quantum numbers and $Y_l^m(\mathbf{r})$ are spherical harmonics (for simplicity, we select the real spherical harmonics), are non always orthogonal (in fact when we consider more than one atom in the system they are *almost always* non-orthogonal). This can be fixed by employing the so-called linear-combination atomic orbitals (LCAO) [89] and orthogonalized via selected method: either the Löwdin symmetrical orthogonalization [90] or the bilinear forms method - see paper A-4.

The other necessity of the EDABI is to select a number of parameters $\{\alpha_i\}$, renormalizing basis' single-particle wavefunctions. It can obviously be done in several ways, but we chose the natural coefficients - the inverse wave-function size α_{nlm} embedded in Slater-type orbitals. For clarity we will use only n explicitly, l we will traditionally refer to as s (0), p (1), d (2), etc. and instead of m we will write main symmetry axes (i.e., α_{210} becomes α_{2p^z}). See Fig. 2.3 for examples of Slate-type orbitals for different α coefficients.

Gaussian contraction of Slater-type orbitals

As the calculation of integrals (2.6) for the Slater-type orbitals based single-particle basis is problematic in general case (especially when it comes to three– and four–site terms) it is convenient to use approximated and integrable representation of STO in terms of Gaussian orbitals (the so called STO-pG basis, where p is the number of Gaussian function approximating a single Slater-type orbital)

$$\psi_i(\mathbf{r}) \approx \psi_i^G(\mathbf{r}) = \alpha^{\frac{3}{2}} \sum_{q=1}^{p} B_q \left(\frac{2\Gamma_q^2}{\pi}\right)^{\frac{3}{4}} e^{-\alpha^2\Gamma_q^2|\mathbf{r}-\mathbf{R}_i|^2}, \tag{2.13}$$

where $\mathbf{R}_i$ denotes ionic coordinates, α is the STO inverse wave-function size, and B_q are the contraction coefficients and Γ_q are the inverse Gaussian sizes, both obtain by a proper minimization procedure of the error function

$$\mathcal{E} \equiv \int d^3r(\psi_i(\mathbf{r}) - \psi_i^G(\mathbf{r}))^2. \tag{2.14}$$

Results

Employing the EDABI approach with concomitant optimization of all the Slater-type orbitals (represented as $p = 5$ Gaussians ($1s$,$2s$) and $p = 10$ Gaussians ($2p$) contractions each) we are able to reproduce many-electron states of atoms of the first two periods of the Mendeleev periodic table with all ionization energies for the full Hamiltonian in the form

$$\mathcal{H} = \sum_{ij}\sum_{\sigma} t_{ij}\hat{c}_{i\sigma}^{\dagger}\hat{c}_{j\sigma} + \sum_{ijkl}\sum_{\sigma,\sigma'} V_{ijkl}\hat{c}_{i\sigma}^{\dagger}\hat{c}_{j\sigma'}^{\dagger}\hat{c}_{l\sigma'}\hat{c}_{k\sigma}. \tag{2.15}$$

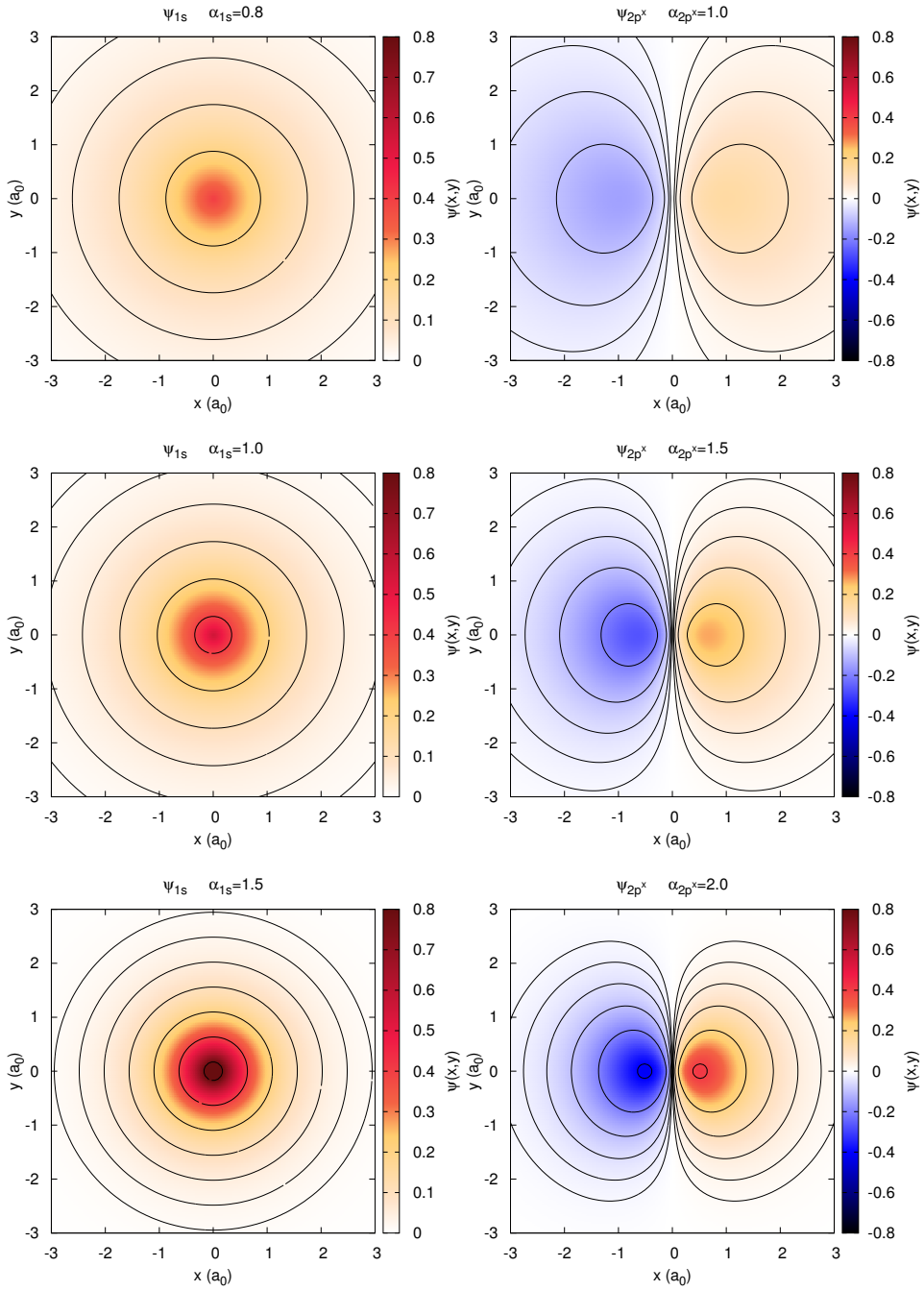

Figure 2.3: Slater functions $\psi_{1s}(\mathbf{r})$ and $\psi_{2p^x}(\mathbf{r})$ on the xy-plane for different values of inverse wave-function size α_{1s} and α_{2p^x} respectively.

Table 2.1: Ground-state energy E_G and ionization energies E_i^{ion} for selected light atoms in Rydbergs (Ry). Optimiziation of $1s$, $2s$, $2p^x$, $2p^y$, and $2p^z$ real Slater-type orbitals. Note that systems with more-than-half-filling (number of electrons > 5, marked with red color) have their values differ from the results presented in literature [91] (cf. Table 2.2). This is due to the fact, that the single-particle basis is no longer *rich enough* for the purpose of *ab initio* description.

	E_G	E_1	E_2	E_3	E_4	E_5	E_6	E_7	E_8	E_9	E_{10}
H	-0.999878	1.000									
He	-5.77524	1.776	4.000								
Li	-14.7287	0.245	5.484	8.999							
Be	-29.165	0.6183	1.3134	11.2352	15.9981						
B	-48.928	0.558	1.652	2.740	18.981	24.997					
C	-74.9426	0.590	1.702	3.314	4.568	28.773	35.996				
N	-107.852	0.723	1.868	3.342	5.426	7.022	40.477	48.994			
O	-147.863	0.414	2.159	3.644	5.473	8.033	9.923	54.225	63.992		
F	-195.917	0.511	1.898	4.093	5.913	7.905	11.319	13.316	69.972	80.990	
Ne	-252.657	0.603	2.154	3.880	6.520	8.672	11.199	14.677	17.245	87.719	99.988

Table 2.2: Ground-state E_G and ionization E_i energies from Lide [91] for comparison with results presented in Table 2.1. Please note that for system not differing much from half-filling the results are similar.

	E_G	E_1	E_2	E_3	E_4	E_5	E_6	E_7	E_8	E_9	E_{10}
H	-0.999	0.999									
He	-5.807	1.807	4.000								
Li	-14.956	0.396	5.559	9.000							
Be	-29.337	0.685	1.338	11.311	16.002						
B	-49.316	0.610	1.849	2.788	19.064	25.006					
C	-75.711	0.828	1.792	3.520	4.740	28.818	36.014				
N	-109.224	1.068	2.176	3.487	5.694	7.195	40.577	49.027			
O	-150.217	1.001	2.581	4.038	5.690	8.371	10.152	54.337	64.047		
F	-199.612	1.281	2.570	4.609	6.405	8.397	11.551	13.611	70.111	81.078	
Ne	-258.101	1.585	3.011	4.663	7.138	9.276	11.608	15.234	17.573	87.892	100.120

Table 2.3: Hydrogeniclike atoms in the EDABI approach (optimiziation of $1s$, $2s$, $2p^x$, $2p^y$, and $2p^z$ real Slater-type orbitals). Note that the exact solution of Schrödinger equation provides $\alpha_{1s} = Z(a_0)$, $E_{HL} = -Z^2(Ry)$.

	Z	α_{1s} (a_0^{-1})	E_{HL} (Ry)
H	1	1.00802	-0.999878
He^{1+}	2	1.99596	-3.9995
Li^{2+}	3	3.02355	-8.9989
Be^{3+}	4	4.0038	-15.9981
B^{4+}	5	5.04009	-24.997
C^{5+}	6	6.0057	-35.9957
N^{6+}	7	7.00665	-48.9941
O^{7+}	8	8.0076	-63.9923
F^{8+}	9	9.00855	-80.9903
Ne^{9+}	10	10.0095	-99.988

The results are listed in Table 2.1. As a test of the method, one may also compare results for the Hydrogeniclike atoms obtained by the solving the single-electron Schrödinger equation with the results obtained from EDABI method (listed in Table 2.3).

2.3 Gutzwiller (GA) and Statistically consistent Gutzwiller Approximations (SGA)

When we consider a system with the strong electronic correlations, the perturbation theory is no longer a effective approach, opening the doors to the variational treatment with the trial wave functions. Such an approach was devised by Gutzwiller [92–94] and generalized over the years to fulfill requirements of different models, e.g., multiband [95, 96], time-dependent case [97], as well as t-J, t-J-U [98–101], and periodic Anderson model [102–105].

2.3.1 Gutzwiller wave function method

Let us take the Hubbard Hamiltonian

$$\mathcal{H} = \sum_{ij\sigma} t_{ij} \hat{c}^{\dagger}_{i\sigma} \hat{c}_{j\sigma} + U \sum_{i} \hat{n}_{i\uparrow} \hat{n}_{i\downarrow}, \tag{2.16}$$

where $\hat{c}^{\dagger}_{i\sigma}$ and $\hat{c}_{i\sigma}$ are the fermionic creation and annihilation operators, $\hat{n}_{i\sigma} \equiv \hat{c}^{\dagger}_{i\sigma} \hat{c}_{i\sigma}$ is the fermionic particle number operator, t_{ij} is the hopping amplitude, and U is the Hubbard on-site repulsion term. Its expectation value is calculated with respect to the Gutzwiller

trial wave function

$$|\psi_G\rangle \equiv \mathcal{P}\,|\psi_0\rangle \equiv \prod_i \mathcal{P}_i\,|\psi_0\rangle\,, \tag{2.17}$$

where $|\psi_0\rangle$ is the uncorrelated single-particle product state (Slater determinant) - to be determined explicitly later, and $\mathcal{P}_i$ is the local Gutzwiller correlator defined for the single-band case in the form

$$\mathcal{P}_i \equiv \left(1-(1-g)\hat{n}_{i\uparrow}\hat{n}_{i\downarrow}\right), \tag{2.18}$$

where g is the variational parameter. The case $g=0$ refers to the situation with no *double occupancy*, as all these terms are projected out from the wave function $|\psi_0\rangle$. Following Bünemann *et al.* [96], we can redefine the local Gutzwiller correlator according to

$$\mathcal{P}_i \equiv \sum_\Gamma \lambda_{i\Gamma}\,|\Gamma\rangle_{ii}\langle\Gamma|\,, \tag{2.19}$$

where $\lambda_{i\Gamma}$ are the variational parameters describing the occupation probabilities of possible local states $|\Gamma\rangle_i$ ($|\Gamma\rangle_i \in \{|-\rangle_i, |\uparrow\rangle_i, |\downarrow\rangle_i, |\updownarrow\rangle_i\}$ for one-band case), where $|-\rangle_i$ is the empty-site i configuration, $|\sigma\rangle_i$ is that with the single occupation with spin $\sigma =\uparrow$ or $\downarrow$, and $|\updownarrow\rangle_i$ is the site occupied by an electron pair.

2.3.2 Gutzwiller approximation: Ground-state energy

For given (2.17) trial wave function we can calculate the ground-state energy E_G per site in the so-called Gutzwiller approximation (GA) and obtain

$$\frac{E_G}{\Lambda} = \frac{\langle\psi_G|\,\mathcal{H}\,|\psi_G\rangle}{\langle\psi_G|\,\psi_G\rangle} \equiv \frac{\langle\psi_0|\,\mathcal{P}\mathcal{H}\mathcal{P}\,|\psi_0\rangle}{\langle\psi_0|\,\mathcal{P}^2\,|\psi_0\rangle} \approx q_\uparrow\epsilon_\uparrow + q_\downarrow\epsilon_\downarrow + Ud^2, \tag{2.20}$$

where Λ is the number of sites, d^2 is the average number of double occupancies,

$$\epsilon_\sigma \equiv \frac{1}{\Lambda}\left\langle \psi_0 \middle| \sum_{ij} t_{ij}\hat{c}^\dagger_{i\sigma}\hat{c}_{i\sigma} \middle| \psi_0 \right\rangle = \frac{1}{\Lambda}\sum_{\mathbf{k}} \epsilon_{\mathbf{k}} \tag{2.21}$$

is the average bare band energy per site for particles of spin σ, and the band narrowing factor is

$$q_\sigma \equiv q_\sigma(d, n_\sigma, n_{\bar{\sigma}}) = \frac{\left(\sqrt{(n_\sigma - d^2)(1-n_\sigma-n_{\bar{\sigma}}+d^2)} + d\sqrt{n_{\bar{\sigma}}-d^2}\right)^2}{n_\sigma(1-n_\sigma)}, \tag{2.22}$$

where n_σ is the average number of particles with spin σ, and $d^2 = \left\langle \hat{n}_{i\uparrow}\hat{n}_{i\downarrow}\right\rangle$. We see that the bare band energies are renormalized by the factor q_σ. Additionally, an essential new feature appears, namely the two-particle correlation function d^2. It is the variational parameter for given ratio U/W (W is the bare bandwidth) and the band filling n.

2.3.3 Effective Hamiltonian in GA

It more convenient to formulate the problem in a different manner. Namely, we assume that there exists an effective, single-particle Hamiltonian $\mathcal{H}_{GA}$, with its expectation value equal to the (2.20), but now calculated with respect to the uncorrelated wave function $|\psi_0\rangle$. Thus, instead of the diagonalizing the Hamiltonian (2.16), we minimize the eigenvalue of the effective Hamiltonian

$$\begin{aligned}\mathcal{H}_{GA} &= \sum_{ij\sigma} q_\sigma(d,n,m) t_{ij} \hat{c}^\dagger_{i\sigma}\hat{c}_{j\sigma} - \sum_{i\sigma}\sigma h \hat{c}^\dagger_{i\sigma}\hat{c}_{i\sigma} + \Lambda U d^2 \\ &= \sum_{\mathbf{k}\sigma} \left(q_\sigma(d,n,m)\epsilon_{\mathbf{k}} - \sigma h\right) \hat{c}^\dagger_{\mathbf{k}}\hat{c}_{\mathbf{k}} + \Lambda U d^2,\end{aligned} \tag{2.23}$$

where $\epsilon_{\mathbf{k}}$ is the dispersion relation and depends on the lattice geometry (examples are listed in Table 1.1), $\sum_{i\sigma}\sigma h \hat{c}^\dagger_{i\sigma}\hat{c}_{i\sigma}$ is the Zeeman term with the reduced magnetic field $h = 1/2 g\mu_B H_a$ (that we can take into account without complicating our case), whereas $n \equiv n_\uparrow + n_\downarrow$ and $m = n_\uparrow - n_\downarrow$ are the more convenient variational parameters, satisfying

$$\begin{cases} n &\equiv \frac{1}{\Lambda}\sum_{\mathbf{k}\sigma}\left\langle \hat{c}^\dagger_{\mathbf{k}}\hat{c}_{\mathbf{k}}\right\rangle, \\ m &\equiv \frac{1}{\Lambda}\sum_{\mathbf{k}\sigma}\sigma\left\langle \hat{c}^\dagger_{\mathbf{k}}\hat{c}_{\mathbf{k}}\right\rangle. \end{cases} \tag{2.24a}$$

The two above quantities represent, respectively, the band filling (average number of particles per site) and the magnetic moment (spin polarization) per site.

2.3.4 GA: Grand Canonical Ensemble Approach

We describe the system at nonzero temperature by constructing the grand potential functional

$$\mathcal{F}^{GA} = -\frac{1}{\beta}\log\mathcal{Z}, \tag{2.25}$$

where $\beta = 1/k_B T$, k_B is the Boltzmann constant, and the grand partition function $\mathcal{Z}$

$$\mathcal{Z} \equiv Tr\left(e^{-\beta(\mathcal{H}_{GA}-\mu\hat{n})}\right), \tag{2.26}$$

where μ is the system chemical potential. Using (2.23) we can write that

$$\mathcal{Z} = \prod_{\mathbf{k}\sigma}\mathcal{Z}_1 = \prod_{\mathbf{k}\sigma}\sum_{n_i=0}^{1} e^{-\beta n_i E^{GA}_{\mathbf{k}\sigma}} e^{-\beta U d^2} = e^{-\beta\Lambda U d^2}\prod_{\mathbf{k}\sigma}\left(1 + e^{-\beta E^{GA}_{\mathbf{k}\sigma}}\right), \tag{2.27}$$

with the quasiparticle energy defined by

$$E^{GA}_{\mathbf{k}\sigma} \equiv q_\sigma\epsilon_{\mathbf{k}} - \sigma h - \mu. \tag{2.28}$$

We can insert (2.27) to (2.25) and obtain

$$\mathcal{F}^{GA} = -\frac{1}{\beta}\sum_{\mathbf{k}\sigma}\log\left(1+e^{-\beta E^{GA}_{\mathbf{k}\sigma}}\right) + \lambda U d^2, \tag{2.29}$$

related to the free energy functional via a simple redefinition

$$F^{GA} = \mathcal{F}^{GA} + \Lambda\mu n. \tag{2.30}$$

In the next Section we describe in detail the minimization procedure of this effective Landau functional for our fermionic system.

2.3.5 Statistical consistency for the Gutzwiller approximation (SGA)

To find the ground-state energy of Hamiltonian (2.16) we minimize the potential (2.29) with respect to quantities d, n and m. This leads to the set of equations

$$\begin{cases} \sum_{\mathbf{k}\sigma}\frac{\partial q_\sigma}{\partial d} f(E^{GA}_{\mathbf{k}\sigma})\epsilon_{\mathbf{k}} &= -2\Lambda U d, \\ \sum_{\mathbf{k}\sigma}\frac{\partial q_\sigma}{\partial n} f(E^{GA}_{\mathbf{k}\sigma})\epsilon_{\mathbf{k}} &= 0, \\ \sum_{\mathbf{k}\sigma}\frac{\partial q_\sigma}{\partial m} f(E^{GA}_{\mathbf{k}\sigma})\epsilon_{\mathbf{k}} &= 0, \end{cases} \tag{2.31a}$$

where $f(E) \equiv 1/(1+e^{\beta E})$ is the Fermi-Dirac distribution. On the other hand, we also have, directly from their definition (2.24), the self-consistent equations for n and m

$$\begin{cases} \Lambda n = \sum_{\mathbf{k}\sigma} f(E^{GA}_{\mathbf{k}\sigma}), \\ \Lambda m = \sum_{\mathbf{k}\sigma} \sigma f(E^{GA}_{\mathbf{k}\sigma}), \end{cases} \tag{2.31b}$$

that produce constrains on the average value of the particle number and the magnetization operator per site, $\hat{n}$ and $\hat{m}$, respectively. At this point, it is essential to include in the minimization procedure the statistical consistency conditions of the solution. To do so, following Jędrak *et al.* [106], we employ the Lagrange multiplier method and define the new effective Hamiltonian

$$\mathcal{H}_{SGA} = \mathcal{H}_{GA} - \lambda_n(\hat{n}-n) - \lambda_m(\hat{m}-m), \tag{2.32}$$

where Lagrange multipliers λ_n and λ_m are the molecular fields, coupled respectively to the total charge and the spin polarization. In effect, we define the Landau grand potential functional in the form

$$\mathcal{F}^{SGA} = -\frac{1}{\beta}\sum_{\mathbf{k}\sigma}\log\left(1+e^{-\beta E^{SGA}_{\mathbf{k}\sigma}}\right) + \lambda\left(U d^2 + \lambda_n n + \lambda_m m\right), \tag{2.33}$$

where the quasiparticle energy is now

$$E^{SGA}_{\mathbf{k}\sigma} \equiv q_\sigma\epsilon_{\mathbf{k}} - \sigma(h+\lambda_m) - (\mu+\lambda_n). \tag{2.34}$$

To minimize (2.33) we need now to solve the modified set of self-consistent equations, namely

$$\begin{cases} \sum_{\mathbf{k}\sigma} \frac{\partial q_\sigma}{\partial d} f(E^{SGA}_{\mathbf{k}\sigma})\epsilon_{\mathbf{k}} & = -2\Lambda U d, \\ \sum_{\mathbf{k}\sigma} \frac{\partial q_\sigma}{\partial n} f(E^{SGA}_{\mathbf{k}\sigma})\epsilon_{\mathbf{k}} & = -\Lambda\lambda_n, \\ \sum_{\mathbf{k}\sigma} \frac{\partial q_\sigma}{\partial m} f(E^{SGA}_{\mathbf{k}\sigma})\epsilon_{\mathbf{k}} & = -\Lambda\lambda_m, \\ \sum_{\mathbf{k}\sigma} f(E^{SGA}_{\mathbf{k}\sigma}) & = \Lambda n, \\ \sum_{\mathbf{k}\sigma} \sigma f(E^{SGA}_{\mathbf{k}\sigma}) & = \Lambda m, \end{cases} \tag{2.35a}$$

where the $\mathbf{k}$ summation goes over the first Brillouin zone. Note that by enabling the Lagrange multipliers, we ensure the statistical consistency of the system. This is not the case for the standard set of equations (2.31). The consistency amounts to forcing the condition that the averages calculated with the help of the self-consistent equations (2.35) coincide with those obtained from a direct minimization of the Landau functional (2.33). This feature is a fundamental correction to GA and has been elaborated earlier in our group [106]. Here it will be applied to the interesting problem of Mott localization in hydrogeniclike systems. Parenthetically, only after including the statistical consistency conditions, our SGA results coincide with those obtained within the slave-boson approach in the saddle-point approximation.

Chapter 3

Published Papers with their summaries

In this chapter we present the published papers, constituting this Thesis, together with its brief summaries. The papers are in the chronological order.

3.1 Paper A-1 – Extended Hubbard model with renormalized Wannier wave functions in the correlated state III: Statistically consistent Gutzwiller approximation and the metallization of atomic solid hydrogen

In this paper we consider a 3-dimensional, atomic model of hydrogen. This is a semi-realistic approach to the problem of metallization, in the regime of atomic crystal, as we do not know the predictions of the atomic phase structure. Hence, we start our discussion with a model case of simple cubic (sc) lattice. For the first-principle system description, we employ the **E**xact **D**iagonalization – **Ab I**nitio Approach (EDABI) with the **S**tatistically-Consistent **G**utzwiller **A**pproximation (SGA) as the parametrized Hamiltonian diagonalization scheme. This is no longer an *exact* approach, nevertheless, it provides useful information about an infinite system. We describe the model with the so-called extended Hubbard model with the single-particle energy ϵ_a, the nearest neighbor hopping term t, the on-site Hubbard interaction U and the intersite Coulomb repulsion K_{ij}, where the microscopic parameters are obtained by integrating either single-particle Hamiltonian (for one-body parameters ϵ_a and t) or Coulomb potential (for two-body parameters U and K_{ij}), both with properly prepared single-particle basis wave functions. This is a problematic case to be treated by means of SGA, therefore we make two more approximations. First, we only consider the basis functions as linear combinations of atomic orbitals (LCAO [89]) up to the certain limit, that is we require the hopping terms to be only between orthogonal functions. Secondly, we

rearrange the Hamiltonian in a way, that intersite Coulomb interaction parameters K_{ij} and ion–ion repulsion renormalize the single-particle energy ϵ_a, leaving the remaining terms to be of negligible influence, when the ground-state energy is calculated, taking advantage of the one-electron-per-lattice-site scenario. Hamiltonian prepared in that way is now tractable with the SGA, thus exchanging the problem of diagonalization the Hamiltonian to the minimization of corresponding Landau functional.

We calculated the ground-state and all its components for varying lattice parameter (interatomic distance) $R \in [3.25, 8]$ and magnetic field H_a, and observed the first order transition at $R_C = 4.1a_0$ (Fig. 1), where the average double occupancy $d^2 = \left\langle \hat{n}_{i\uparrow}\hat{n}_{i\downarrow} \right\rangle$ drops discontinuously to zero with the increasing lattice parameter R (Fig. 2) indicating a metal $\rightarrow$insulator transition. This claim can be backed up by the divergence of magnetic susceptibility (Fig. 5) and the disappearance of Hubbard gap $E_{gap} = U - W$ (Fig. 11), where U is the Hubbard repulsion and $W = 12|t|$ is the bandwidth. We obtain the microscopic parameters of the Hamiltonian (Fig. 3) in the correlated state (cf. the renormalized inverse wave-function size α (Fig. 9)), as well as the Landau functional minimization parameters, the most interesting being magnetization m (Fig. 6) and the molecular field λ_m coupled with m (Fig. 4). For the sake of completeness we supply critical scaling of the ground-state energy (Fig. 7) and of the inverse wave-function size (Fig. 8).

As an extra result, we assessed the critical pressure to stabilize metallic phase and have found it to be $\sim 100GPa$ (Fig. 12). As we disregarded the molecular phases, this paper can be treated only as an first estimate, as there can still be a stable, lower-energy molecular structure. Nevertheless, even in the model case of simple cubic lattice, the metallization under pressure can be obtained.

The paper was published in European Physical Journal B (Eur. Phys. J. B **86**, 252 (2013)), pp. 1–9.

Eur. Phys. J. B (2013) 86: 252
DOI: 10.1140/epjb/e2013-40127-y

THE EUROPEAN PHYSICAL JOURNAL B

Regular Article

Extended Hubbard model with renormalized Wannier wave functions in the correlated state III

Statistically consistent Gutzwiller approximation and the metallization of atomic solid hydrogen

Andrzej P. Kądzielawa[1], Jozef Spałek[1,2,a], Jan Kurzyk[3], and Wlodzimierz Wójcik[3]

[1] Marian Smoluchowski Institute of Physics, Jagiellonian University, ul. Reymonta 4, 30-059 Kraków, Poland
[2] Faculty of Physics and Applied Computer Science, AGH University of Science and Technology, ul. Reymonta 19, 30-059 Kraków, Poland
[3] Institute of Physics, Kraków University of Technology, Podchorążych 1, 30-084 Kraków, Poland

Received 14 February 2013 / Received in final form 15 April 2013
Published online 6 June 2013 –

Abstract. We extend our previous approach [J. Kurzyk, W. Wójcik, J. Spalek, Eur. Phys. J. B **66**, 385 (2008); J. Spałek, J. Kurzyk, R. Podsiadły, W. Wójcik, Eur. Phys. J. B **74**, 63 (2010)] to modeling correlated electronic states and the metal-insulator transition by applying the so-called *statistically consistent Gutzwiller approximation* (SGA) to carry out self-consistent calculations of the renormalized single-particle Wannier functions in the correlated state. The transition to the Mott-Hubbard insulating state at temperature $T = 0$ is of weak first order even if antiferromagnetism is disregarded. The magnitude of the introduced self-consistent magnetic correlation field is calculated and shown to lead to a small magnetic moment in the magnetically uniform state. Realistic value of the applied magnetic field has a minor influence on the metallic-state characteristics near the Mott-Hubbard localization threshold. The whole analysis has been carried out for an extended Hubbard model on a simple cubic (SC) lattice and the evolution of physical properties is analyzed as a function of the lattice parameter for the renormalized $1s$-type Wannier functions. Quantum critical scaling of the selected physical properties is analyzed as a function of the lattice constant $R \to R_c = 4.1a_0$, where R_c is the critical value for metal-insulator transition and $a_0 = 0.53$ Å is the Bohr radius. A critical pressure for metallization of solid atomic hydrogen is estimated and is $\sim 10^2$ GPa.

1 Motivation

One of the important quantum-mechanical problems in both the solid-state [1–4] and the optical-lattice [5] systems is the localization-delocalization transitions of fermionic states which is called *the Mott* or *Mott-Hubbard transition*. In electron systems it corresponds to the delocalization of atomic states (usually of $3d$ or $4f$ type) and the formation of a Fermi liquid of heavy quasiparticles composed mainly of the transforming electrons, irrespectively of the fact that there may be other valence electrons present also there [4]. In the extreme version, the transition is driven solely by the interparticle interaction, in which the presence of lattice plays only a secondary role. In that situation, the localization-delocalization transition is called *the Wigner transition* [6,7]. The description of these two transitions minimally provides a bridge between the atomic physics with the localized single-particle electron states and the theory of fermionic quantum liquids with delocalized states, for which (quasi)momentum $\boldsymbol{p} = \hbar\boldsymbol{k}$ characterizes quasiparticle states. A principal dynamic quantity driving the transition is the particle density (or interatomic distance for fixed number of particles, as is the case here).

A second impetus to the physics of these phenomena has been provided by the introduction by Anderson [8,9] and Hubbard [10] of second-quantization or quantum-particle language, with the help of which the revised *Mott-Hubbard transition* can be analyzed in terms of microscopic parameters. In the simplest, half-filled single-band model the relevant microscopic parameter is the ratio U/W, where U is the magnitude of the intraatomic (Hubbard) interaction and $W = 2z|t|$ is the bare bandwidth (i.e., that for the uncorrelated particles), with z being the coordination number (i.e., the number of nearest neighbors) and $|t|$ is the magnitude of intersite transfer (hopping) of individual fermions. It is amazing that a similar type of approach can be formulated for both fermions and the bosons, in the latter situation in the optical-lattice situation [2,3].

[a] e-mail: ufspalek@if.uj.edu.pl

The principal question is how to combine the Mott [1] and the Hubbard [11] aspects of this quantum phase transition in a purely electronic system. Once achieved, the whole description can be analyzed as a function of the lattice parameter (or interatomic distance, R). In the series of papers [12,13] we have formulated such an approach starting from the Gutzwiller-ansatz approximation (GA) for the extended Hubbard model, with a simultaneous readjustment of the single-particle Wannier functions in the correlated state. The method provides, among others, a direct connection of the Mott criterion for localization/delocalization ($n_C^{1/3} a_B \approx 0.2$) with that of Hubbard ($U \approx W$). As an extra bonus coming from such a formulation we obtain the quantum-critical behavior of single-particle wave function size α^{-1} [13], as well as the detailed evolution of the correlated metallic state into the Mott-Hubbard insulator. One principal methodological advantage of the present formulation is that, in distinction to the LDA + U [14,15] or LDA + DMFT [16,17] approaches our formulation avoids the problem of double counting of electron-electron interaction. However, unlike LDA + U or LDA + DMFT methods, the present approach is still on the stage of modeling only the simplest (one-band) systems. Nonetheless, it may provide a formally proper starting point for more complex situations such as many-band systems. Our formulations can certainly be also reformulated for Bose-Hubbard optical-lattice systems. It is unique in the sense of discussing of quantum critical behavior of single-particle wave function characteristics such as the inverse wave function size (the inverse effective Bohr radius).

As a concrete application of our results we calculate the critical pressure for the metallization of solid atomic hydrogen with the electronic correlations included within our renormalized mean-field theory.

The structure of the paper is as follows. In Section 2 we characterize briefly the method used in the paper and the modification of our previous approach [12,13]. In Section 3 we analyze in detail the numerical results obtained with the help of the so-called *Statistically Consistent Gutzwiller Approximation* (SGA). As a physical application, we also provide there the estimate of the critical pressure for the solid atomic hydrogen metallization. Section 4 contains an outlook with summary of main results and a brief discussion of possible extensions.

2 Model and method applied

2.1 Starting Hamiltonian

We start with the Extended Hubbard Hamiltonian for $1s$ hydrogenic-like system

$$\mathcal{H} = \epsilon_a \sum_i n_i + \sum_{i \neq j,\sigma} t_{ij} a^\dagger_{i\sigma} a_{j\sigma} + U \sum_i n_{i\uparrow} n_{i\downarrow} + \sum_{i<j} K_{ij} n_i n_j + \sum_{i<j} V_{ion\text{-}ion}\left(\boldsymbol{r}_j - \boldsymbol{r}_i\right), \quad (1)$$

where t_{ij} is the hopping integral, U the intraatomic interaction magnitude, ϵ_a the atomic energy per site, and $V_{ion\text{-}ion}$ corresponds to classical Coulomb interaction between two H^+ ions, equal (in atomic units) to

$$V_{ion\text{-}ion}\left(\boldsymbol{r}_j - \boldsymbol{r}_i\right) = \frac{2}{|\boldsymbol{r}_j - \boldsymbol{r}_i|}. \quad (2)$$

By following [18], we introduce $N_e = \sum_i n_i$ – the total number of electrons, and $\delta n_i = n_i - 1$ as the deviation from neutral-atom configuration. We can now rearrange the interatomic interaction in the following manner:

$$\begin{aligned}\sum_{i<j} K_{ij} n_i n_j &= \sum_{i<j} K_{ij}(n_i - 1)(n_j - 1) \\ &\quad - \sum_{i<j} K_{ij} + 2N_e \frac{1}{N} \sum_{i<j} K_{ij} \\ &= \sum_{i<j} K_{ij} \delta n_i \delta n_j + N_e \frac{1}{N} \sum_{i<j} K_{ij} \\ &\quad + (N_e - N) \frac{1}{N} \sum_{i<j} K_{ij}. \end{aligned} \quad (3)$$

By introducing now *effective* atomic energy per site, i.e., containing both the atomic binding part ϵ_a and the ion-ion repulsion, we can write it down in the form

$$\epsilon_a^{eff} = \epsilon_a + \frac{1}{N} \sum_{i<j} \left(K_{ij} + \frac{2}{R_{ij}} \right), \quad (4)$$

where $R_{ij} \equiv |\boldsymbol{r}_j - \boldsymbol{r}_i|$. In effect, we can rewrite Hamiltonian (1) in the following manner:

$$\mathcal{H} = \epsilon_a^{eff} \sum_i n_i + \sum_{i \neq j,\sigma} t_{ij} a^\dagger_{i\sigma} a_{j\sigma} + U \sum_i n_{i\uparrow} n_{i\downarrow} + \frac{1}{2} \sum_{i \neq j} K_{ij} \delta n_i \delta n_j. \quad (5)$$

We also add $(-\sum_{i,\sigma} \sigma \frac{1}{2} g \mu_B H_a n_{i\sigma})$ – a simple magnetic Zeeman term, where g is the Landé factor, μ_B the Bohr magneton and H_a the external magnetic field. By introducing the reduced magnetic field $h \equiv \frac{1}{2} g \mu_B H_a$, we obtain our starting Hamiltonian

$$\mathcal{H} = \epsilon_a^{eff} \sum_i n_i + \sum_{i \neq j,\sigma} t_{ij} a^\dagger_{i\sigma} a_{j\sigma} + U \sum_i n_{i\uparrow} n_{i\downarrow} + \frac{1}{2} \sum_{i \neq j} K_{ij} \delta n_i \delta n_j - h \sum_{i,\sigma} \sigma n_{i\sigma}. \quad (6)$$

This lattice Hamiltonian describing the system of $1s$-type states in a solid contains the following microscopic parameters: t_{ij}, U, K_{ij} and the band filling n. Additionally, close to the metal-insulator boundary we can assume that $\langle \delta n_i \delta n_j \rangle \simeq 0$.

2.2 Incorporation of single-particle wave function optimization

The microscopic parameters of (6) can be expressed via the single-particle Wannier functions in the following manner:

$$\begin{aligned} t_{ij} &= \langle w_i | H_1 | w_j \rangle , \\ U &= \left\langle w_i w_i \left| \frac{e^2}{|\boldsymbol{r}_1 - \boldsymbol{r}_2|} \right| w_i w_i \right\rangle , \\ K_{ij} &= \left\langle w_i w_j \left| \frac{e^2}{|\boldsymbol{r}_1 - \boldsymbol{r}_2|} \right| w_i w_j \right\rangle , \\ \epsilon_a &= \langle w_i | H_1 | w_i \rangle , \end{aligned} \tag{7}$$

where H_1 is the Hamiltonian for a single particle in the system, and $e^2/|\boldsymbol{r}_1 - \boldsymbol{r}_2|$ is interparticle interaction. The numerical value is obtained by approximating first the Wannier functions $w_i \equiv w_i(\boldsymbol{r}) = w_i(\boldsymbol{r} - \boldsymbol{R}_i)$ by $1s$ Slater orbitals and those, in turn, by series of the Gaussian functions, i.e.,

$$\begin{aligned} w_i(\boldsymbol{r}) &= \beta \Psi_i(\boldsymbol{r}) - \gamma \sum_{j=1}^{z} \Psi_j(\boldsymbol{r}) , \\ \Psi_i(\boldsymbol{r}) &= \sqrt{\frac{\alpha^3}{\pi}} e^{-\alpha |\boldsymbol{r} - \boldsymbol{R}_i|} \\ &\approx \alpha^{\frac{3}{2}} \sum_{a=1}^{p} B_a \left(\frac{2\Gamma_a^2}{\pi} \right)^{\frac{3}{4}} e^{-\Gamma_a^2 |\boldsymbol{r} - \boldsymbol{R}_i|^2} , \end{aligned} \tag{8}$$

where the parameters β and γ are defined through equations (24) and (25) in part I [12] to make the basis normalized and orthogonal, i.e., $\langle w_i | w_{j(i)} \rangle = 0$. Parameters B_a and Γ_a are derived by minimizing energy of single atom (Hamiltonian $\mathcal{H} \overset{a.u.}{=} -\nabla^2 - 2|\boldsymbol{r} - \boldsymbol{R}_i|^{-1}$). p is the number of Gaussian functions used. Parameter α is found by minimizing the system energy of the trial correlated state (see below). The difference with our previous approach [13] is that we include the statistical consistency conditions, as discussed next.

2.3 Statistically-consistent Gutzwiller approximation (SGA)

To obtain optimal value of the inverse size α given intraatomic distance R we have to obtain the system energy. It was shown [19] that the Gutzwiller approximation (GA) does not always provide the variational results consistent with those obtained from the corresponding self-consistent equations. To assure this consistency we minimize the GA free-energy functional $\mathcal{F}$ supplemented with two additional molecular fields λ_m and λ_n, coupled with m and n, respectively:

$$\begin{aligned} \mathcal{F}^{(SGA)} = &-\frac{1}{\beta} \sum_{\boldsymbol{k}\sigma} \log \left(1 + e^{-\beta E_{\boldsymbol{k}\sigma}^{(SGA)}} \right) \\ &+ \Lambda \left(\lambda_n n + \lambda_m m + U d^2 + \mu n \right) , \end{aligned} \tag{9}$$

where the trial eigenvalues $E_{\boldsymbol{k}\sigma}^{(SGA)}$ are:

$$\begin{aligned} E_{\boldsymbol{k}\sigma}^{(SGA)} &\equiv E_{\boldsymbol{k}\sigma} - \sigma\lambda_m - \lambda_n \\ &= q_\sigma \epsilon_{\boldsymbol{k}} - \sigma (h + \lambda_m) - (\mu + \lambda_n) , \end{aligned} \tag{10}$$

where $d^2 = \langle n_{i\uparrow} n_{i\downarrow} \rangle$, and

$$\begin{aligned} q_\sigma = \Big(&\sqrt{(n_\sigma - d^2)(1 - n_\sigma - n_{\overline{\sigma}} + d^2)} \\ &+ d\sqrt{n_{\overline{\sigma}} - d^2} \Big)^2 / n_\sigma (1 - n_\sigma) \end{aligned} \tag{11}$$

is the band narrowing renormalization factor and $\epsilon_{\boldsymbol{k}}$ is dispersion relation for bare particles (here taken for simple cubic structure, $\epsilon_{\boldsymbol{k}} = 2t(\cos k_x + \cos k_y + \cos k_z)$). The eigenvalues $E_{\boldsymbol{k}\sigma}$ are obtained by Fourier transform of the effective GA Hamiltonian

$$\begin{aligned} \mathcal{H} = &\epsilon_a^{eff} \sum_{i\sigma} n_{i\sigma} + \sum_{ij\sigma} t_{ij} q_\sigma a_{i\sigma}^\dagger a_{j\sigma} \\ &+ \Lambda U d^2 - \mu \sum_{i\sigma} n_{i\sigma} , \end{aligned} \tag{12}$$

additionally supplemented with the Lagrange-multiplier constrains

$$-\lambda_m \sum_i (m_i - m) - \lambda_n \sum_i (n_i - n) , \tag{13}$$

where $m_i \equiv n_{i\uparrow} - n_{i\downarrow}$, $m \equiv \langle m_i \rangle$, $n_i \equiv n_{i\uparrow} + n_{i\downarrow}$, and $n \equiv \langle n_i \rangle$.

The operator $\mathcal{K} \equiv \mathcal{H} - \sum_i (\lambda_m m_i + \lambda_n n_i) + \Lambda(\lambda_m m + \lambda_n n)$ plays the role of the effective Hamiltonian, in which the mean fields (m, d^2) and the Lagrange multipliers (λ_m, λ_n), as well as μ, are all determined variationally, in addition to the wave function parameter α. In the next section we analyze in detail the physical results obtained by minimizing though that procedure the functional (9).

2.4 Overview of numerical methods

Numerical analysis was carried out with the help of method different from that used in references [12,13] by introducing the lower-level minimization for each single-particle basis optimization step. In other words – for each and every step of minimizing energy with respect to the reverse function size α, where *Golden Section Search* [20] was empirically proven to be the most efficient, there is introduced a new minimization of functional $\mathcal{F}^{(SGA)}$ with respect to the double occupancy d, the magnetization m, the chemical potential μ and the molecular fields λ_m and λ_n. The latter procedure was carried using *GSL - GNU Scientific Library*[1], with the order of magnitude of zero-precision 10^{-8} and all the following up calculations with the double precision.

Due to new minimization step and new parameter (external magnetic field H_a), the numerical complexity increases by two orders of magnitude, and it enforces new

[1] http://www.gnu.org/software/gsl/

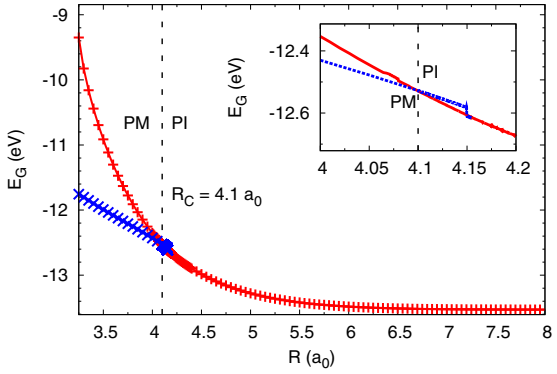

Fig. 1. Ground state energy (per atom) of the metallic state $(PM, \times)$ for $R < R_c$ and the insulating $(PI, +)$ for $R \geqslant R_c$, as a function of interatomic distance R (in units of Bohr radius a_0). Inset: detailed representation of the first-order $PM \to PI$ transition near $R = R_c \approx 4.1a_0$. The upper curve for $R < R_c$ represents the energy of the unstable PI state. Note that as $E_G > -1$ Ry, the lattice can only be stabilized by the external pressure (see Sect. 3.3).

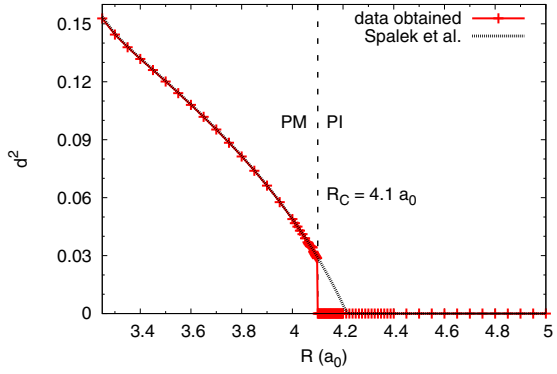

Fig. 2. Double occupancy probability $d^2 = \langle n_{i\uparrow} n_{i\downarrow} \rangle$ versus R. Note a weak discontinuous jump to zero at $R = R_c \approx 4.1a_0$, as compared to the continuous evolution for $PM \to PI$ of the Gutzwiller approximation obtained previously [12,13].

optimization. To decrease the computing time we chose the basis of three Gaussians ($p = 3$ in (8)) instead of seven (as in Refs. [12,13]). After comparing the results for constant external magnetic field H_a for $p = 3$ and $p = 7$ we observe no qualitative change of behavior. Below we discuss the basic physical properties obtained within SGA and just discussed numerical procedure, as well as compare them with those obtained previously without the statistical consistency [12,13].

3 Results and discussion

3.1 Ground-state properties

The calculated ground state energy E_G as a function of interatomic distance R (lattice parameter) is shown in Figure 1. In the inset a detailed dependence of E_G in the transition regime $R \approx R_c = 4.1a_0$ is displayed. For the sake of comparison, the energy of PI state (for $H_a = 0$) has been also shown for $R < R_c$, where this phase is not stable. The principal difference with our previous Gutzwiller ansatz (GA) results is that in the present (SGA) approach the transition is weakly discontinuous, as one can see explicitly from the circumstance that dE_G/dR, which is proportional to the internal pressure, is discontinuous.

In Figure 2 we plot the double occupancy probability $d^2 = \langle n_{i\uparrow} n_{i\downarrow} \rangle$ versus R and again see a weak discontinuity at $R = R_c$. The present SGA results are compared with the previous GA results of Spałek et al. [13].

The R-dependent evolution of the microscopic parameters are shown in Figures 3 and 4. In Figure 3 we plot the values of U and the nearest-neighbor hopping magnitude $|t|$, whereas in the inset the U/W ratio, with $W = 2z|t|$ being the bare bandwidth, is shown in the regime $R \approx R_c$. Note that at $R_c = 4.1a_0$ the U/W is

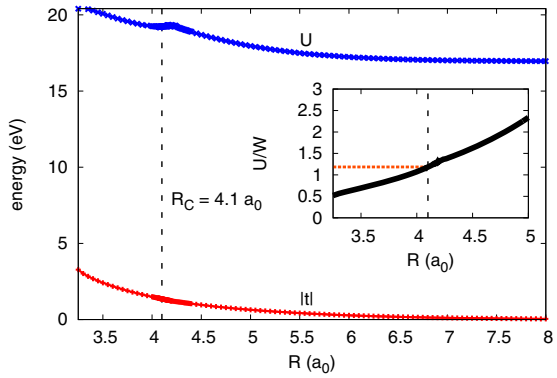

Fig. 3. Microscopic parameters: hopping integral $|t|$ and the Hubbard interaction parameter U, both as a function of R. Inset: U/W ratio vs. R. The U/W ratio for $R = R_c$ is $(U/W)_C \simeq 1.18$. The vertical dashed line marks the $PM \to PI$ transition point. In the large-R limit U reaches the atomic value $U_{at} = (5/4)$ Ry.

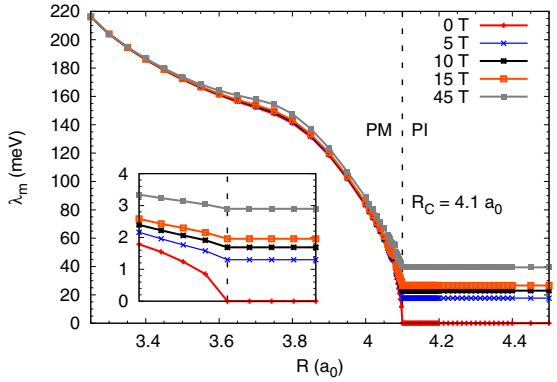

Fig. 4. Correlation-induced effective magnetic field λ_m vs. R for selected values of applied magnetic field H_a. For $H_a = 0$, λ_m vanishes at $PM - PI$ boundary (see inset for details). The presence of the applied field triggers $\lambda_m \neq 0$ in the insulating state.

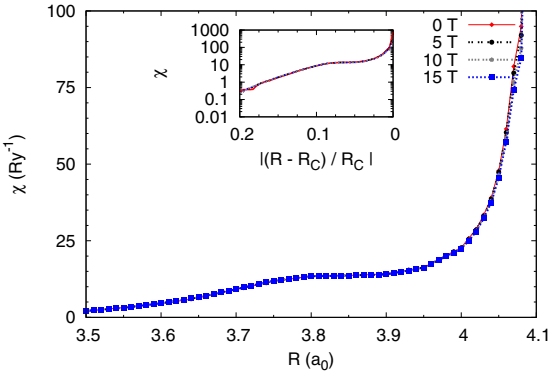

Fig. 5. Differential static magnetic susceptibility vs. R for selected values of the applied magnetic field. The χ divergence at $R_c = 4.1a_0$ accompanies the $PM-PI$ transition and is associated with localization of the itinerant electrons when $R \to R_c$. Overall χ behavior in the metallic state does not depend much on the value of H_a. Inset: double logarithmic plot $\chi(R)$ showing absence of any simple exponential type of scaling.

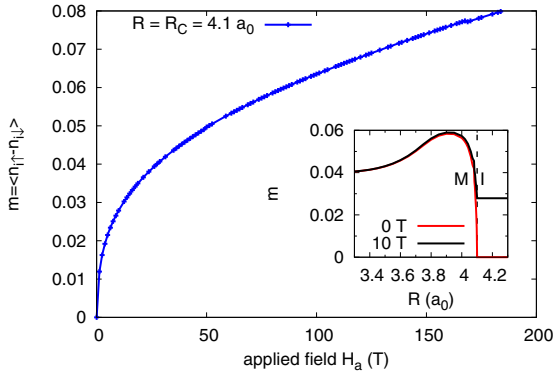

Fig. 6. Magnetic moment $m = \langle n_{i\uparrow} - n_{i\downarrow} \rangle$ as a function of the applied magnetic field at the critical interatomic distance $R_c = 4.1a_0$. Inset: a residual uniform moment in the metallic state vs. R near R_c, induced by the correlation field when it is assumed as spatially uniform.

of the order of unity, in accordance with the results obtained when U/W is treated as a free parameter [11]. The atomic limit is reached effectively when $|t| \approx 0$, i.e. for $R \sim 6.5a_0$. The value of U in that limit is $U = (5/4)$ Ry. Amazingly, one should also note that at the transition $R_c^{-1}\alpha^{-1} = n_c^{1/3}a_B \sim 0.25$, in accordance with the original criterion due to Mott [2,3] for the Mott localization ($n_C = 1/R_c^3$ is the particle density at $R = R_c$ and $a_B = \alpha^{-1}$ in the effective Bohr radius at that point). This approach does allow to relate directly the Mott and the Hubbard criteria for localization of fermions. This was achieved by readjusting the Wannier functions, determining t and U parameters in the correlated state.

In Figure 4 we exhibit the evolution of the consistency field λ_m, which plays the role of the self-consistent (correlation) field, also for selected nonzero applied magnetic field. One should note that the lowermost curve corresponds to the case with $H_a = 0$. The nonzero value of the effective field in the metallic phase will introduce a small but nonzero value of the spin magnetic moment in the uniform (weakly magnetic) phase as discussed below. The situation is highlighted in the inset to this figure. However, one should emphasize that the field λ_m is dependent on the phase discussed and in the antiferromagnetic state it takes the form of a staggered field [21]. The latter phase will not be analyzed in detail here, as the first and the foremost aim of this paper is to underline the first-order nature of the $M \to I$ transition if the statistical consistency conditions are properly taken into account, as well as the quantum scaling of the single-particle atomic wave function inverse size α^{-1}. The corresponding behavior of the renormalized but less pronounced (cf. [13]), so we will not discuss it in detail here.

To visualize directly the type of magnetism accompanying the metal-insulator transition (MIT), we have plotted in Figure 5 the zero-field magnetic susceptibility versus R (the inset illustrates an overall behavior). The principal feature of χ quasi-divergence for $R \to R_c$ is roughly independent of the applied field magnitude specified. It does not follow exactly the Brinkman-Rice dependence [22] as here the unrenormalized (χ_0) value is strongly R dependent as well, so χ cannot be parametrized by U/W ratio only. For the sake of completeness we plot in Figure 6 the magnetization curve at the localization threshold. The dependence roughly emulates the Brillouin curve for the localized particles of spin 1/2. However, one has to take into account a nonlinear increase of the molecular field for nonzero H_a value. (cf. Fig. 4). In the inset to this figure we provide the uniform magnetic-moment magnitude as a function of R if a uniform $\lambda_m \neq 0$ is assumed. In the metallic state the spontaneous value of spin polarization is very small and practically field independent.

For the sake of completeness, we also provide in Table 1 the numerical values of the selected quantities vs. R. Note that we compared the values of E_G in SGA and GA. The slightly higher values of E_G obtained in the present (SGA) case should not be surprising for R away from R_c. It is rewarding that they are lower as R_c is approaching, since then the results are more realistic, i.e. the tight-binding approximation works better. The last column describes the effective mass enhancement ($q_\sigma^{-1} = \frac{m*}{m_B}$) due to the interparticle correlations. One should note that the bare band value m_B is also dependent on R. Additionally, for the half-filled band case (and only then) the mass enhancement is not explicitly spin-direction ($\sigma = \pm 1$) dependent. The scaling with R of the selected just discussed quantities is carried out next.

3.2 Scaling laws of physical parameters

The question arises whether the scaling properties proposed earlier [13] of selected physical quantities near the quantum critical point (located at $R = R_c$), where χ is divergent, take place also within the present SGA approach. To address this question, we have plotted in Figure 7 the relative ground state energy per site

Table 1. Computed quantities in SGA (except additional results for ground-state energy added, calculated in GA), all as a function of the lattice parameter, for the simple cubic structure. For their definition, see main text. The values, if not specified explicitly, are in rydbergs (Ry). The $\chi(0)$ value for $R \geqslant R_c$ is infinite.

$R(a_0)$	E_G^{SGA}	E_G^{GA}	t	U	$\alpha^{-1}(a_0)$	d^2	λ_m	$\chi\,(\mathrm{Ry}^{-1})$	q^{-1}
3.25	−0.8640	−0.8644	−0.2409	1.4996	0.9474	0.152774	0.015884	0.1809	1.17728
3.50	−0.8814	−0.8816	−0.1773	1.4749	0.9220	0.120128	0.012641	2.0598	1.36818
4.00	−0.9136	−0.9136	−0.1098	1.4152	0.9200	0.048886	0.006084	22.6577	2.82781
4.05	−0.9171	−0.9171	−0.1046	1.4139	0.9175	0.038973	0.004256	47.3562	3.47235
4.09	−0.9200		−0.1005	1.4140	0.9147	0.030193	0.027281	253.7567	4.40375
4.10	−0.9209	−0.9207	−0.0995	1.4143	0.9138	0.000000	0.000000	∞	∞
4.20	−0.9315	−0.9288	−0.0896	1.4217	0.9021	0.000000	0.000000		
4.50	−0.9544	−0.9517	−0.0705	1.3742	0.9263	0.000000	0.000000		
5.00	−0.9760	−0.9732	−0.0471	1.3200	0.9556	0.000000	0.000000		
7.00	−0.9939		−0.0082	1.2504	0.9972	0.000000	0.000000		
∞	−1.0000	−1.0000	0.0000	1.2500	1.0000	0.000000	0.000000		

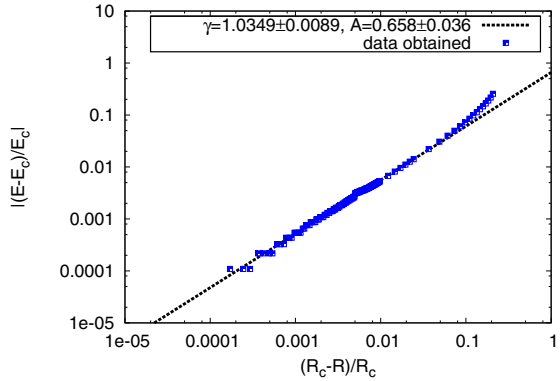

Fig. 7. Scaling of the relative ground state energy near $R = R_c$. For detailed explanation see main text.

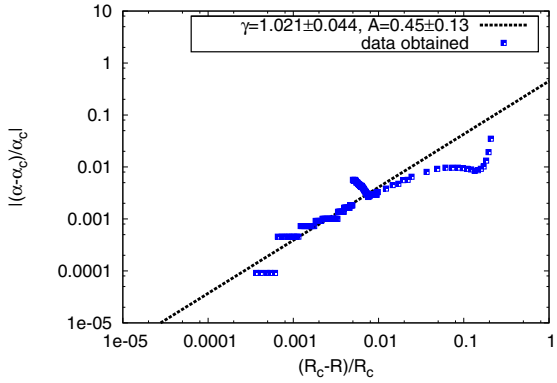

Fig. 8. Scaling of the inverse orbital size α near $R = R_c$. For detailed explanation see main text.

$|(E_G(R)-E_G(R_c))/E_G(R_c)| \equiv |(E-E_C)/E_C|$ vs. relative interatomic distance $(R_c - R)/R_c$ for $R \to R_c - 0$. As before, we observe an almost linear scaling $|(E-E_C)/E_C| = A((R_c - R)/R_c)^\gamma$, since $\gamma = 1.035 \pm 0.009$ and additionally, $A = 0.66 \pm 0.04$. One should note that this type of scaling for the ground state energy near QCP is very different from the corresponding behavior in the atomic limit $R \gg R_c$, where the corresponding energy per site is roughly dominated by the Coulomb contribution, so $E_G \sim R^{-1}$. This type of scaling means that the first derivative is nonzero and constant for $R \to R_c$. This feature will be taken upon and interpreted in Section 3.3.

In Figure 8 we plot the relative inverse renormalized atomic-orbital size $|(\alpha(R) - \alpha(R_c))/\alpha(R_c)| \equiv |(\alpha - \alpha_c)/\alpha_c|$ vs. $(R_c - R)/R_c$. Again, we have an almost linear scaling, though the behavior is not as regular as before [13]. It is thus more legible to display the actual behavior of the renormalized orbital size $\alpha(R)$ vs. R, as shown in Figure 9. The quantum critical behavior corresponds to the cusp-like feature around R_c, where we observe a clear discontinuity of $d\alpha/dR$ at $R = R_c$. The most important feature of this figure is the fact that we observe this type of quantum critical behavior for the renormalized inverse size of the single-particle wave function. We are not aware of any other result of that type appearing in the literature, apart from the analogical result obtained by us earlier within the GA [13]. Note also, as already said earlier, this type of critical behavior will translate into the same type of behavior for the renormalized Wannier functions. It is important to emphasize that this quantum critical behavior of the principal characteristic (α) of the renormalized wave function is independent of the fact whether the actual two-particle characteristic – d^2 vanishes continuously (as in GA) or discontinuously (as in SGA), as well as whether the states are paramagnetic (PM, PI) or have a small "parasitic" magnetic moment. This analysis should certainly be extended and carried out for the antiferromagnetic (AFM, AFI) cases, but that requires a separate treatment, as it will certain a large number of additional variational parameters. This is certainly planned as the next stage of work.

Finally, we would like to discuss at this point two important physical characteristics of our correlated single narrow-band system. First of them is exhibited in Figure 10 and shows the effective mass enhancement q_σ^{-1} vs. H_a for selected values of R close to R_c, but on the metallic side. We observe the two important features. First, the quasiparticle mass is spin-independent in this half-filled band case, unlike in the non-half-filled case [23,24]. Also, the mass enhancement due to the

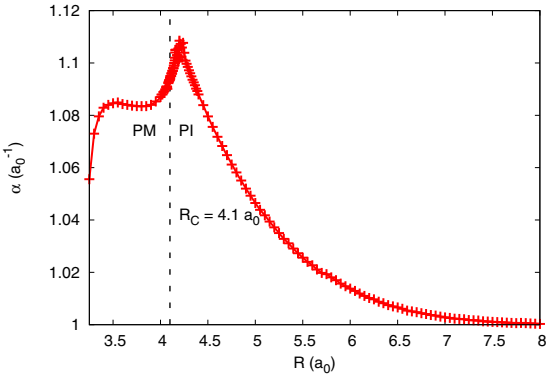

Fig. 9. Inverse atomic-orbital size vs. R. The critical behavior near $R = R_c = 4.1a_0$. The dependence is practically independent of the applied field. Note that the cusp has its maximum slightly above R_c.

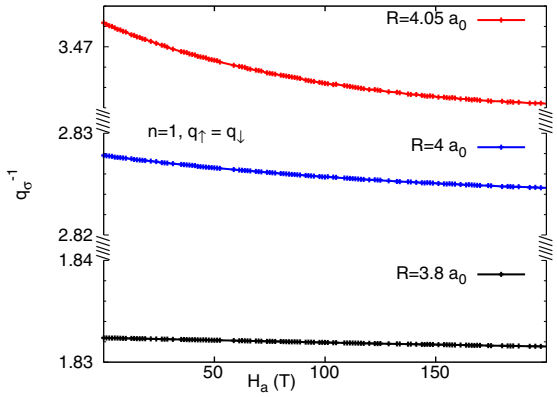

Fig. 10. Effective mass enhancement as a function of magnetic field for the situation with one electron per atom. In this case it is spin direction independent and dependent only on the interatomic distance. Note that this enhancement does not include the change of the bare mass which increases also with increasing R.

correlations increases in SGA relatively slowly compared to that in the parametrized GA approach [25] as $R \to R_c - 0$. Second, this slow increase of q^{-1} when confronted with the rather fast dependence of the susceptibility (cf. Fig. 5, Tab. 1) means that the magnetic contribution to the renormalized susceptibility (corresponding to the "renormalized Stoner part", cf. [22,25]) has an essential contribution to the susceptibility. Also, as mentioned earlier, there may be an essential contribution due to the bare bandwidth W narrowing with the increasing R. In effect, the resultant behavior of quantities such as χ or the linear specific-heat coefficient $\gamma = \gamma_0 q^{-1}$ in the strong-correlation limit (here $U \approx W$) is much more subtle than it was discussed within the pure parametrized model (GA) picture, where the renormalization of the Wannier functions, as well as the correlation fields λ_m and λ_n, are absent. Simply put, our approach goes beyond the parametrized-model approach as it provides the correlated system evolution as a function of experimentally accessible parameter – the lattice parameter.

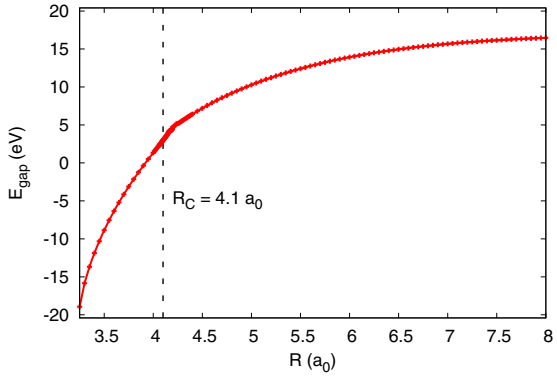

Fig. 11. Hubbard gap evolution $E_{gap} = U - W$ as a function of interatomic distance. Note a continuous dependence near R_c even though the transition is weakly discontinuous (cf. Figs. 1, 2). As the gap is increasing rapidly with increasing R ($R > R_c$), the Mott insulators for $R > 4.5a_0$ cannot be regarded as wide-gap semiconductors.

Finally, in Figure 11 we plot the value of the Mott-Hubbard gap $E_{gap} = U - W$ versus R. Obviously, in the metallic phase it does not appear (for the sake of completeness, we show it as having a negative value). Above the transition it reaches relatively fast with increasing $R > R_c$ the asymptotic value $E_{gap} \sim U$. A weak cusp-like behavior should be noted just above $R = R_c$. This feature is reminiscent of the cusp-like behavior of the renormalized Wannier functions. It would be interesting to study the pressure dependence of the gap for the Mott insulator located just above the transition point and determine its scaling with $(R - R_c)/R_c$. It does not scale linearly, as the quantities earlier.

3.3 Supplement: Application to solid atomic hydrogen: estimate of the critical pressure for metallization

Our formulation represents a fully microscopic model of the solid atomic hydrogen undergoing a Mott insulator-metal transition. This model differs from the standard treatment [26], in which the phase diagram is treated as a function of microscopic parameter U/W, since we include here a fully self-consistent procedure of evaluating the renormalized-by-correlations wave functions. In effect, we can calculate explicitly the critical pressure for metallization. In this approach the external pressure is the factor stabilizing the system in a particular phase (M or I). This task can be carried out by using the classical definition of pressure p as the force F, applied to make the present atomic solid stable, over the area A. This force is obtained by differentiating $F = |-\nabla_R E_G|$. The corresponding external pressure we have to exert on the system in order to stabilize the crystal as a function of interatomic distance (with energy E_G per site and the elementary cell area $A/N = R^2$) is plotted in Figure 12. Note that the physical meaning has the critical pressure for metallization as the point $R = R_c$ is the terminal point of stability of *the almost localized Fermi liquid*. It differs from other results [27] as those results concern a molecular (H_2) solid;

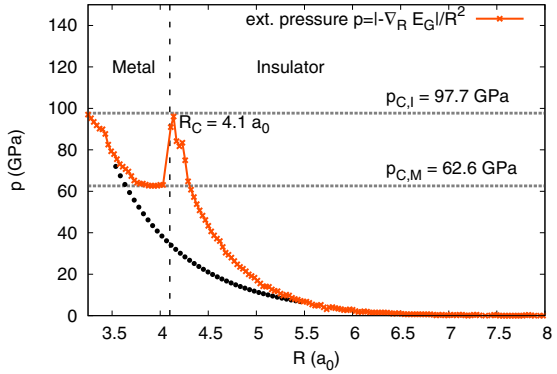

Fig. 12. External pressure (in GPa $= 10^9$ Pa) one has to exert in order to stabilize the crystal vs. interatomic distance (with cell area $A/N = R^2$). Note two critical values of pressure: $p_{C,I} = 97.7$ GPa required in the insulating state and $p_{C,M} = 62.6$ GPa in the metallic state. The lattice becomes very rigid as $R \to R_c$. The dotted line marks naive extrapolation $M \to I$.

for detailed comment see e.g. [28]. Note that the pressure behavior $p(R)$ for $R \to R_c$ traces the difference on the slopes dE/dR for metallic ($R < R_c$) and insulating ($R > R_c$) regimes. Roughly, it shows a critical (divergent) behavior at R_c. To determine that more accurately we require a refined numerical analysis. Nonetheless, the trend is clear and provides a promising starting point for a further analysis.

One must emphasize that this discussion is based on an implicit assumption that the positive ions (protons in this case) form a lattice in both the metallic (M) and insulating (I) states. This may turn only a rather crude approximation on the possible role of their zero-point motion in increasing the value of the critical pressure. Additionally, a possible transition to solid-liquid plasma as an alternative scenario, should certainly not be ruled out (for the relevant discussion of that point e.g. [29,30]).

4 Outlook

We have provided ground-state principal characteristics of the correlated narrow-band system involving first-principle variational calculations of the renormalized Wannier functions of 1s-type in the correlated state described by the statistically consistent Gutzwiller approximation (SGA). Our model is fully microscopic as it contains an explicit calculations of microscopic parameters of the extended Hubbard model. In this manner, we can track the correlated Fermi-liquid evolution with the increasing lattice parameter R into the Mott-Hubbard insulator. As an extra bonus, we obtain an estimate of the critical pressure for the metallization of solid atomic hydrogen which is roughly equal to 100 GPa. Obviously, the solid atomic hydrogen is a molecular crystal up to much higher pressures [26,27], but it may be possible that the states of this type can be synthesized in the optical-lattice experiments.

We would like to emphasize that our model calculations contain two attractive features from a general methodological point of view of the computational solid state physics. First, they do not include twice the Coulomb interactions among electrons, as it is the case for LDA + U or LDA + DMFT methods. Those latter methods have their own merits as they can be (and are) applied to complex real materials. But the correctness of the present approach is still worth mentioning, even when applied so far to the mode system only. Second, within the present approach the calculation of the renormalized characteristics of the single-particle wave function and of the interelectronic correlations, are both treated on the same footing. This is the crucial feature of the Mott-Hubbard systems, for which the single-particle energy (e.g. the renormalized band energy) is of the same magnitude as the interparticle (Coulomb in this case) interaction. The approach of the present type should be extended to the multiband situation to discuss the realistic strongly correlated materials (the magnetic oxides such as V_2O_3) evolving, when varying the lattice parameter (i.e., applying the pressure), and not only as a function of the microscopic parameters such as U/W, as they vary very rapidly in the vicinity of the Mott-Hubbard transition. However, this program execution may represent a long road ahead.

One has to mention that the present approach requires some other basic extensions. First of all, as any Gutzwiller-type approach, it does not include explicitly the intersite kinetic exchange appearing deeply in the Mott insulating state (for R substantially larger than R_c). The trace of this interaction is coded in the correlation fields λ_m, as has been shown in a related context before [21]. Second, the case with partial band filling ($n < 1$) should be also treated. Third and most importantly, the antiferromagnetic state should be included in the analysis. This is our plan for the near future. However, we believe that this simple analysis shows up in a clear manner the quantum critical behavior of the renormalized-by-correlations single-particle wave function, not obscured by the complicated magnetic structure (i.e., that with a staggered magnetic moment). Fourth and finally, the approach, even in the present single-band case, should be extended to the close packed lattices such as *fcc* and *hcp*, as this are the typical structures for metals. But then, one has to include at least first two hopping integrals (between the nearest and the next-nearest neighbors). Such treatment is certainly tractable. Nonetheless, we believe that our first estimate of the critical pressure for the metallization of solid atomic hydrogen, carried out for the *sc* structure, provides a promising starting point.

Finally, one can extend our analysis to nonzero temperatures in a straightforward manner, starting from the free-energy functional (9). This should be carried out separately and the results can be compared with GA results providing the first-order line ending in a classical critical point, as well as the reentrant metallic behavior [23,24,31,32].

Discussions with Jan Kaczmarczyk are greatly appreciated. The work was carried out partly within the Project TEAM awarded to our group by the Foundation for Polish Science (FNP) for the years 2011-2014 (APK and JS). We also

acknowledge partial support by the special Grant MAESTRO from the National Science Center (NCN) for the years 2012-2017.

References

1. N.F. Mott, Proc. Phys. Soc. Sect. A **62**, 416 (1949)
2. N.F. Mott, *Metal-Insulator Transitions*, 2nd edn. (Taylor and Francis, London, 1990)
3. F. Gebhard, *The Mott Metal-Insulator Transition* (Springer, Berlin, 1997)
4. M. Imada, A. Fujimori, Y. Tokura, Rev. Mod. Phys. **70**, 1039 (1998)
5. I. Bloch, in *Understanding Quantum Phase Transitions*, edited by L.D. Carr (CRC Press, Boca Raton, 2011), Chap. 19
6. E. Wigner, Trans. Faraday Soc. **34**, 29 (1938)
7. E. Wigner, Phys. Rev. **46**, 1002 (1934)
8. P.W. Anderson, Phys. Rev. **115**, 2 (1959)
9. P.W. Anderson, in *Solid State Physics*, edited by F. Seitz, D. Turnbull (Academic Press, New York, 1963), Vol. 14, pp. 99−213
10. J. Hubbard, Proc. Roy. Soc. **276**, 238 (1963)
11. J. Hubbard, Proc. Roy. Soc. **281**, 401 (1964)
12. J. Kurzyk, W. Wójcik, J. Spałek, Eur. Phys. J. B **66**, 385 (2008), Part I
13. J. Spałek, J. Kurzyk, R. Podsiadły, W. Wójcik, Eur. Phys. J. B **74**, 63 (2010), Part II
14. V.I. Anisimov, J. Zaanen, O.K. Andersen, Phys. Rev. B **44**, 943 (1991)
15. V.I. Anisimov, F. Aryasetiawan, A.I. Lichtenstein, J. Phys.: Condens. Matter **9**, 767 (1997)
16. G. Kotliar, S.Y. Savrasov, K. Haule, V.S. Oudovenko, O. Parcollet, C.A. Marianetti, Rev. Mod. Phys. **78**, 865 (2006)
17. D. Vollhardt, Ann. Phys. **524**, 1 (2012)
18. A. Rycerz, Ph.D. thesis, Marian Smoluchowki Institute of Physics, Jagiellonian University, 2003
19. J. Jędrak, J. Kaczmarczyk, J. Spałek, `arXiv:1008. 0021 [cond-mat.str-el]` (2010)
20. W.H. Press, S.A. Teukolsky, W.T. Vetterling, B.P. Flannery, *Numerical Recipes: The Art of Scientific Computing*, 3rd edn. (Cambridge University Press, New York, 2007)
21. P. Korbel, W. Wójcik, A. Klejnberg, J. Spałek, M. Acquarone, M. Lavagna, Eur. Phys. J. B **32**, 315 (2003)
22. W.F. Brinkman, T.M. Rice, Phys. Rev. B **2**, 4302 (1970)
23. J. Spałek, Physica B **378-380**, 654 (2006)
24. J. Spałek, Phys. Stat. Sol. B **243**, 78 (2006)
25. J. Spałek, J. Sol. Stat. Chem. **88**, 70 (1990)
26. K. Shibata, T. Ohashi, T. Ogawa, R. Kodama, Phys. Rev. B **82**, 195123 (2010)
27. S.T. Weir, A.C. Mitchell, W.J. Nellis, Phys. Rev. Lett. **76**, 1860 (1996)
28. I. Silvera, Proc. Natl. Acad. Sci. USA **107**, 12743 (2010)
29. M.A. Morales, C. Pierleoni, E. Schwegler, D.M. Ceperley, Proc. Natl. Acad. Sci. USA **107**, 12799 (2010)
30. I. Tamblyn, S.A. Bonev, Phys. Rev. Lett. **104**, 065702 (2010)
31. J. Spalek, A. Datta, J.M. Honig, Phys. Rev. Lett. **59**, 728 (1987)
32. J. Spałek, in *Encyclopedia of Condensed Matter Physics*, edited by F. Bassani et al. (Elsevier, Amsterdam, 2005), Vol. 3, pp. 126−36

3.2 Paper A-2 – Metallization of Atomic Solid Hydrogen within the Extended Hubbard Model with Renormalized Wannier Wavefunctions

This is a follow-up paper to paper A-1. In this contribution to the XVI National Conference on Superconductivity in which we expand the discussion of the most important outcome of that previous work, namely, the critical pressure of metallization of solid atomic hydrogen crystal. Using the extended Hubbard model, with the single-particle energy ϵ_a, the nearest-neighbor hopping term t, the on-site Hubbard interaction U, and the intersite Coulomb repulsion K_{ij}, we model the metal–insulator transition using better approximation for the single-particle basis states with $p = 9$ instead of $p = 3$ Gaussians per wave function. This is discussed briefly with Gaussian fit results presented in Table 1 and the basis wave-functions profiles displayed in Fig. 1. We show that although the results change slightly quantitatively, they do not change qualitatively the previous results (cf. the ground-state energy E_G in Fig. 2 and microscopic parameters t, U and $K \equiv K_{i,z(i)}$, where $z(i)$ is the nearest neighbor of site i).

We also discuss a fine outcome of our approach - the possibility of comparing both Mott and Mott-Hubbard criteria. The first being $n_c^{1/3} a_B \approx 0.2$, where for critical concentration n_c we have $n_c \equiv R_C^{-3}$, and effective Bohr radius $a_B = \alpha_C^{-1}$, where R_C is the critical value of lattice parameter R, and α_C is the critical value of the inverse wave-function size. This lead the Mott criterion to be $n_c^{1/3} a_B = R_C^{-1} \alpha_C^{-1} \approx 0.22$, close to the expected value. Similarly, we obtain the Mott-Hubbard ratio $U/W \approx 1.18$, close to the critical value of unity.

Finally, we assessed the zero-point motion energy E_{ZPM} of the interacting ions in the simple cubic lattice. The zero-point motion represents the primary effect of non-classical character of the H^+ ions (protons). As a starting point, we assume a small ion displacement $\delta\mathbf{R}$, so that only the nearest neighbor contribution to the total energy will change significantly. Then, we derive the formula for the total energy for such displacement, including estimation of the kinetic energy of an ion through the uncertainty principle $\delta\mathbf{P}^2 \delta\mathbf{R}^2 \geqslant 3\hbar^2/4$. This allowed us to find all modes, the one with smallest energy being diagonal. We display the value of E_{ZPM}, as well as its ratio to the ground-state energy in Fig. 5.

The paper was published in Acta Physica Polonica A (Acta Phys. Polon. A **126**, 4A (2014)), pp. A58-A62.

Proceedings of the XVI National Conference on Superconductivity and Strongly Correlated Systems, Zakopane 2013

Metallization of Atomic Solid Hydrogen within the Extended Hubbard Model with Renormalized Wannier Wave Functions

A.P. Kądzielawa*

Marian Smoluchowski Institute of Physics, Jagiellonian University, W.S. Reymonta 4, PL-30-059 Kraków, Poland

We refer to our recent calculations *Eur. Phys. J. B* **86**, 252 (2013) of metallization pressure of the three-dimensional simple-cubic crystal of atomic hydrogen and study the effect on the crucial results concocting from approximating the $1s$ Slater-type orbital function with a series of p Gaussians. As a result, we find the critical metallization pressure $p_{\rm C} = 102$ GPa. The latter part is a discussion of the influence of zero-point motion on the stabilizing pressure. We show that in our model the estimate magnitude of zero-point motion carries a little effect on the critical metallization pressure at zero temperature.

DOI: 10.12693/APhysPolA.126.A-58

PACS: 71.30.+h, 71.27.+a, 71.10.Fd, 62.50.–p

1. Motivation

This year we are celebrating the 50th anniversary of the Hubbard model, a second-quantization language to describe strongly correlated systems provided independently by Hubbard [1], Gutzwiller [2, 3] and Kanamori [4]. This description shed some light on many-body quantum systems, in particular on the localization–delocalization transitions of fermions states in the solid-state [5–8], and optical-lattice [9] systems. This transition is called the Mott or Mott–Hubbard transition.

In the series of papers [10–12], we have conducted model calculations combining both the Mott [5] and the Hubbard [13] aspects of the phase transition, within the extended Hubbard model, with a simultaneous renormalization of the single-particle Wannier basis, connecting first- and second-quantization approach. In [12] we obtained, using proposed model, the critical metallization pressure $p_{\rm C} = 97.7$ GPa required to stabilize the atomic-hydrogen-like crystal, while having both the Mott ($n_{\rm C}^{1/3} a_{\rm B} \approx 0.2$) and the Hubbard ($U \approx W$) criteria satisfied at the same time. Thus, those two criteria represent two sides of the same coin.

Ever since Ashcroft proposed an explanation for greater-than-expected magnetic field of Jovian planets [14] by applying the BCS theory to the metallic hydrogen, the pursuit of the metallization of this element began. Predicted by Wigner and Huntington in 1935 [15] the conducting phase of hydrogen is claimed to have various properties, including hypothesis of being superconducting up to the room temperature [14].

In this paper we briefly describe the model in Sect. 2. Then in Sect. 3 we review the validity of approximations made in [12] and show that they were in fact sufficient (explicitly redoing all calculations and showing no qualitative changes). We also show that both Mott and Hubbard criteria of localization-delocalization transition are satisfied. In Sect. 4 we estimate the magnitude of zero-point motion energy, omitted in our calculations to test the strength of our results, keeping in mind the possibility of quantum melting of hydrogen.

2. Model

We start with the extended Hubbard Hamiltonian describing a single-band hydrogen system [10–12]:

$$\mathcal{H} = \epsilon_a \sum_i n_i + \sum_{i\neq j,\sigma} t_{ij} a^\dagger_{i\sigma} a_{j\sigma} + U \sum_i n_{i\uparrow} n_{i\downarrow} + \sum_{i<j} K_{ij} n_i n_j + \sum_{i<j} \frac{2}{R_{ij}}, \tag{1}$$

where t_{ij} is the hopping integral, U — the intraatomic interaction magnitude, ϵ_a — the atomic energy per site, and $2/R_{ij} = 2|\boldsymbol{R}_j - \boldsymbol{R}_i|^{-1}$ — ion–ion interaction corresponding to the classical Coulomb repulsion (in atomic units).

We have the total number of electrons $N_{\rm e} = \sum_i n_i$, and define the deviation from one-electron-per-atom configuration $\delta n_i = n_i - 1$. We rearrange [16]:

$$\sum_{i<j} K_{ij} n_i n_j = \sum_{i<j} K_{ij} \delta n_i \delta n_j + N_{\rm e} \frac{1}{N} \sum_{i<j} K_{ij} + (N_{\rm e} - N) \frac{1}{N} \sum_{i<j} K_{ij}. \tag{2}$$

For half band-filling $n = N_{\rm e}/N = 1$ the latter part disappears, and we can write $\sum_{i<j} K_{ij} \approx \sum_{i<j} K_{ij} n_i n_j$, thus introducing the *effective* atomic energy per site $\epsilon_a^{\rm eff} = \epsilon_a + \frac{1}{N} \sum_{i<j} \left(K_{ij} + \frac{2}{R_{ij}} \right)$. Let us rewrite the Hamiltonian 1 in a following manner:

$$\mathcal{H} = \epsilon_a^{\rm eff} \sum_i n_i + \sum_{i\neq j,\sigma} t_{ij} a^\dagger_{i\sigma} a_{j\sigma} + U \sum_i n_{i\uparrow} n_{i\downarrow} + \frac{1}{2} \sum_{i\neq j} K_{ij} \delta n_i \delta n_j. \tag{3}$$

Since we are interested in calculating explicitly the aver-

*e-mail: kadzielawa@th.if.uj.edu.pl

age value $\langle\mathcal{H}\rangle$, we note that close to the metal–insulator boundary $\langle\delta n_i \delta n_j\rangle \approx 0$, hence we disregard this term in the calculation of energy.

2.1. Wave-function optimization

To calculate the microscopic parameters ϵ_a, t_{ij}, K_{ij}, U of the Hamiltonian (3) we choose the basis of the orthogonalized-to-the-nearest-neighbors Wannier w_i functions constructed from $1s$ Slater-type orbitals (STO) Ψ_i:

$$w_i(\boldsymbol{r}) = \beta\,\Psi_i(\boldsymbol{r}) - \gamma\sum_{j=1}^{z}\Psi_j(\boldsymbol{r}), \tag{4}$$

where β and γ (see [10] Eqs. (24) and (25)) are mixing parameters specified for the topology of the crystal, and depending explicitly on the overlap integrals of the single--particle functions. z is the number of nearest neighbors.

Obtaining the microscopic parameters from the first principles requires several integrations, since

$$\epsilon_a = \langle w_i|H_1|w_i\rangle, \quad t_{ij} = \langle w_i|H_1|w_j\rangle,$$

$$U = \left\langle w_i w_i \left| 2|\boldsymbol{r}_1 - \boldsymbol{r}_2|^{-1} \right| w_i w_i \right\rangle,$$

$$K_{ij} = \left\langle w_i w_j \left| 2|\boldsymbol{r}_1 - \boldsymbol{r}_2|^{-1} \right| w_i w_j \right\rangle, \tag{5}$$

where H_1 is the Hamiltonian for a single particle in the system, and $2|\boldsymbol{r}_1 - \boldsymbol{r}_2|^{-1}$ interparticle interaction in atomic units. Calculating (5) with basis as given in (4) requires solving very complicated series of integrals and can be simplified by approximating STO with a series of Gaussian functions

$$\Psi_i(\boldsymbol{r}) = \sqrt{\frac{\alpha^3}{\pi}}\,\mathrm{e}^{-\alpha|\boldsymbol{r}-\boldsymbol{R_i}|} \approx \alpha^{\frac{3}{2}}\sum_{a=1}^{p} B_a \left(\frac{2\Gamma_a^2}{\pi}\right)^{\frac{3}{4}} \mathrm{e}^{-\alpha^2\Gamma_a^2|\boldsymbol{r}-\boldsymbol{R_i}|^2}, \tag{6}$$

where B_a and Γ_a are parameters found by minimizing energy of the single atom ($\mathcal{H}_1 \overset{\text{a.u.}}{=} -\bigtriangledown^2 - 2|\boldsymbol{r} - \boldsymbol{R_i}|^{-1}$). p is a number of Gaussian functions used for the approximation. α is the inverse function size and will remain a variational parameter, allowing us to renormalize the ground state function to find the minimal energy for given lattice parameter R. For the sake of completeness we explicitly illustrate the quality of the approximation (Fig. 1) and the coefficient for different STO-pG basis (Table I).

TABLE I

B_a and Γ_a coefficient obtained by minimizing the single-particle energy with wave functions given by (6).

STO-3G		STO-5G		STO-7G		STO-9G		a
B_a	Γ_a^2	B_a	Γ_a^2	B_a	Γ_a^2	B_a	Γ_a^2	
0.7079069	0.4037496	0.4862397	0.3428813	0.3347926	0.3073439	0.2333815	0.2832535	1
0.3460096	0.897739	0.4687430	0.6489746	0.4947580	0.5341995	0.4735227	0.4656983	2
0.0691531	1.9705714	0.1446282	1.2283203	0.2218991	0.9285009	0.2825582	0.7656564	3
		0.0307340	2.3248533	0.0674427	1.6138428	0.1065788	1.2588187	4
		0.0093803	4.4002717	0.0188009	2.8050467	0.0341750	2.0696289	5
				0.0038829	4.8754978	0.0099417	3.4026852	6
				0.0018480	8.4741829	0.0032307	5.5943683	7
						0.0006094	9.1977233	8
						0.0004466	15.1220138	9

2.2. Ground-state energy

As stated earlier we would like to determine the inverse wave function size α minimizing the ground-state energy. To obtain the values for given α and the fixed lattice parameter R we use statistically-consistent Gutzwiller approximation (SGA) [17]. We extend the Gutzwiller approximation Hamiltonian

$$\mathcal{H}_{\mathrm{GA}} = \epsilon_a^{\mathrm{eff}}\sum_{i\sigma} n_{i\sigma} + \sum_{ij\sigma} t_{ij} q_\sigma a_{i\sigma}^\dagger a_{j\sigma} + NUd^2, \tag{7}$$

where the double occupancy number $d^2 = \langle n_{i\uparrow} n_{i\downarrow}\rangle$ and $q_\sigma = 2\left(d\sqrt{1-2d^2-m} + \sqrt{d^2(1-2d^2+m)}\right)^2/(1-m^2)$ for $n = 1$, by introducing the Lagrange-multiplier constraints

$$\mathcal{C}_\lambda = -\lambda_m\sum_i (m_i - m) - \lambda_n\sum_i (n_i - n), \tag{8}$$

where $m_i \equiv n_{i\uparrow} - n_{i\downarrow}$, $m \equiv \langle m_i\rangle$, $n_i \equiv n_{i\uparrow} + n_{i\downarrow}$, and $n \equiv \langle n_i\rangle$.

Finally, we use the operator $\mathcal{K} = \mathcal{H}_{GA} + \mathcal{C}_\lambda$ as our effective Hamiltonian. Mean fields d^2 and m, as well as the Lagrange multipliers λ_m and λ_n, and the chemical potential μ are all determined variationally.

Once the ground-state energy is found as a minimal value for some $\alpha_{\min}$, we get the set of values — the microscopic parameters (5) in the ground state. Below we discuss the properties of our results in comparison to those obtained earlier [12].

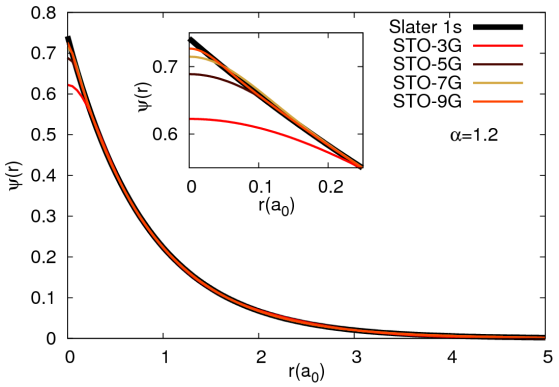

Fig. 1. Approximations of Slater $1s$ function centered on-site with different Gaussian resolution p (see (6) and Table I) for $\alpha = 1.2$ with respect to distance r from the ion. Inset: details for small distances. Note that the biggest contribution to the error is given by the part close to the node, hence small total error after integrating over whole space. As expected the 9 Gaussian basis (STO-9G) is far the best approximation.

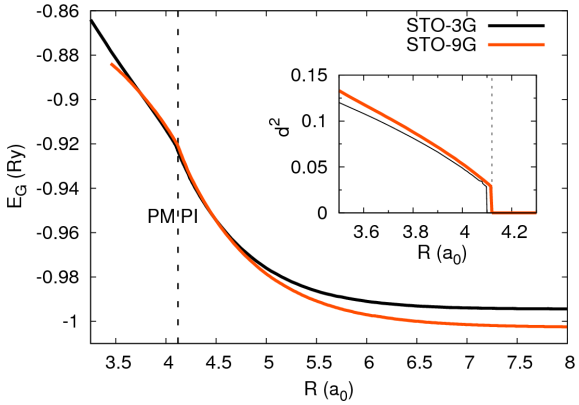

Fig. 2. Ground-state energy versus lattice parameter R for different STO-pG basis. Note more realistic behavior in the metallic ($R < R_C = 4.12a_0$) regime with non-trivial R dependence. Inset: double occupancy mean field versus lattice parameter R for different STO-pG basis. Note no qualitative changes of behavior.

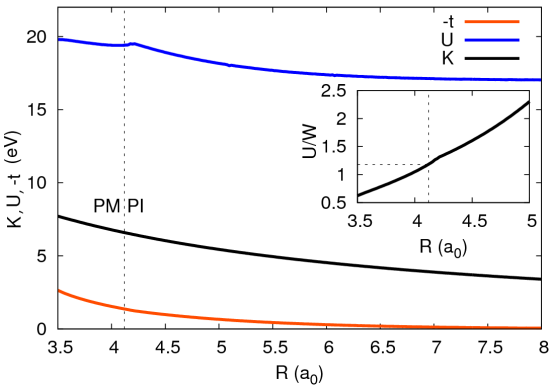

Fig. 3. The microscopic parameters t, U and K versus lattice parameter R. Inset: U/W ratio with bandwidth $W = 2z|t|$ and on-site repulsion U.

3. Gaussian basis resolution

In our previous approach [12] we favored the Gaussian basis consisting of 3 functions. We argued that the quality of such an approximation is sufficient, and that the numerical effort to obtain results in higher Gaussian resolutions ($p > 3$) is unnecessary. The computational complexity scales

$$\epsilon_a, t \propto p^2,$$

$$U, K_{ij} \propto p^4, \tag{9}$$

where p is the resolution. Hence the time of calculating the full set of data points is increased by a factor of 200 when replacing STO-3G to STO-9G basis.

3.1. STO-3G versus STO-9G

For our *ab initio* calculations we have selected STO-9G basis. It is much better (cf. Fig. 1) than STO-3G, while time of the calculation is still acceptable.

The dependence of the ground-state energy E_G with respect to the lattice parameter R (Fig. 2) is the main outcome. Similarly to the previous case [12], there are two local minima — one associated with the metallic phase ($d^2 \neq 0$), and one with the Mott insulating phase ($d^2 = 0$). The transition occurs at $R = R_C = 4.12a_0$ (compared to $R_C^{old} = 4.1a_0$), but its nature is not changed, as it still is a weakly discontinuous transition (observe the obvious discontinuity of double occupancy number, cf. inset in Fig. 2).

In Fig. 3 we plot the values of the nearest-neighbor hopping ($-t$), on-site repulsion U, and the nearest--neighbor intersite repulsion K. Even though there are no qualitative changes in the values in comparison with [12] we present this for the sake of completeness.

In Ref. [12] we have shown that our transition satisfies both the Mott and the Hubbard criteria for metal–insulator transition. Below we refer to them while discussing the new results.

3.2. The Mott and the Hubbard criteria

The original Mott criterion [5,6] $n_C^{1/3} a_B \approx 0.2$ can be rewritten by substituting α^{-1} for the effective Bohr radius a_B and defining the particle density as $n_C = R_C^{-3}$. We get $n_C^{1/3} a_B = R_C^{-1} \alpha^{-1} \approx 0.22$, a slightly better outcome than in [12] (as it is predicted with a better accuracy).

As shown in inset to Fig. 3, the ratio (U/W) for critical lattice parameter $R_C = 4.12a_0$ is equal to 1.18 in consistence with [13].

3.3. Metallization pressure

Our model represents a 3-dimensional simple-cubic crystal of the atomic hydrogen (one electron per ion, $1s$ orbitals) undergoing the Mott–Hubbard transition. It is clear that the minimal value of energy (cf. Fig. 2) of such a crystal is reached for lattice parameter $R \to \infty$. Thus one require external pressure p for its stabilization, that can be obtained classically as the force per cell $F = |-\nabla_{\mathrm{R}} E_{\mathrm{G}}|$ over the elementary cell area $A/N = R^2$. In Fig. 4 we plot such pressure versus lattice parameter R and provide a comparison between the previously obtained (STO-3G [12]) results and the new ones.

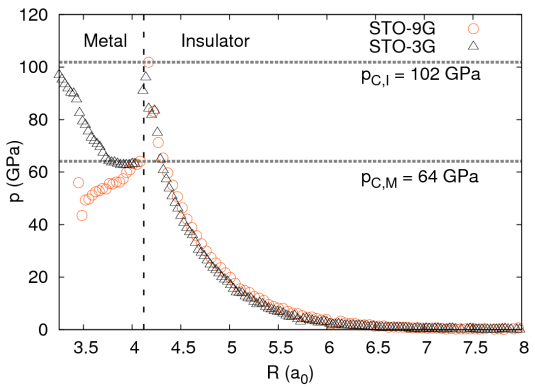

Fig. 4. Stabilizing pressure for a simple-cubic atomic solid hydrogen crystal versus lattice parameter R for different STO-nG basis. Note only a slight change in obtained critical pressure $p_{\mathrm{C}} = 102$ GPa for significantly larger STO-9G basis. The qualitatively different behavior of stabilizing pressure in the metallic ($R < R_{\mathrm{C}} = 4.12a_0$) regime is caused by non-trivial behavior of energy in this regime (see Fig. 2 for details).

We have calculated the metallizing pressure $p_{\mathrm{C}} = 102$ GPa assuming that our model is static — this assumption is not quite correct within the quantum-mechanical world, where there is always a non-zero energy of zero-point oscillations. In the next section we deal with this problem by estimating the contribution of zero-point motion to the total energy.

4. Zero-point motion energy

We introduce (following approach similar to [18]) the uncertainties of the momentum $\delta\boldsymbol{P}$ and position $\delta\boldsymbol{R}$. The energy of a distortion per ion is

$$\Delta E = \frac{\delta \boldsymbol{P}^2}{2M_{H^+}} + \frac{1}{2}\sum_{i\,\in\,\{x,y,z\}} \left(\frac{e^2}{R+\delta R_i} + \frac{e^2}{R-\delta R_i} \right). \tag{10}$$

By applying the uncertainty relation $\delta\boldsymbol{P}^2 \cdot \delta\boldsymbol{R}^2 \geq 3\hbar^2/4$ and minimizing 10 with respect to R_i's we get a set of local extrema, from which the global minimum is

$$\Delta E_0 = 3\frac{e^2}{R} + \frac{\hbar\left(4\sqrt{6}eMR + \sqrt{M}\sqrt{R}\hbar\right)}{8M^{3/2}R^{5/2}}, \tag{11}$$

$$|\delta \boldsymbol{R}_0| = \sqrt{\frac{3R^2}{2\sqrt{6}\frac{e}{\hbar}\sqrt{M}\sqrt{R}+1}}, \tag{12}$$

where R is the lattice parameter. The first term of (11) is related to the Coulomb repulsion of ions and the second $E_{\mathrm{ZPM}} \equiv \Delta E_0 - 3e^2R^{-1}$ is the zero-point oscillation energy.

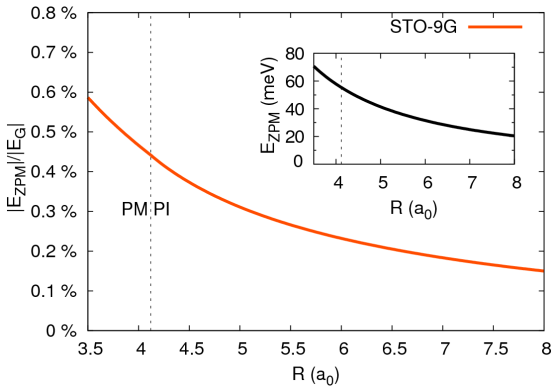

Fig. 5. The relative magnitude of estimated zero-point motion energy with respect to ground-state energy at given lattice parameter R. Note that result below 0.5 at the metal–insulator transition shows that the correction from ZPM to the critical pressure can be disregarded. Inset: explicit value of estimated zero-point motion energy.

In Fig. 5 we show the ratio of $|E_{\mathrm{ZPM}}|$ to the ground-state energy $|E_{\mathrm{G}}|$. Since it is slowly-changing and is about two orders of magnitude smaller than the ground-state energy, our approach of omitting it in the calculation of metallization pressure holds.

5. Conclusions

In this paper we established that the choice of the STO-3G basis in [12] was not influencing results qualitatively, and that the computational simplicity and total CPU time conservation are allowing us to examine also a full picture with an external magnetic field, preserving main properties of the system. Better accuracy (Sect. 2.1) increases the quality of the results (cf. Fig. 2), but does not change our understanding of the metal–insulator transition in this model.

The analysis of zero-point motion carried out in Sect. 4 reinforces our previous results and suggests that the energy of oscillations does not increase the stabilization pressure significantly.

Acknowledgments

I would like to thank Prof. Józef Spałek for critical reading of this paper as well as Dr. Andrzej Biborski and Marcin Abram for discussions.

The work was realized as a part of the TEAM project awarded to our group by the Foundation for Polish Science (FNP) for the years 2011–2014.

References

[1] J. Hubbard, *Proc. R. Soc. (London)* **276**, 238 (1963).

[2] M.C. Gutzwiller, *Phys. Rev. Lett.* **10**, 159 (1963).

[3] M.C. Gutzwiller, *Phys. Rev.* **137**, A1726 (1965).

[4] J. Kanamori, *Prog. Theor. Phys.* **30**, 275 (1963).

[5] N.F. Mott, *Proc. Phys. Soc. Sec. A* **62**, 416 (1949).

[6] N.F. Mott, *Metal–Insulator Transitions*, 2nd ed., Taylor and Francis, London 1990.

[7] F. Gebhard, *The Mott Metal–Insulator Transition*, Springer, Berlin 1997.

[8] M. Imada, A. Fujimori, Y. Tokura, *Rev. Mod. Phys.* **70**, 1039 (1998).

[9] I. Bloch, *Understanding Quantum Phase Transitions*, Ed. L.D. Carr, CRC Press, Boca Raton 2011, Ch. 19.

[10] J. Kurzyk, W. Wójcik, J. Spałek, *Eur. Phys. J. B* **66**, 385 (2008), Part I.

[11] J. Spałek, J. Kurzyk, R. Podsiadły, W. Wójcik, *Eur. Phys. J. B* **74**, 63 (2010), Part II.

[12] A.P. Kądzielawa, J. Spałek, J. Kurzyk, W. Wójcik, *Eur. Phys. J. B* **86**, 252 (2013), Part III.

[13] J. Hubbard, *Proc. R. Soc. (London)* **281**, 401 (1964).

[14] N.W. Ashcroft, *Phys. Rev. Lett.* **21**, 1748 (1968).

[15] E. Wigner, H.B. Huntington, *J. Chem. Phys.* **3**, 764 (1935).

[16] A. Rycerz, Ph.D. thesis, Jagiellonian University 2003.

[17] J. Jędrak, J. Kaczmarczyk, J. Spałek, arXiv:1008.0021 2010.

[18] J. Spałek, R. Podsiadły, W. Wójcik, A. Rycerz, *Phys. Rev. B* **61**, 15676 (2000).

3.3 Paper A-3 – H_2 and $(H_2)_2$ molecules with an ab initio optimization of wavefunctions in correlated state: electron–proton couplings and intermolecular microscopic parameters

In this paper we utilize the **E**xact **D**iagonalization – **Ab** **I**nitio Approach (EDABI) to describe the H_2 molecule with more precise approach (in comparison to that in paper A-2) to assess the zero-point motion amplitude and corresponding energy, taking the contributions up to the ninth order. We also provide a full microscopic picture of van der Waals-like attraction between two H_2 molecules, that eventually led to the one-dimensional molecular chain discussed in the papers A-4 and A-5. We also present the methodology of including higher (than $1s$) orbitals into the model, thus opening the door for description of different atoms that is planned for the near future.

We start from the full two-site Hamiltonian (2.5), with explicit expressions for all six microscopic parameters: the single-particle energy ϵ, the hopping term t, the on-site Hubbard interaction U and the intersite Coulomb repulsion K, the exchange integral J and the so-called correlated hopping V. As we have real-valued single-particle basis wave functions, the so-called pair hopping-term amplitude is equal to the exchange integral. We calculate explicitly the form of these parameters as a function of inverse wave-function size α and the intersite distance R, for the single-particle-basis wave functions, composed of $1s$ Slater-type orbitals (all formulas can be found in Appendix A). Then, for given R, we minimize the system ground-state energy $E_G = E_- + 2/R$ with respect to the inverse wave-function size α, where E_- is the exact eigenvalue for the Hamiltonian and $2/R$ is classical Coulomb repulsion of the ions. Within this simple model, we find the minimum of E_G for $R_B = 1.43042a_0$ and $E_B = -2.29587Ry$, $\sim 2\%$ from the almost exact result $R_{K-W} = 1.3984a_0$, $E_{K-W} = -2.349Ry$ of Kołos and Wolniewicz [107]. The results are presented in Figs. 1–5. The next step is to estimate the zero-point motion amplitude and energy. For this purpose we consider the oscillations of interionic distance $R = R_B + \delta R$, and: *(i)* we expand the system energy around minimum, in terms of δR up to the ninth order; *(ii)* calculate the additional term $\delta\mathcal{H}$ of Hamiltonian, that covers the change of energy caused by the change $\delta\Xi$ of the microscopic parameters, here labeled generically via Ξ; these are calculated explicitly (the corresponding formulas can be found in Appendix B) and presented in Figs. 7–8; *(iii)* obtain explicitly the averages of the operator part of Hamiltonian in the ground-state (cf. Fig. 6); *(iv)* estimate the kinetic energy of the ions and the change of the interionic Coulomb repulsion. We combine steps *(i)–(iv)* and minimize the expression for the total energy of the system with respect to the δR. The result is the zero-point motion amplitude $\delta R_0 = 0.189a_0$ and the energy $E_{ZPM} = 0.0241Ry$.

We supplement the results with the solution of the $(H_2)_2$ system with all two-site parameters of interaction (three– and four-site terms are of negligible magnitude) and present the results in Figs. 10–14. We observe the van der Waals-like behavior of the energy difference

per molecule $\Delta E_{H_2}(a) = E_{(H_2)_2}/2 - E_B$, with a shallow minimum for the intermolecular distance $a = 4.5a_0$. In Appendix D, we sketch how to incorporate higher orbitals to the model on the example of one-body microscopic parameters for $1s$ and $2s$ Slater-type orbitals.

The paper was published in New Journal of Physics (New J. Phys **16**, 123022 (2014)), pp. 1–26. It has also been selected by the Institute of Physics Publishing as one of the papers of the year 2014 (the so-called IOPSelect).

New Journal of Physics
The open access journal at the forefront of physics
Deutsche Physikalische Gesellschaft DPG | IOP Institute of Physics

H_2 and $(H_2)_2$ molecules with an *ab initio* optimization of wave functions in correlated state: electron–proton couplings and intermolecular microscopic parameters

Andrzej P Kądzielawa[1], Agata Bielas[2], Marcello Acquarone[3], Andrzej Biborski[4], Maciej M Maśka[2] and Józef Spałek[1,4]

[1] Instytut Fizyki im. Mariana Smoluchowskiego, Uniwersytet Jagielloski, ulica Łojasiewicza 11, PL-30348 Kraków, Poland
[2] Instytut Fizyki, Uniwersytet Śląski, ulica Uniwersytecka 4, PL-40007 Katowice, Poland
[3] Dipartimento di Fisica e Scienze della Terra dellUniversità di Parma, I-43100 Parma, Italy
[4] Akademickie Centrum Materiałów i Nanotechnologii, AGH Akademia Górniczo-Hutnicza, Aleja Mickiewicza 30, PL-30059 Kraków, Poland
E-mail: kadzielawa@th.if.uj.edu.pl and ufspalek@if.uj.edu.pl

Received 19 August 2014, revised 4 November 2014
Accepted for publication 12 November 2014
Published 8 December 2014

New Journal of Physics **16** (2014) 123022

doi:10.1088/1367-2630/16/12/123022

Abstract

The hydrogen molecules H_2 and $\left(H_2\right)_2$ are analyzed with electronic correlations taken into account between the $1s$ electrons in an exact manner. The optimal single-particle Slater orbitals are evaluated in the correlated state of H_2 by combining their variational determination with the diagonalization of the full Hamiltonian in the second-quantization language. All electron–ion coupling constants are determined explicitly and their relative importance is discussed. Sizable zero-point motion amplitude and the corresponding energy are then evaluated by taking into account the anharmonic contributions up to the ninth order in the relative displacement of the ions from their static equilibrium value. The applicability of the model to solid molecular hydrogen is briefly analyzed by calculating intermolecular microscopic parameters for the $2 \times H_2$ rectangular configuration, as well its ground state energy.

Keywords: hydrogen molecules, electron-proton coupling for hydrogen molecule, electronic correlations for hydrogen molecule, intermolecular hopping and interaction parameters

1. Motivation

The few-site models of correlated fermions play an important role in singling out, in an exact manner, the role of various local intra- and inter-site interactions against hopping (i.e., containing both covalent and the ionic factors) and thus, in establishing the optimal correlated state of fermions [1–8] on a local (nanoscopic) scale. The model has also been used to obtain a realistic analytic estimate of the hydrogen-molecule energies of the ground and the excited states in the correlated state [9]. For this purpose, we have developed the so-called EDABI method, which combines *E*xact *D*iagonalization in the Fock space with a concomitant *Ab I*nitio determination of the single-particle basis in the Hilbert space. So far, the method has been implemented by taking only 1*s* Slater orbitals, one per site [10]. The method contains no parameters; the only approximation made is taking a truncated single-particle basis (i.e., one Slater orbital per site) when constructing the field operator, that in turn is used to derive the starting Hamiltonian in the second-quantization representation. This Hamiltonian represents an extended Hubbard Hamiltonian, with *all* two-site interactions taken into account and the solution comprises not only the exact eigenvalues of the few-site Hamiltonian, but also at the same time an evaluation of the adjustable single-particle wave functions in the correlated state. Also, the calculated thermodynamic properties rigorously exemplify [12, 11] the low- and high-energy scales, corresponding to spin and local charge fluctuations, respectively. The former represents the precursory magnetic-ordering effect whereas the latter represents local effects accompanying the Mott–Hubbard transition. In general, our approach follows the tradition of accounting for interelectronic correlations via the second-quantization procedure, with the adjustment of single-particle wave functions, contained in microscopic parameters of the starting model, in the correlated state.

The first aim of this paper is to extend a previously established fully microscopic approach [9, 10] and calculate all six possible electron–ion coupling constants for H_2 as a function of the bond length. As a byproduct, we obtain an accurate estimate of the zero-point-motion amplitude and its energy to a high (ninth) order in the relative displacement of the ions. This evaluation shows explicitly the dominant contributions to the vibronic spectra of the molecule. In effect, the work formulates a complete two-site model of correlated states with all the coupling parameters calculated from an *ab initio* procedure. It also forms a starting point to full scale dynamic calculations involving a richer basis in the Hilbert space, at least in the adiabatic limit. So, although the importance of the present results to the discussion of the exact evaluation of the ground-state energy of the H_2 molecule is limited, the approach may be extended to treat molecular solid hydrogen with the inclusion of interelectronic correlations. Explicitly, as a starting point we calculate the intermolecular hopping integrals and the principal electron–electron interaction microscopic parameters as a function of intermolecular distance.

A methodological remark is in place here. As we determine the local ion–electron and electron–electron coupling parameters, they can be regarded as a starting estimate of those for the bulk solid molecular hydrogen, as we have recently studied a critical pressure of metallization of the *atomic* solid (Mott insulating) state [13]. The obtained pressure of atomic-

hydrogen metallization is about 100 *GPa*, a value which squares well with that observed for the case of fluid molecular hydrogen (140 *GPa*)[14], although the recent simulations provide quite different values for fluid hydrogen analyzed at high temperature [15]. Obviously, our previous work is not related directly to the molecular-hydrogen metallization in the solid state [16–19]. So far, we have discussed rigid-lattice properties. We believe that the present results form the first step in incorporating the vibrational spectrum and correlations to extended systems.

The structure of the paper is as follows. Even though the main purpose of the paper is to calculate the local electron–proton and electron–electron coupling constants, for the sake of the completeness, in sections 2 and 3 we reproduce some of the results of [9] and correct some minor errors (see also appendix A). In section 4 we define the method of calculation of both the electron–ion (proton) coupling constants (see also appendix B), as well as estimate the zero-point motion to the ninth order versus the interionic distance. In section 5 we extend the single-molecule treatment and provide the intermolecular hopping amplitudes and the electron–electron microscopic parameters which may serve for analysis of the solid molecular hydrogen. Section 6 contains physical discussion and a brief outlook, where we also refer to the finite-size quantum Monte Carlo results. In the series of appendices we provide some analytical details, as they may form an analytical basis for the electron–lattice coupling supplementing the classic Slater results for the electronic part of H_2 molecule [20].

2. Model and summary of purely electronic properties

2.1. Wannier basis

To describe the behavior of an electron in the system of two ions we start from 1*s* Slater–type orbitals

$$\Psi_i(\mathbf{r}) = \sqrt{\frac{\alpha^3}{\pi}}\, e^{-\alpha|\mathbf{r}-\mathbf{R_i}|}, \tag{1}$$

where α is the inverse size of the orbital. To ensure orthogonality we use Wannier functions, which in this case reduce the superposition of the atomic states, i.e.,

$$w_i(\mathbf{r}) = \beta\Big[\,\Psi_i(\mathbf{r}) - \gamma\Psi_j(\mathbf{r})\Big], \tag{2}$$

with the mixing parameters

$$\begin{cases} \beta = \dfrac{1}{\sqrt{2}}\sqrt{\dfrac{1+\sqrt{1-S^2}}{1-S^2}} \\ \gamma = \dfrac{S}{1+\sqrt{1-S^2}} \end{cases} \tag{3}$$

where $S = S(\alpha, R) \equiv \langle\Psi_1|\Psi_2\rangle$ is the atomic functions' overlap.

Equations (3) ensure both the orthogonality and proper behavior in the atomic limit i.e., $\lim_{R\to\infty}\beta = 1$, where R is the average interatomic distance. $\lim_{R\to\infty}\gamma = 0$.

2.2. Second-quantization picture

The two-site Hamiltonian with one orbital per site has the general form

$$\begin{aligned}\mathcal{H} = {} & \epsilon\left(\hat{n}_1 + \hat{n}_2\right) + t\sum_{\sigma}\left(\hat{a}^{\dagger}_{1\sigma}\hat{a}_{2\sigma} + \hat{a}^{\dagger}_{2\sigma}\hat{a}_{1\sigma}\right) \\ & + U\left(\hat{n}_{1\uparrow}\hat{n}_{1\downarrow} + \hat{n}_{2\uparrow}\hat{n}_{2\downarrow}\right) - 2\,J\mathbf{S}_1\mathbf{S}_2 \\ & + \left(K - \frac{J}{2}\right)\hat{n}_1\hat{n}_2 + J\left(\hat{a}^{\dagger}_{1\uparrow}\hat{a}^{\dagger}_{1\downarrow}\hat{a}_{2\downarrow}\hat{a}_{2\uparrow} + h.\,c.\right) \\ & + V\sum_{\sigma}\Big[\left(\hat{n}_{1\sigma} + \hat{n}_{2\sigma}\right)\left(\hat{a}^{\dagger}_{1\bar{\sigma}}\hat{a}_{2\bar{\sigma}} + \hat{a}^{\dagger}_{2\bar{\sigma}}\hat{a}_{1\bar{\sigma}}\right)\Big],\end{aligned} \tag{4}$$

where $\hat{a}_{i\sigma}$ and $\hat{a}^{\dagger}_{i\sigma}$ are the fermionic operators of annihilation and creation of the electron with spin σ on the $1s$ orbital of hydrogen atom $i \in \{1, 2\}$.

The microscopic parameters $\epsilon = T_{11}$, $t = T_{12}$, $U = V_{1111}$, $J = V_{1122}$, $K = V_{1212}$ and $V = V_{1112}$ correspond to one–and two-particle interactions [9]

$$T_{ij} = \left\langle w_i \left| \mathcal{T} \right| w_j \right\rangle, \tag{5a}$$

$$V_{ijkl} = \left\langle w_i w_j \left| \mathcal{V} \right| w_k w_l \right\rangle, \tag{5b}$$

where in atomic units $\mathcal{T} = -\nabla^2 - 2/|\mathbf{r} - \mathbf{R}|$, and $\mathcal{V} = 2/|\mathbf{r} - \mathbf{r}'|$. In appendix A we provide explicitly the form of microscopic parameters as a function of both intersite static distance R and the inverse wave-function size α. In what follows we first diagonalize (4), and subsequently optimize the wave functions contained in the microscopic parameters of (4). This program will be carried out systematically in what follows.

2.3. Exact solution

The system described by the Hamiltonian (4) has an exact solution previously studied in detail in [9]. For the two-electron system ($n_1 + n_2 = 2$), i.e. with one particle per site, the starting basis is

$$|1\rangle = \hat{a}^{\dagger}_{1\uparrow}\hat{a}^{\dagger}_{2\uparrow}\,|0\rangle, \tag{6a}$$

$$|2\rangle = \hat{a}^{\dagger}_{1\downarrow}\hat{a}^{\dagger}_{2\downarrow}\,|0\rangle, \tag{6b}$$

$$|3\rangle = \frac{1}{\sqrt{2}}\left(\hat{a}^{\dagger}_{1\uparrow}\hat{a}^{\dagger}_{2\downarrow} + \hat{a}^{\dagger}_{1\downarrow}\hat{a}^{\dagger}_{2\uparrow}\right)|0\rangle, \tag{6c}$$

representing the intersite spin-triplet states with eigenvalues $E_1 = E_2 = E_3 = 2\epsilon + K - J$, and

$$|4\rangle = \frac{1}{\sqrt{2}}\left(\hat{a}^{\dagger}_{1\uparrow}\hat{a}^{\dagger}_{2\downarrow} - \hat{a}^{\dagger}_{1\downarrow}\hat{a}^{\dagger}_{2\uparrow}\right)|0\rangle, \tag{6d}$$

$$|5\rangle = \frac{1}{\sqrt{2}}\left(\hat{a}^{\dagger}_{1\uparrow}\hat{a}^{\dagger}_{1\downarrow} + \hat{a}^{\dagger}_{2\uparrow}\hat{a}^{\dagger}_{2\downarrow}\right)|0\rangle, \tag{6e}$$

$$|6\rangle = \frac{1}{\sqrt{2}}\left(\hat{a}^{\dagger}_{1\uparrow}\hat{a}^{\dagger}_{1\downarrow} - \hat{a}^{\dagger}_{2\uparrow}\hat{a}^{\dagger}_{2\downarrow}\right)|0\rangle, \tag{6f}$$

representing the spin-singlet states, with the corresponding Hamiltonian matrix involving the matrix elements $\langle i\,|\mathcal{H}|\,j\rangle \equiv \left(\mathcal{H}_{ij}\right)$:

$$\left(\mathcal{H}_{ij}\right) = \begin{pmatrix} 2\epsilon + K + J & 2(t+V) & 0 \\ 2(t+V) & 2\epsilon + U + J & 0 \\ 0 & 0 & 2\epsilon + U - J \end{pmatrix}. \tag{7}$$

The state (6*f*) is an eigenvector of (7) with eigenvalue $E_6 = 2\epsilon + U - J$. The diagonalization supplies us with the two other eigenvectors [1]

$$|\pm\rangle = [2\mathcal{D}(\mathcal{D} \mp U \pm K)]^{-\frac{1}{2}} \\ [\mp(\mathcal{D} \mp U \pm K)|4\rangle + 4|t+V||5\rangle], \tag{8}$$

with eigenvalues

$$E_{\pm} = 2\epsilon + \frac{U+K}{2} + J \pm \frac{1}{2}\mathcal{D}, \tag{9}$$

where $\mathcal{D} = \sqrt{(U-K)^2 + 16(t+V)^2}$. The state $|-\rangle$ from (8) is the lowest-energy spin-singlet eigenstate. It is this state for which we determine explicitly the single-particle wave function and subsequently determine the microscopic parameters ϵ, t, U, J, K, and V explicitly, all as a function of interionic distance R.

2.4. Optimization of the atomic basis

The ground-state energy is the energy E_- of (9), supplemented with the ion–ion repulsion, i.e. by

$$E_G = E_- + \frac{2}{R}, \tag{10}$$

where $(2/R)$ is also represented in atomic units. As all the microscopic parameters are only a function of the distance R and the inverse wave-function size α, we have $E_G = E_G(\alpha, R)$. For each distance R, we minimize E_G with respect to α, thus closing the solution. Finally, we select $R = R_B$ as the equilibrium solution, for which the zero-point motion still has to be taken into account.

3. The stationary state for the H_2 molecule

In figure 1 we plot the energy of H_2 (dimer) versus the distance R. It is crucial that we obtain a local (and global) minimum at $R = R_B \equiv 0.757$ Å. This simple result obtained in [9] differs with respect to the virtually exact solution by Kołos and Wolniewicz [21, 22], $R_{K-W} = 0.74$ Å by 2.5% only.

In figure 2 we plot the sequence of the spin-singlets and the spin-triplet states. Parenthetically, the start from second-quantization language allows for evaluation of the ground-state and the lowest excited states, on an equal footing. This feature provides the difference with purely variational calculations in the first-quantization language. Namely,

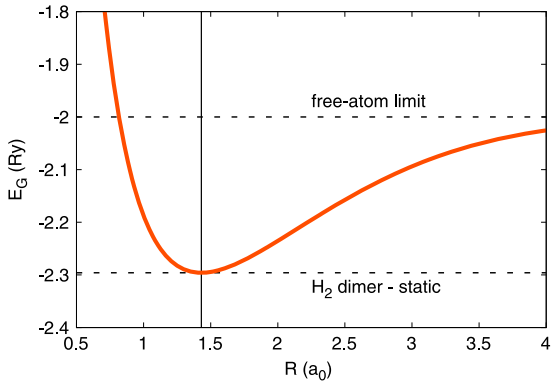

Figure 1. Ground-state energy—as defined by (10)—versus interionic static distance R. Note that the minimum value is $E_B = -2.295\,87\ Ry$ (marked by the vertical line here and below) at $R_B = 1.430\,42\ a_0$.

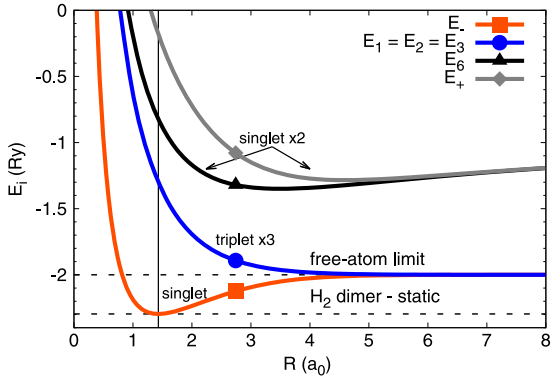

Figure 2. Solutions for the states: the spin-triplets ($E_1 = E_2 = E_3$) and the spin-singlets ($E_\pm$, E_6) versus the interionic distance R. The spin-singlet state $|-\rangle$ is the equilibrium state.

within this basis the spin-singlet state is stable at arbitrary interionic distance R. In figures 3–5 the inverse wave function size α, as well as all the microscopic parameters, are displayed as a function of the bond length R. One can see that with increasing R, the values tend to the proper free-atom limits. Those quantities form an input for the subsequent evaluation of electron–proton coupling constants discussed next.

4. Adiabatic approximation for the electron–ion coupling

Our principal aim here is to extend our previous model [9, 10] by allowing the ions to oscillate around the equilibrium positions. Thus the interionic distance R is taken now in the form

$$R = R_B + \delta R, \tag{11}$$

where δR is responsible for the zero-point motion. The electronic part of the ground-state energy is expanded next on δR in terms of a Taylor series, which to the ninth order reads

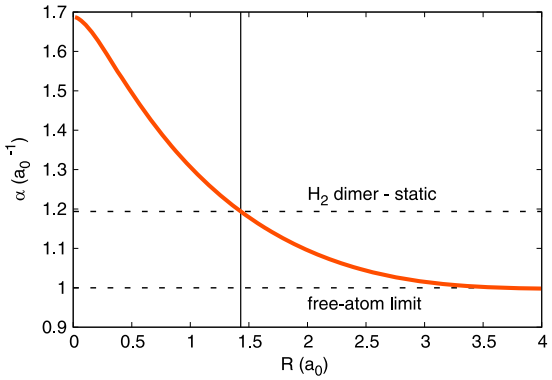

Figure 3. The optimal inverse wave-function size α versus the proton–proton average distance R. Note that $\alpha_B = 1.193\,78 a_0^{-1}$.

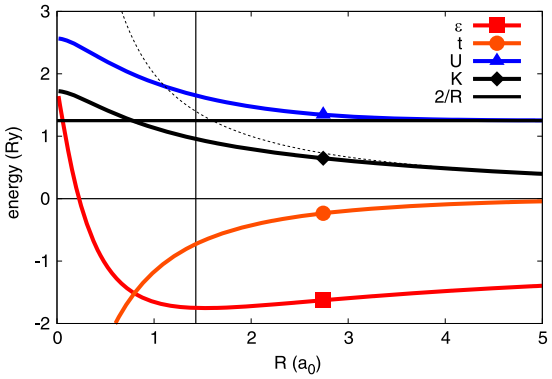

Figure 4. Microscopic parameters ϵ, t, U, and K versus average interionic distance R. Note the convergence of the intersite Coulomb repulsion K to the classical value $2/R$ (dashed line) at $R \to \infty$. The on-site repulsion U also reaches its atomic limit $U_{at} = 1.25\,Ry$, whereas the hopping parameter $t \to 0$.

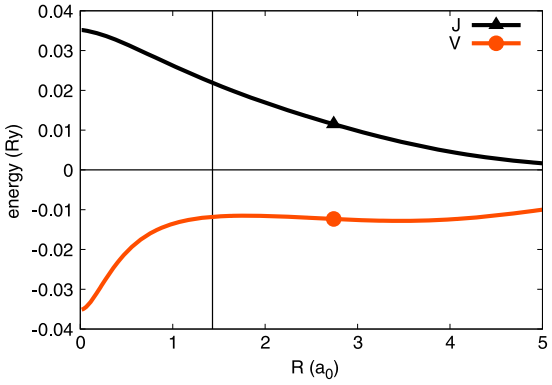

Figure 5. Microscopic parameters J and V versus R. Note that the exchange integral is always ferromagnetic, and the so-called correlated hopping parameter is $V < 0$.

$$\langle \mathcal{H} \rangle_{\delta R} = E_B + \sum_{i=2}^{9} \frac{1}{i!} E_B^{(i)} \delta R^i + O\left(\delta R^{10}\right), \tag{12}$$

where $E_B^{(i)} = \left.\frac{\partial^i E_B}{\partial R^i}\right|_{R_B}$ and $E_B^{(1)} = 0$, whereas all the remaining terms but for the energy E_B describe the oscillations (see table 2 for numerical values). We have modified the Hamiltonian (4) accordingly by taking into account δR, i.e.,

$$\mathcal{H} \to \mathcal{H} + \delta\mathcal{H}, \tag{13}$$

where $\delta\mathcal{H}$ is the additional term. Also, $\mathcal{H}$ simplifies to the form

$$\mathcal{H} = \sum_i \Xi_i \hat{O}_i, \tag{14}$$

where $\Xi = \{\epsilon, t, U, J, K, V\}$ and $\hat{O}_i$ are the corresponding operator parts of Hamiltonian: the two- and four-operator terms of (4) standing next to the respective microscopic parameter (for example $\hat{O}_\epsilon = \hat{n}_1 + \hat{n}_2$). With the Hamiltonian in this form we now have the energy change due to the change of the microscopic parameters

$$\delta\mathcal{H} = \sum_i \delta\Xi_i \hat{O}_i = \sum_i \xi_i \delta R\ \hat{O}_i, \tag{15}$$

where $\xi_i \equiv \frac{\delta \Xi_i}{\delta R}$. Since $\delta R \propto (b_i^\dagger + b_i)$, where $b_i^\dagger$, b_i are bosonic creation and annihilation operators of the system deformation and the set $\{\xi_i\}$ defines a new set of microscopic parameters—the electron–ion coupling constants. They can be derived by differentiation in a way similar to that of [23, 24] (see appendix B for details).

The shift of the ions changes the system properties in the following manner

$$\langle \delta\mathcal{H} \rangle = \sum_i \xi_i \left\langle \hat{O}_i \right\rangle_0 \delta R, \tag{16}$$

where the average $\langle \hat{O}_i \rangle_0 = \langle - \left| \hat{O}_i \right| - \rangle$ is taken with respect to the ground state. In effect, we obtain

$$\left\langle \hat{O}_\epsilon \right\rangle_0 = 2, \tag{17a}$$

$$\left\langle \hat{O}_t \right\rangle_0 = \frac{8|t+V|}{\mathcal{D}}, \tag{17b}$$

$$\left\langle \hat{O}_U \right\rangle_0 = \frac{16(t+V)^2}{2\mathcal{D}(\mathcal{D}+U-K)}, \tag{17c}$$

$$\left\langle \hat{O}_J \right\rangle_0 = 1, \tag{17d}$$

$$\left\langle \hat{O}_K \right\rangle_0 = \frac{\mathcal{D}+U-K}{2\mathcal{D}}, \tag{17e}$$

$$\left\langle \hat{O}_V \right\rangle_0 = \frac{8|t+V|}{\mathcal{D}}. \tag{17f}$$

The R dependence of the parameters $\langle \hat{O}_i \rangle$ given by (17) is displayed in figure 6. As they are of the order of unity, the principal factor determining the relative strength of the coupling

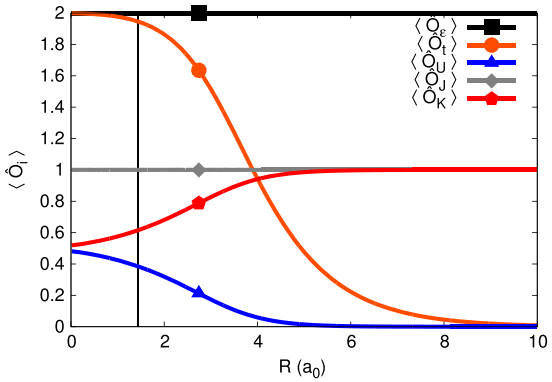

Figure 6. Averages (17) calculated in the ground-state versus distance R. They are of the order of unity.

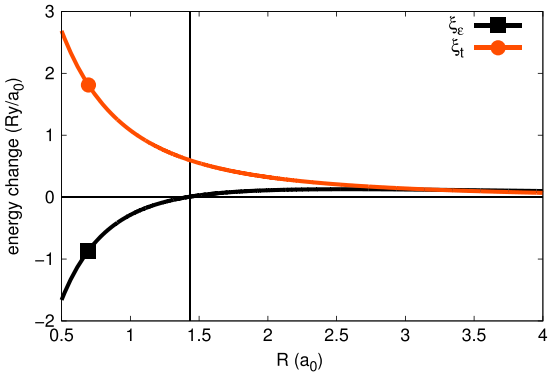

Figure 7. Coupling constants ξ_ϵ and ξ_t versus intersite distance R.

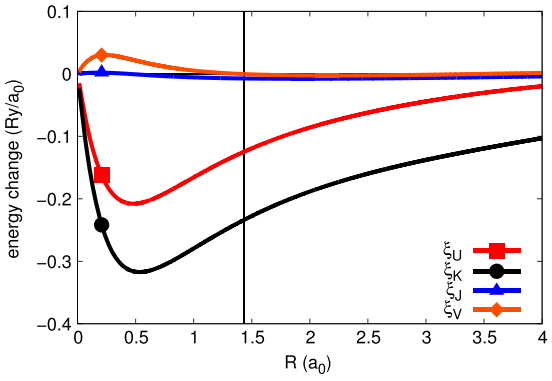

Figure 8. Coupling constants ξ_U, ξ_K, ξ_J and ξ_V versus intersite distance R

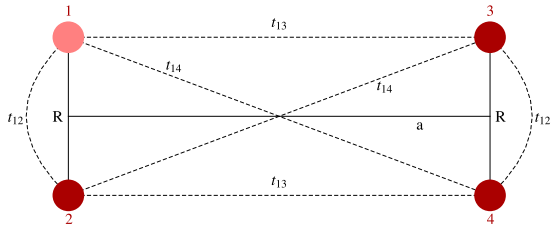

Figure 9. The system of two H_2 molecules at the relative distance a. The hopping integrals t_i are marked next to the respective dashed lines. Note that the orthogonalization procedure for four sites produces a different basis than that obtained in (3).

constants is provided by the parameters $\{\xi_i\}$ displayed in figures 7 and 8. At the equilibrium bond distance marked by the vertical line, the largest values are (on the absolute scale) those coming from modulation of the hopping parameter (ξ_t) and the change of intersite Coulomb interaction (ξ_K). The first of the two has been included in the Su, Schrieffer and Heeger model [25]. The second may play an important role in the high-T_C superconductivity [24]. Also, we see that the so-called Holstein coupling [26] is not important if calculated near the hydrogen-molecule equilibrium state.

We determine the value of δR by minimizing the total energy of the system:

$$E_{\text{total}} \equiv \langle \mathcal{H} \rangle + \langle \delta \mathcal{H} \rangle + \left\langle \mathcal{H}_{\text{ion}} \right\rangle. \tag{18}$$

where

$$\left\langle \mathcal{H}_{\text{ion}} \right\rangle = 2\frac{\delta P^2}{2\,M} + \frac{2}{R + \delta R}. \tag{19}$$

where the ionic momentum δP is evaluated via the Heisenberg principle and $M \overset{a.u.}{\approx} 1836.152\,67$ is the mass of the proton.

5. Evaluation of the microscopic parameters for the two-molecule system

We extend our approach by considering a system of two H_2 dimers at a relative distance a from each other (see figure 9). We calculate the respective hopping integrals, where t_{12} should approach t defined in (A.1*b*) for large a, and the new single-particle energy ϵ should again converge to previously obtained value (A.1*a*). We determine all the two-particle interaction integrals, thus going beyond the Hubbard model solved in [5]. Additionally, in table 1 we list the numerical values of the most relevant microscopic parameters.

The results are presented in figures 10–13. Note that all the results converge to the free-molecule ($a \to \infty$) values. The calculated hopping values of t_{13} and t_{14} may serve as input parameters for H_2 molecular crystal.

Explicitly, in figure 10 we display the intermolecular dependence of single-particle parameters. For the distances $a \gtrsim 2\,a_0$ the hoppings t_{13} and t_{14} can be regarded as small on the scale $t_{12} = t$. Hence, the system in a solid will preserve its molecular character, with no magnetism involved even though we have nominally one electron per atom. In other words, the lowest band will be full and no simple-minded Hubbard subband (HOMO-LUMO) picture in the ground state appears. In figure 11 we compare the relative values of intramolecular (U,

Table 1. Numerical values of single-particle energy (ϵ), the hopping integrals ($t_{\alpha\beta}$), the on-site Coulomb repulsion U and the intramolecular Coulomb interaction K_{12} for the two-molecule system; values refer to the points marked in the figure 13.

R (a_0)	a (a_0)	ϵ (Ry)	t_{12} (Ry)	t_{13} (Ry)	t_{14} (Ry)	U (Ry)	K_{12} (Ry)	K_{13} (Ry)	K_{14} (Ry)
0.715	1.43	−3.4265	−1.5534	−0.9320	0.2799	1.9210	1.2082	1.0480	0.8405
0.715	2.86	−2.9068	−1.3948	−0.2349	0.0993	1.7875	1.1386	0.6790	0.5976
0.715	4.29	−2.5229	−1.3671	−0.0499	0.0339	1.7557	1.1233	0.4674	0.4369
1.43	1.43	−3.4500	−0.8030	−0.8030	0.1023	1.8143	1.0127	1.0127	0.7514
1.43	2.86	−3.0007	−0.7504	−0.2232	0.0279	1.6903	0.9699	0.6732	0.5655
1.43	4.29	−2.6483	−0.7380	−0.0535	0.0096	1.6585	0.9587	0.4666	0.4245
2.145	1.43	−3.2344	−0.4278	−0.7651	0.0500	1.7359	0.8269	0.9858	0.6552
2.145	2.86	−2.8805	−0.4211	−0.2294	0.0013	1.6162	0.8047	0.6674	0.5223
2.145	4.29	−2.5668	−0.4185	−0.0610	−0.0019	1.5839	0.7977	0.4655	0.4056
2.86	1.43	−3.0007	−0.2232	−0.7504	0.0279	1.6903	0.6732	0.9699	0.5655
2.86	2.86	−2.7193	−0.2354	−0.2354	−0.0075	1.5712	0.6631	0.6631	0.4739
2.86	4.29	−2.4410	−0.2385	−0.0670	−0.0066	1.5383	0.6593	0.4646	0.3816

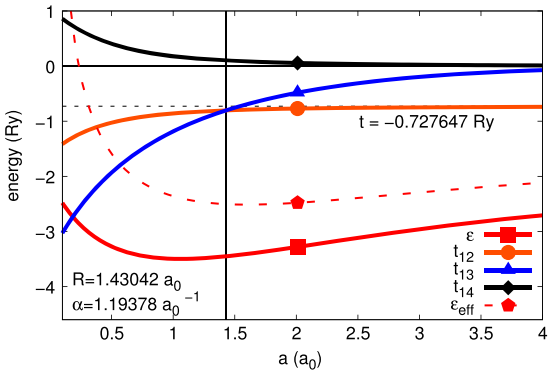

Figure 10. The one-particle microscopic parameters for two H_2 molecules system versus intermolecular distance a. The red dashed line marks the effective (renormalized by ion–ion repulsion) single-particle energy per site $\epsilon_{\text{eff}} = \epsilon + 1/N\sum_i 2/R_i$. Note the convergence of $t_{12} \to t$, and $t_{13},\ t_{14} \to 0$ with $a \to \infty$. The equality of t_{12} and t_{13} at $a = R_B = 1.430\,42\,a_0$ should be observed as well.

Table 2. The numerical values of coefficients in Taylor series of ground-state energy. Up to the term $E_B^{(6)}$ all of the derivatives are calculated analytically from equation (10). Orders seventh–ninth (marked by an asterisk) were calculated numerically due to complicated analytical expression for ground-state energy.

$E_B^{(1)}\left(\frac{Ry}{a_0}\right)$	0.0
$\frac{1}{2!}E_B^{(2)}\left(\frac{Ry}{a_0^2}\right)$	0.430 045
$\frac{1}{3!}E_B^{(3)}\left(\frac{Ry}{a_0^3}\right)$	−0.464 021
$\frac{1}{4!}E_B^{(4)}\left(\frac{Ry}{a_0^4}\right)$	0.354 584
$\frac{1}{5!}E_B^{(5)}\left(\frac{Ry}{a_0^5}\right)$	−0.253 393
$\frac{1}{6!}E_B^{(6)}\left(\frac{Ry}{a_0^6}\right)$	0.174 863
$\frac{1}{7!}E_B^{(7)}\left(\frac{Ry}{a_0^7}\right)^*$	−0.119 178
$\frac{1}{8!}E_B^{(8)}\left(\frac{Ry}{a_0^8}\right)^*$	0.081 758 6
$\frac{1}{9!}E_B^{(9)}\left(\frac{Ry}{a_0^9}\right)^*$	−0.056 383 7

$K_{12} = K$) versus intermolecular (K_{13}, K_{14}) Coulomb interactions. Again, intramolecular interactions dominate for $a \gtrsim 2\,a_0$. From figures 10 and 11 it follows then that in the insulating (molecular-crystal) state, virtual hopping processes will contribute and renormalize the gap between the full-band (valence) and the conduction-band (excited single electron) states in a similar manner to the kinetic exchange. This gap will have the form of the Hubbard gap, as the value of U, corresponding to the transition $2H_2 \to H_2^- + H_2^+$ will have the value

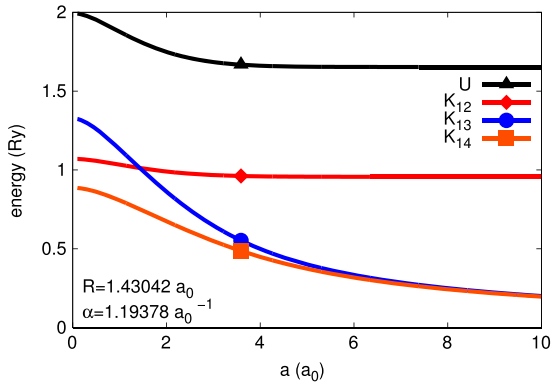

Figure 11. Coulomb-interaction microscopic parameters: the on-site part (U), intramolecular (K_{12}), and intermolecular K_{13} and K_{14} for two H_2-molecule system versus intermolecular distance a.

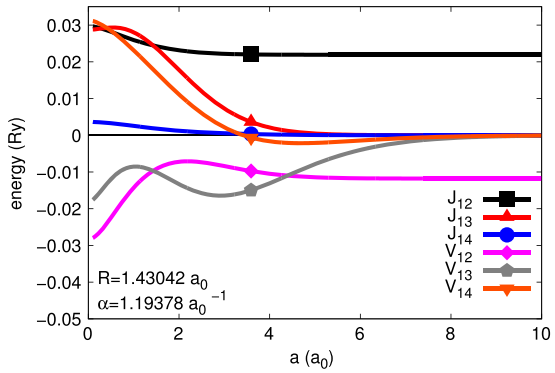

Figure 12. Two-particle microscopic parameters: intramolecular spin-exchange J_{12} and correlated hopping V_{12}, as well as the intermolecular parameters J_{13}, J_{14}, V_{13} and V_{14} for two H_2 molecules system versus intermolecular distance a. Note that all the intermolecular parameters converge to zero quickly.

$U - K_{12} \approx 0.6\,Ry$, by far the largest energy in the insulating state. For the sake of completeness, we have plotted in figure 12 the remaining interaction parameters: the exchange integrals, intra- (J_{12}) and inter-molecular (J_{13} and J_{14}), as well as the correlated hopping amplitudes: V_{12} and (V_{13} and V_{14}), respectively.

In figure 14 we show the difference between the energies of the $\left(H_2\right)_2$ system and that of the free molecules (per molecule):

$$\Delta E_{H_2} = \frac{E_{(H_2)_2}}{2} - E_B, \tag{20}$$

where $E_{(H_2)_2}$ is the energy of the $\left(H_2\right)_2$ system and $E_B = -2.295\,87\,Ry$ is the energy of single molecule. The equilibrium parameters are $\Delta E_{H_2} = -0.011\,29\,Ry$ and $a = 4.5a_0$. Those results are in agreement with the earlier estimates [28]. The stability of hydrogen molecular clusters were also studied in [29, 30]; our approach coherently incorporates electronic correlations (a

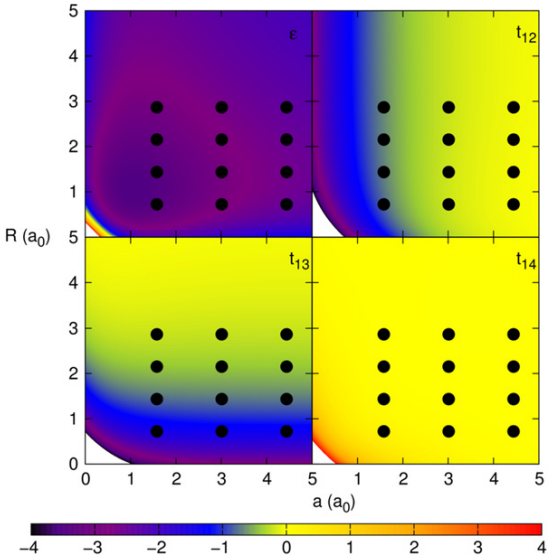

Figure 13. The one-particle microscopic parameters (in Ry) for the two H_2 molecule system versus intermolecular distance a and interionic distance R. Note the symmetry of ϵ and t_{14}. As expected for relatively small distances, values of t_{12} and t_{13} are negative whereas t_{14} is positive. When approaching point (0, 0) all parameters diverge to negative (t_{12} and t_{13}) or positive (ϵ and t_{14}) infinity. The explicit values of the marked points are given in table 1

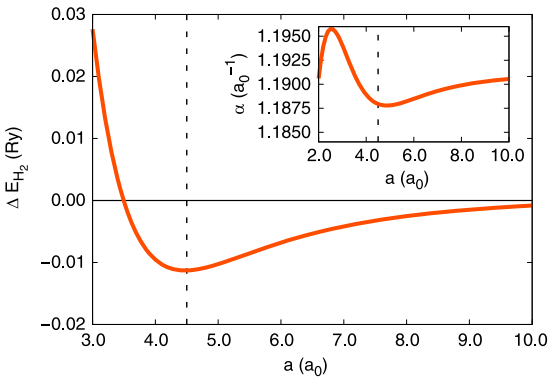

Figure 14. Difference between the energies of the $\left(H_2\right)_2$ system and that of the free molecules (per molecule) versus intermolecular distance a. Note the van der Waals-like behavior with the shallow minimum at $a = 4.5\ a_0$. Inset: inverse atomic wave-function size α versus a. For $a \to \infty$, it approaches the value $\alpha_B = 1.193\ 78\ a_0^{-1}$. The behavior is similar to the one in [27].

necessity in describing the non-polar systems) into the molecular picture, which plays an important role in view of the existence of the minima of the $\Delta E_{H_2}(a)$ curve [28, 29].

Table 3. The values (in atomic units) of the microscopic parameters of Hamiltonian (4) and the electron–ion coupling constants from (15) at the hydrogen-molecule equilibrium ($R = R_B$ and $\alpha = \alpha_B$).

microscopic paramters (Ry)		coupling constants (Ry/a_0)	
ϵ	−1.750 79	ξ_ϵ	0.006 161 65
t	−0.727 647	ξ_t	0.598 662
U	1.653 21	ξ_U	−0.124 934
K	0.956 691	ξ_K	−0.234 075
J	0.021 9085	ξ_J	−0.007 463 03
V	−0.011 7991	ξ_V	−0.000 426 452

6. Discussion of results and outlook

The evaluation of the global parameters of the system can be summarized as follows:

1. The H_2 binding energy is $E_B = -2.295\,87Ry$. This value can be compared to the Kołos-Wolniewicz value [21]: $E_{\mathrm{K-W}} = -2.349\,Ry$, which is about 2.26% lower than the value obtained here.
2. The increase of the binding energy here is due to the zero-point motion, which is

$$E_{ZPM} = 0.024\,072Ry, \tag{21}$$

   and is of the order 1.0485% of the binding energy.
3. Whereas the bond length is here $R_B = 1.430\,42\,a_0$ (as compared to $R_{\mathrm{K-W}} = 1.3984\,a_0$, which is 2.29% lower), the zero-point motion amplitude is $|\delta\mathbf{R}| = 0.189\,028\,a_0$, a rather large value. Note that the optimal size of the inverse orbit of the $1s$ component hydrogen orbital is $\alpha_B = 1.193\,78\,a_0^{-1}$, so that the effective Bohr orbit is $a \equiv \alpha^{-1} = 0.8377\,a_0$. The Bohr orbit decrease is due to the increased binding of electron in the molecule $\sim$0.2932 Ry with respect to that in the hydrogen atom. The size a is substantially smaller than that of $1s$ orbit (1.06 Å) in H atom [9].
4. The ion–electron coupling constants versus R are shown in figures 7 and 8, whereas their values for $R = R_B$ are listed in table 3. We also provide the second-order coupling constants values at the hydrogen-molecule equilibrium in table 4. Our first-principle calculations allow us to claim that the coupling constant appearing in the Holstein model [26] (ξ_ϵ) is decisively smaller than those of the Su, Schrieffer and Heeger model [25] (ξ_t) as well as of those coming from the intersite direct Coulomb interaction (ξ_K). This should not be surprising, as the dominant coupling parameters represent interatomic-vibration contributions. A separate branch is represented by phonon excitations, but their analysis requires a construction of a spatially extended system of the molecules.

The question is to what extent the calculated local characteristics will represent their local counterparts in the molecular-solid phase. Certainly, the phonons and the molecule-rotational degrees of freedom will represent low-energy excitations. But the zero-point motion energy of

Table 4. The values (in atomic units) of the second-order electron–ion coupling constants $\xi_i^2 = \delta^2\Xi/\delta R^2$ at the hydrogen-molecule equilibrium ($R = R_B$ and $\alpha = \alpha_B$).

coupling constants (Ry/a_0^2)	
ξ_ϵ^2	0.327 335
ξ_t^2	−0.560 426
ξ_U^2	0.050 4027
ξ_K^2	0.013 028
ξ_J^2	−0.006 715 66
ξ_V^2	−0.010 5204

the whole molecule should have to be added. Will this provide a reliable description of the molecular or atomic hydrogen even though our accuracy in determining the individual-molecule energy is about 2% higher than the virtually exact value of Kołos and Wolniewicz [21]? One has to check and this task is under consideration in our group. Such consideration must include the inter-molecular hopping integrals t_{13} and t_{14}. One should also note that the proper method of treating the few-site H_2-molecule system is the quantum-Monte-Carlo-method [31–33]. Nonetheless, our method evaluates both the system energetics and the wave-function renormalization at the same time in the correlated state.

One can also extend the present model of the molecular binding by also including $2s$ and $2p$ adjustable hydrogen orbitals in the Hilbert space of the single-particle states via the corresponding Gaussian representation. The first estimate of the $2s$-orbital contribution to selected microscopic parameters is briefly discussed in appendix D. Their numerical values are provided in 6. One can see that the basis extension leads to the numerically relevant corrections. This is an additional route to follow, but only after the first-principle calculations of the solid phase along the lines discussed here is undertaken and tested.

Very recently [34], the dynamical mean field theory (DMFT) has been applied to the H_2 molecule and its accuracy tested. Our approach in this respect is much simpler, but still provides comparable accuracy. Also, we have calculated the vibronic coupling constants, which have been determined accurately recently [35]. Those results compare well with our estimates. This circumstance shows again that our method forms a proper starting point for treatment of solid molecular hydrogen, as a correlated state, at least in the insulating phase.

Acknowledgments

The authors (APK & JS) are grateful the Foundation for Polish Science (FNP) for financial support within the TEAM Project. MA is grateful to the Jagiellonian University for hospitality and FNP for a partial support for his visit. JS is grateful to the National Science Center (NCN) for the support within the MAESTRO project, grant no. DEC-2012/04/A/ST3/00342. APK's visit to the University of Parma has been financially supported by the grant of the Polish Ministry of Science and Higher Education, grant no. 7150/E-338/M/2013. MMM acknowledges support by the Polish National Science Center (NCN) under grant no. DEC-2013/11/B/ST3/00824.

Appendix A. Exact solution without the zero-point motion

For the sake of completeness we express the microscopic parameters defined in (5) in terms of *single-particle parameters* via (2)

$$\epsilon = \beta^2\Big(1+\gamma^2\Big)\epsilon' - 2\beta^2\gamma t', \tag{A.1a}$$

$$t = \beta^2\Big(1+\gamma^2\Big)t' - 2\beta^2\gamma\epsilon', \tag{A.1b}$$

$$U = \beta^4\Big[\Big(1+\gamma^4\Big)U' + 2\gamma^2K' - 4\gamma\Big(1+\gamma^2\Big)V' + 4\gamma^2J'\Big], \tag{A.1c}$$

$$K = \beta^4\Big[2\gamma^2U' + \Big(1+\gamma^4\Big)K' - 4\gamma\Big(1+\gamma^2\Big)V' + 4\gamma^2J'\Big], \tag{A.1d}$$

$$J = \beta^4\Big[2\gamma^2U' + 2\gamma^2K' - 4\gamma\Big(1+\gamma^2\Big)V' + \Big(1+\gamma^2\Big)^2J'\Big], \tag{A.1e}$$

$$V = \beta^4\Big[-\gamma\Big(1+\gamma^2\Big)U' - \gamma\Big(1+\gamma^2\Big)K' + \Big(1+6\gamma^2+\gamma^4\Big)V' - 2\gamma\Big(1+\gamma^2\Big)J'\Big], \tag{A.1f}$$

where Ξ' parameters are

$$T_{ij}{}' = \Big\langle \Psi_i \,|\mathcal{T}|\, \Psi_j \Big\rangle, \tag{A.2a}$$

$$V'_{ijkl} = \Big\langle \Psi_i\Psi_j \,\Big|\, \mathcal{V}_{12} \,\Big|\, \Psi_k\Psi_l \Big\rangle, \tag{A.2b}$$

with $\mathcal{T} = -\bigtriangledown^2 - 2/|\mathbf{r}-\mathbf{R}|$, and $\mathcal{V} = 2/|\mathbf{r}-\mathbf{r}'|$. *The single-particle parameters* read

$$\epsilon' = \alpha^2 - 2\alpha - \frac{2}{R} + 2\Big(\alpha + \frac{1}{R}\Big)e^{-2\alpha R}, \tag{A.3a}$$

$$t' = \alpha^2 e^{-\alpha R}\Big(1 + \alpha R - \frac{1}{3}\alpha^2R^2\Big) - 4\alpha e^{-\alpha R}(1+\alpha R), \tag{A.3b}$$

$$U' = \frac{5}{4}\alpha, \tag{A.3c}$$

$$K' = \frac{2}{R} - \alpha e^{-2\alpha R}\Big(\frac{2}{\alpha R} + \frac{3}{2}\alpha R + \frac{1}{3}\alpha^2R^2 + \frac{11}{4}\Big), \tag{A.3d}$$

$$V' = \alpha e^{-\alpha R}\left(2\alpha R + \frac{1}{4} + \frac{5}{8\alpha R}\right) - \frac{1}{4}\alpha e^{-3\alpha R}\left(1 + \frac{5}{2\alpha R}\right), \tag{A.3e}$$

$$J' = \alpha e^{-2\alpha R}\left(\frac{5}{4} - \frac{23}{10}\alpha R - \frac{6}{5}\alpha^2 R^2 - \frac{2}{15}\alpha^3 R^3\right) + \frac{12}{5R}\left(S^2 C_E + S^2 \log(\alpha R) - 2\, S\bar{S}\,\mathrm{Ei}(-2\alpha R) + \bar{S}^2\mathrm{Ei}(-4\alpha R)\right), \tag{A.3f}$$

where the overlaps are given by

$$S = e^{-\alpha R}\left(1 + \alpha R + \frac{1}{3}\alpha^2 R^2\right), \tag{A.4}$$

$$\bar{S} = e^{\alpha R}\left(1 - \alpha R + \frac{1}{3}\alpha^2 R^2\right). \tag{A.5}$$

C_{E} is so-called Euler constant

$$C_{\mathrm{E}} = \lim_{n\to\infty}\left(\sum_{k=1}^{n}\frac{1}{k} - \log(n)\right) \approx 0.5772, \tag{A.6}$$

and $Ei(x)$ is the exponential integral.

$$Ei(x) = -\int_{-x}^{\infty} e^{-t}t^{-1}\mathrm{d}t. \tag{A.7}$$

Appendix B. Adiabatic-approximation details

For the sake of completeness, we also provide the explicit form of the coupling constants $\xi_i \equiv \mathrm{d}\Xi_i/\mathrm{d}R$. For editorial purposes we calculate first *the single-particle coupling constants* from (A.3*a*). They are

$$\delta\epsilon' = 2R^{-2}e^{-2\alpha R}\left[e^{2\alpha R} - 1 - 2\,R\alpha\left(1 + \alpha R\right)\right], \tag{B.1a}$$

$$\delta t' = \frac{1}{3}e^{-\alpha R}\alpha^3\, R\,[12 + \alpha(-5 + \alpha R)], \tag{B.1b}$$

$$\delta U' = 0. \tag{B.1c}$$

The corresponding derivatives of the two-particle parameters are

$$\delta K' = \frac{1}{3}R^{-2}e^{-2\alpha R}\left[6 - 6e^{2\alpha R} + \alpha R(2 + \alpha R)(6 + \alpha R(3 + 2\alpha R))\right] \tag{B.1d}$$

$$\delta V' = \frac{1}{8}R^{-2}\Big(e^{-3\,R\alpha}\Big[5 + 15\,R\alpha + 6R^2\alpha^2\Big] - e^{-R\alpha}\Big[5 + 5R\alpha - 14R^2\alpha^2 + 16R^3\alpha^3\Big]\Big) \quad \text{(B.1}e\text{)}$$

$$\begin{aligned}\delta J' = \frac{1}{15R^2}e^{-2\,R\alpha}\Big(&-4C_E\Big[9 + 18R\alpha + 21R^2\alpha^2 + 18R^3\alpha^3 + 9R^4\alpha^4 + 2R^5\alpha^5\Big]\\ &+ R^2\alpha^2\Big[72 + 33R\alpha + 30R^2\alpha^2 + 4R^3\alpha^3\Big] + 4e^{4\,R\alpha}\\ &\times\Big[-9 + 18R\alpha - 21R^2\alpha^2 + 18R^3\alpha^3 - 9R^4\alpha^4 + 2R^5\alpha^5\Big]\mathrm{Ei}\Big(-4R\alpha\Big)\\ &- 24e^{2\,R\alpha}\Big(-3 - R^2\alpha^2 + R^4\alpha^4\Big)\mathrm{Ei}\Big(-2R\alpha\Big) - 36\log(R\alpha)\\ &- 4R\alpha\Big(18 + 21R\alpha + 18R^2\alpha^2 + 9R^3\alpha^3 + 2R^4\alpha^4\Big)\log(R\alpha)\Big)\end{aligned} \quad \text{(B.1}f\text{)}$$

with basis mixing-parameters β and γ (see (3)) changes

$$\delta\beta = \frac{S}{4\Big(1 - S^2\Big)\beta}\left(\frac{1}{\sqrt{1 - S^2}} + \frac{1}{2\Big(1 - S^2\Big)}\right)\delta S, \quad \text{(B.2)}$$

$$\delta\gamma = \frac{1}{1 - S^2 + \sqrt{1 - S^2}}\delta S, \quad \text{(B.3)}$$

where S is the overlap (A.4) and δS reads

$$\delta S = -\frac{1}{3}e^{-R\alpha}R\alpha^2\Big(1 + R\alpha\Big). \quad \text{(B.4)}$$

Our final results are

$$\begin{aligned}\xi_\epsilon = 2\frac{\delta\beta}{\beta}\epsilon + \beta^2\Big[&\Big(1 + \gamma^2\Big)\delta\epsilon' - 2\gamma\delta t'\Big]\\ &+ 2\beta^2\delta\gamma\,[\gamma\epsilon' - t'],\end{aligned} \quad \text{(B.5}a\text{)}$$

$$\begin{aligned}\xi_t = 2\frac{\delta\beta}{\beta}t + \beta^2\Big[&\Big(1 + \gamma^2\Big)\delta t' - 2\gamma\delta\epsilon'\Big]\\ &+ 2\beta^2\delta\gamma\,[\gamma t' - \epsilon'],\end{aligned} \quad \text{(B.5}b\text{)}$$

$$\begin{aligned}\xi_U = 4\frac{\delta\beta}{\beta}U + \beta^4\Big[&\Big(1 + \gamma^4\Big)\delta U' + 2\gamma^2\delta K'\\ &- 4\gamma\Big(1 + \gamma^2\Big)\delta V' + 4\gamma^2\delta J'\Big]\\ &+ 4\beta^4\delta\gamma\Big[\gamma^3U' + \gamma K'\\ &- \Big(1 + 3\gamma^2\Big)V' + 2\gamma J'\Big],\end{aligned} \quad \text{(B.5}c\text{)}$$

$$\xi_K = 4\frac{\delta\beta}{\beta}K + \beta^4\Big[\,2\gamma^2\delta U' + \left(1+\gamma^4\right)\delta K' - 4\gamma\left(1+\gamma^2\right)\delta V' + 4\gamma^2\delta J'\Big] + 4\beta^4\delta\gamma\Big[\,\gamma U' + \gamma^3 K' - \left(1+3\gamma^2\right)V' + 2\gamma J'\Big], \tag{B.5d}$$

$$\xi_J = 4\frac{\delta\beta}{\beta}J + \beta^4\Big[\,2\gamma^2\delta U' + 2\gamma^2\delta K' - 4\gamma\left(1+\gamma^2\right)\delta V' + \left(1+\gamma^2\right)^2\delta J'\Big] + 4\beta^4\delta\gamma\,[\gamma U' + \gamma K' - \left(1+3\gamma^2\right)V' + \gamma\left(1+\gamma^2\right)J'\Big], \tag{B.5e}$$

$$\xi_V = 4\frac{\delta\beta}{\beta}V - \beta^4\Big[\,\gamma\left(1+\gamma^2\right)\delta U' + \gamma\left(1+\gamma^2\right)\delta K' - \left(1+6\gamma^2+\gamma^4\right)\delta V' + 2\gamma\left(1+\gamma^2\right)\delta J'\Big] - \beta^4\delta\gamma\Big[\left(1+3\gamma^2\right)U' + \left(1+3\gamma^2\right)K' - 4\gamma\left(3+\gamma^2\right)V' + 2\left(1+3\gamma^2\right)J'\Big]. \tag{B.5f}$$

These parameters are displayed versus R in figures 7 and 8.

Appendix C. Zero-point motion with classical electronic interaction

We ask the question of how important it is to include the quantum nature of the electronic interaction in our evaluation of zero-point motion energy. Let us consider, following [9], the energy of the ions as

$$E_{\text{ion}} = \frac{\delta P^2}{2M} + \frac{e^2}{R+\delta R}, \tag{C.1}$$

where δP and δR are the momentum and position uncertainties, M is ion mass and e its charge. By expressing δP by δR via the uncertainty relation $\delta P^2\delta R^2 \geqslant \frac{3}{4}\hbar^2$ we obtain

$$E_{\text{ion}} = \frac{\frac{3}{4}\hbar^2}{2M\delta R^2} + \frac{e^2}{R+\delta R}, \tag{C.2}$$

Table C.1 The values (in atomic units) of the zero-point motion energy and amplitude. The classical electron interaction approximation versus adiabatic approximation.

	$\lvert\delta\mathbf{R}_0\rvert$ (a_0)	E_{ZPM} (Ry)
classical interaction	0.0901816	0.14434
quantum interaction	0.189028	0.024072

which we can minimize with respect to δR. We calculate

$$\delta R_0 \overset{a.u.}{=} \frac{1}{4\sqrt{2}M}\left(a - 1 + \frac{1 - 8\sqrt{2}MR}{a}\right), \tag{C.3}$$

where

$$a \overset{a.u.}{=} \Big[-1 + 12\,MR\left(\sqrt{2} - 4\,MR\right) + 2^{15/4}\sqrt{M^3R^3\left(-1 + 9\sqrt{2}MR\right)}\Big]^{1/3}. \tag{C.4}$$

We take the mass of the ion $M \overset{a.u.}{\approx} 1836.15267\,m_0$ and the interionic distance $R = R_B = 1.430\,17a_0$. The results are presented in the table C.1.

Appendix D. Inclusion of 2*s* orbitals

We would like to estimate the role of higher orbitals both for more realistic description of H_2 systems and future consideration of other elements. We start by taking the $2s$ Slater-type orbital

$$\Psi^{2s}(\mathbf{r}) \equiv \sqrt{\frac{\alpha_{2s}^5}{3\pi}}\ |\mathbf{r}|\ e^{-\alpha_{2s}|\mathbf{r}|}, \tag{D.1}$$

where α_{2s} is the inverse wave function size. It is obviously non-orthogonal with the $1s$ orbital (1) as we have that

$$S_{on}^{\alpha,\,\alpha_{2s}} \equiv \left\langle \Psi^{1s} \middle| \Psi^{2s} \right\rangle = \frac{8\sqrt{3}\,\alpha^{3/2}\alpha_{2s}^{5/2}}{(\alpha + \alpha_{2s})^4}. \tag{D.2}$$

D.1. On-site orthogonalization

We perform the orthogonalization by introducing realistic orbital functions [36]

$$\chi^{1s}(\mathbf{r}) = \Psi^{1s}(\alpha,\,\mathbf{r}), \tag{D.3}$$

$$\chi^{2s}(\mathbf{r}) = A\Psi^{1s}(\alpha_{2s},\,\mathbf{r}) + B\Psi^{2s}(\alpha_{2s},\,\mathbf{r}), \tag{D.4}$$

where A and B are mixing parameters obtained via orthonormality conditions

$$\left\langle \chi^{1s} \middle| \chi^{2s} \right\rangle = 0,$$
$$\left\langle \chi^{2s} \middle| \chi^{2s} \right\rangle = 1. \tag{D.5}$$

We can solve problem (D.5) analytically and obtain

$$A = -\frac{S_{on}^{\alpha,\,\alpha_{2s}}}{\sqrt{S_{1s}^{\alpha,\,\alpha_{2s}2} - 2S_{1s}^{\alpha,\,\alpha_{2s}}S_{\rm on}^{\alpha,\,\alpha_{2s}}S_{\rm on}^{\alpha_{2s},\,\alpha_{2s}} + S_{\rm on}^{\alpha,\,\alpha_{2s}2}}},$$
$$B = \frac{S_{1s}^{\alpha,\,\alpha_{2s}}}{\sqrt{S_{1s}^{\alpha,\,\alpha_{2s}2} - 2S_{1s}^{\alpha,\,\alpha_{2s}}S_{\rm on}^{\alpha,\,\alpha_{2s}}S_{\rm on}^{\alpha_{2s},\,\alpha_{2s}} + S_{\rm on}^{\alpha,\,\alpha_{2s}2}}}, \tag{D.6}$$

where $S_{\rm on}$ is given by (D.6) and

$$S_{1s}^{\alpha,\,\alpha_{2s}} \equiv \left\langle \Psi^{1s} \middle| \Psi^{1s} \right\rangle = \frac{8(\alpha\alpha_{2s})^{3/2}}{(\alpha + \alpha_{2s})^3}. \tag{D.7}$$

D.2. Intersite orthogonalization

As χ^σ s are orthogonal on-site, one can also introduce intersite orthogonalization. We introduce the following mixing coefficients (2)

$$w_i^\sigma(\mathbf{r}) = \beta^\sigma\left(\chi_i^\sigma(\mathbf{r}) - \gamma^\sigma\chi_j(\mathbf{r})\right), \tag{D.8}$$

where β^σ and γ^σ depend only on the overlap integral $S^\sigma \equiv \langle\chi_1^\sigma|\chi_2^\sigma\rangle$:

$$\beta^\sigma = \frac{1}{\sqrt{2}}\sqrt{\frac{1 + \sqrt{1 - \left(S^\sigma\right)^2}}{1 - \left(S^\sigma\right)^2}} \tag{D.9}$$

$$\gamma^\sigma = \frac{S^\sigma}{1 + \sqrt{1 - \left(S^\sigma\right)^2}}. \tag{D.10}$$

We already have overlap S^{1s} (A.4).

Overlap S^{2s} is only a little bit more complicated

$$\begin{aligned} S^{2s} &= \left\langle \chi_1^{2s} \middle| \chi_2^{2s} \right\rangle = \left\langle A\Psi_1^{1s} + B\Psi_1^{2s} \middle| A\Psi_2^{1s} + B\Psi_2^{2s} \right\rangle \\ &= A^2\left\langle \Psi_1^{1s} \middle| \Psi_2^{1s} \right\rangle + 2\,AB\left\langle \Psi_1^{1s} \middle| \Psi_2^{2s} \right\rangle + B^2\left\langle \Psi_1^{2s} \middle| \Psi_2^{2s} \right\rangle \\ &= A^2S^{1s,\alpha_{2s}} + 2\,ABS^{1s,2s} + B^2S^{2s}, \end{aligned} \tag{D.11}$$

where

$$S^{1s,2s} = \frac{e^{\alpha_{2s}(-R)}\left(\alpha_{2s}R\left(\alpha_{2s}R\left(\alpha_{2s}R + 4\right) + 9\right) + 9\right)}{6\sqrt{3}}, \tag{D.12}$$

$$S^{2s} = \frac{1}{45}e^{\alpha_{2s}(-R)}\left(\alpha_{2s}R\left(\alpha_{2s}R\left(\alpha_{2s}R\left(\alpha_{2s}R + 5\right) + 20\right) + 45\right) + 45\right). \tag{D.13}$$

D.3. Single-particle microscopic parameters

Introducing $2s$ orbitals provides us with four new single-particle microscopic parameters

$$\epsilon_{2s} = \left\langle w_i^{2s}(\mathbf{r}) \left| \mathcal{H}_1 \right| w_i^{2s}(\mathbf{r}) \right\rangle, \tag{D.14a}$$

$$t_{2s} = \left\langle w_i^{2s}(\mathbf{r}) \left| \mathcal{H}_1 \right| w_{\bar{i}}^{2s}(\mathbf{r}) \right\rangle, \tag{D.14b}$$

$$V_{on} = \left\langle w_i^{1s}(\mathbf{r}) \left| \mathcal{H}_1 \right| w_i^{2s}(\mathbf{r}) \right\rangle, \tag{D.14c}$$

$$V_{inter} = \left\langle w_i^{1s}(\mathbf{r}) \left| \mathcal{H}_1 \right| w_{\bar{i}}^{2s}(\mathbf{r}) \right\rangle, \tag{D.14d}$$

where ϵ_{2s} is single-particle energy on the $2s$ orbital, t_{2s} the hopping between $2s$ sites, and V_{on} and V_{inter} are hybridizations on- and inter-site respectively.

Similarly to sections appendix A and B, the exact solution is a function of Slater microscopic parameters

$$\begin{aligned}\epsilon_{2s} = \beta^{2s^2}\Big(A^2\Big(\big(\gamma^2+1\big)\epsilon'_{1s} - 2\gamma t'_{1s}\Big) + 2\,AB\Big(\big(\gamma^2+1\big)V'_{\mathrm{on}} - 2\gamma V'_{\mathrm{inter}}\Big) \\ + B^2\Big(\big(\gamma^2+1\big)\epsilon'_{2s} - 2\gamma t'_{2s}\Big)\Big),\end{aligned} \tag{D.15a}$$

$$\begin{aligned}t_{2s} = \beta^{2s^2}\Big(A^2\Big(\big(\gamma^2+1\big)t'_{1s} - 2\gamma \epsilon'_{1s}\Big) + 2\,AB\Big(\big(\gamma^2+1\big)V'_{\mathrm{inter}} - 2\gamma V'_{\mathrm{on}}\Big) \\ + B^2\Big(\big(\gamma^2+1\big)t'_{2s} - 2\gamma \epsilon'_{2s}\Big)\Big),\end{aligned} \tag{D.15b}$$

$$\begin{aligned}V_{\mathrm{on}} = \beta^{1s}\beta^{2s}\Big(A\Big(\big(\gamma^{1s}\gamma^{2s}+1\big)\epsilon''_{1s} - \big(\gamma^{1s}+\gamma^{2s}\big)t''_{1s}\Big) \\ + B\Big(\big(\gamma^{1s}\gamma^{2s}+1\big)V''_{\mathrm{on}} - \big(\gamma^{1s}+\gamma^{2s}\big)V''_{\mathrm{inter}}\Big)\Big),\end{aligned} \tag{D.15c}$$

$$\begin{aligned}V_{\mathrm{inter}} = \beta^{1s}\beta^{2s}\Big(A\Big(\big(\gamma^{1s}\gamma^{2s}+1\big)t''_{1s} - \big(\gamma^{1s}+\gamma^{2s}\big)\epsilon''_{1s}\Big) \\ + B\Big(\big(\gamma^{1s}\gamma^{2s}+1\big)V''_{\mathrm{inter}} - \big(\gamma^{1s}+\gamma^{2s}\big)V''_{\mathrm{on}}\Big)\Big),\end{aligned} \tag{D.15d}$$

where A and B are found via (D.5), while β^{σ} and γ^{σ} via (D.9). The Slater microscopic parameters can be explicitly written in a form

$$\epsilon'_{1s} = \frac{1}{R}e^{-2\alpha_{2s}R}\Big(2\alpha_{2s}R + e^{2\alpha_{2s}R}\Big(\big(\alpha_{2s}-2\big)\alpha_{2s}R - 2\Big) + 2\Big) \tag{D.16}$$

$$t'_{1s} = -\frac{1}{3}\alpha_{2s}e^{\alpha_{2s}(-R)}\big(\alpha_{2s}\big(R\big(\alpha_{2s}\big(\alpha_{2s}R-3\big)+12\big)-3\big)+12\big), \tag{D.17}$$

$$\begin{aligned}\epsilon'_{2s} = \frac{1}{3R}e^{-2\alpha_{2s}R}\Big(e^{2\alpha_{2s}R}\big(\big(\alpha_{2s}-3\big)\alpha_{2s}R - 6\big) \\ + \alpha_{2s}R\big(2\alpha_{2s}R\big(\alpha_{2s}R+3\big)+9\big)+6\big),\end{aligned} \tag{D.18}$$

$$t'_{2s} = -\frac{1}{45}\alpha_{2s}e^{\alpha_{2s}(-R)}\big(\alpha_{2s}\big(R\big(\alpha_{2s}\big(R\big(\alpha_{2s}R\big(\alpha_{2s}\big(\alpha_{2s}R-5\big)+10\big)+40\big)-15\big)+90\big)-15\big)+90\big), \tag{D.19}$$

$$V'_{on} = \frac{1}{2\sqrt{3}R}e^{-2\alpha_{2s}R}\Big(4\alpha_{2s}^2R^2+8\alpha_{2s}R+e^{2\alpha_{2s}R}\Big(\big(\alpha_{2s}-4\big)\alpha_{2s}R-6\Big)+6\Big), \tag{D.20}$$

$$V'_{inter} = -\frac{1}{6\sqrt{3}}\alpha_{2s}e^{\alpha_{2s}(-R)}\Big(\alpha_{2s}^4R^3-4\alpha_{2s}^3R^2+3\alpha_{2s}^2R(4R-1)+3\alpha_{2s}(8R-1)+24\Big), \tag{D.21}$$

$$\epsilon''_{1s} = \frac{8(\alpha\alpha_{2s})^{3/2}}{R(\alpha+\alpha_{2s})^3}e^{-R(\alpha+\alpha_{2s})}\Big(R(\alpha+\alpha_{2s})+e^{R(\alpha+\alpha_{2s})}\times\big(\big(\alpha-1\big)\alpha_{2s}R+\alpha\big(-R\big)-2\big)+2\Big), \tag{D.22}$$

$$\begin{aligned} t''_{2s} = -\frac{8(\alpha\alpha_{2s})^{3/2}}{R\left(\alpha^2-\alpha_{2s}^2\right)^3}e^{-R(\alpha+\alpha_{2s})}\Big(&e^{\alpha R}\Big(-2\alpha^2\big(\alpha+1\big)\alpha_{2s}\\ &-2\big(\alpha-1\big)\alpha_{2s}^3+\alpha^3\big(\alpha R+2\big)\\ &+\big(\alpha-1\big)\alpha_{2s}^4\big(-R\big)+\alpha\alpha_{2s}^2\Big(\big(\alpha-2\big)\alpha R-2\Big)\Big)\\ &+e^{\alpha_{2s}R}\Big(2\alpha^3\big(\alpha_{2s}-1\big)+2\alpha\alpha_{2s}^2\big(\alpha_{2s}+1\big)\\ &+\alpha^4\big(\alpha_{2s}-1\big)R+\alpha^2\alpha_{2s}\big(2-\big(\alpha_{2s}-2\big)\alpha_{2s}R\big)-\alpha_{2s}^3\big(\alpha_{2s}R+2\big)\Big)\Big), \end{aligned} \tag{D.23}$$

$$V''_{on} = \frac{8\alpha^{3/2}\alpha_{2s}^{5/2}}{\sqrt{3}R(\alpha+\alpha_{2s})^4}e^{-R(\alpha+\alpha_{2s})}\big(R\big(\alpha+\alpha_{2s}\big)\big(R\big(\alpha+\alpha_{2s}\big)+4\big)-e^{R(\alpha+\alpha_{2s})}\big(R\big(\alpha\big(\alpha-2\alpha_{2s}+2\big)+2\alpha_{2s}\big)+6\big)+6\big), \tag{D.24}$$

$$\begin{aligned} V''_{inter} = \frac{8\alpha^{3/2}\alpha_{2s}^{5/2}}{\sqrt{3}R(\alpha-\alpha_{2s})^4(\alpha+\alpha_{2s})^4}e^{-5\alpha R-4\alpha_{2s}R}\Big(&e^{4R(\alpha+\alpha_{2s})}\\ &\times\Big(2\alpha^5+8\alpha^3\alpha_{2s}\big(2\alpha_{2s}-1\big)+2\alpha\alpha_{2s}^3\big(3\alpha_{2s}+4\big)\\ &+\alpha^6R+2\alpha^4\Big(\big(\alpha_{2s}-1\big)\alpha_{2s}R+1\Big)+\alpha^2\alpha_{2s}^2\Big(\alpha_{2s}\big(4-3\alpha_{2s}\big)R+4\Big)\\ &-2\alpha_{2s}^4\big(\alpha_{2s}R+3\big)\Big)\\ &-e^{5\alpha R+3\alpha_{2s}R}\Big(\big(\alpha-1\big)\alpha_{2s}^6R^2+\alpha^4\Big(\alpha\Big(R\big(\alpha R+2\big)+2\Big)+2\Big)\\ &-4\alpha^3\alpha_{2s}\big(\alpha\big(\alpha+1\big)R+2\big)\Big) \end{aligned}$$

Table D.1 The values of single-particle microscopic parameters without optimization of $2s$ orbitals for $1s$ and $2s$ band ($R = R_B$, $\alpha = \alpha_B$, $\alpha_{2s} = \alpha_B/2$). Note that the last column describes atomic limit, where $\alpha \to 1$, $\alpha_{2s} \to 0.5$. We can observe that the model fulfills requirements, as the Wannier function w_i^{2s} approaches the exact solution of Hydrogen atom.

	Equilibrium system			Atomic limit
microscopic parameter Ξ	$\Xi^{2s}(Ry)$	$\Xi^{1s}(Ry)$	Ξ^{2s}/Ξ^{1s}	$\Xi^{2s}(Ry)$
ϵ	−0.518585	−1.75079	29.62%	−0.25
t	−0.292465	−0.727647	40.19%	0
V_{on}	0.0773174			0
V_{inter}	−0.110457			0

$$+\alpha^2\alpha_{2s}^2\Big(\alpha\Big(R\Big(\big(\alpha-3\big)\alpha R-4\Big)+16\Big)+4\Big)+4\big(\alpha-1\big)\alpha_{2s}^5 R$$
$$+\alpha_{2s}^4\Big(\alpha\Big(R\Big(\alpha\big(3-2\alpha\big)R+2\Big)+6\Big)-6\Big)+8\alpha\alpha_{2s}^3\Big(\alpha R+1\Big)\Big)\Big). \quad \text{(D.25)}$$

One can obtain the exact values for the optimal inter-ionic distance $R = R_B = 1.430\,42$ and $\alpha = \alpha_B = 1.193\,78$. The results, together with comparison to the one-orbital case, are listed in table D.1. Note that the new estimates are carried out for the optimal bond length and the inverse wave-functions size for the case of $1s$ functions only ($R = R_B = 1.430\,42$ and $\alpha = \alpha_B = 1.193\,78$, respectively).

References

[1] Spalek J, Oleś A M and Chao K A 1981 *Phys. Stat. Sol.* (b) **108** 329
[2] Penson K A and Kolb M 1986 *Phys. Rev.* B **33** 1663
[3] de Boer J and Schadschneider A 1995 *Phys. Rev. Lett.* **75** 4298
[4] Iglesias J R, Gusmão M A, Acquarone M, Romano A and Noce C 1997 *Physica* B **230–232** 1047
[5] Schumann R 2002 *Ann. Phys. (Leipzig)* **11** 49
[6] Schumann R 2008 *Ann. Phys. (Leipzig)* **17** 221
[7] Acquarone M, Iglesias J R, Gusmão M A, Noce C and Romano A 1997 *Il Nuovo Cimento* D **19** 1345
[8] Matlak M, Grabiec B and Krawiec S 2007 *Acta Phys. Polon.* A **112** 537
[9] Spałek J, Podsiadły R, Wójcik W and Rycerz A 2000 *Phys. Rev.* B **61** 15676
[10] For review see: Spałek J, Görlich E M, Rycerz A and Zahorbeński R 2007 *J. Phys.: Condens. Matter* **19** 255212
[11] Oleś A M, Spałek J and Chao K A 1979 *Physica* A **97** 565
[12] Spałek J, Oleś A M and Chao K A 1979 *Physica* A **97** 552
[13] Kadzielawa A P, Spałek J, Kurzyk J and Wójcik W 2013 *Eur. Phys. J.* B **86** 252
[14] Weir S T, Mitchell A C and Nellis W J 1996 *Phys. Rev. Lett.* **76** 1860–3
[15] Sorella S and Capriotti L 2010 *J. Chem. Phys.* **133** 234111
[16] Ashcroft N W 2000 *J. Phys.: Condens. Matter* **12** A129
[17] Shibata K, Ohashi T, Ogawa T and Kodama R 2010 *Phys. Rev.* B **82** 195123
[18] McMahon J M and Ceperley D M 2011 *Phys. Rev. Lett.* **106** 165302
[19] Naumov I I, Cohen R E and Hemley R J 2013 *Phys. Rev.* B **88** 045125
[20] Slater J C 1963 *Quantum Theory of Molecules and Solids* vol 1 (New York: McGraw-Hill)

[21] Kołos W and Wolniewicz L 1968 *J. Chem. Phys.* **49** 404
Kołos W and Wolniewicz L 1964 *J. Chem. Phys.* **41** 3663
[22] Szabo A and Ostlund N S 1989 *Modern Quantum Chemistry* (Mineola, New York: Dover Publications)
[23] Acquarone M and Noce C 1999 *Int. J. Mod. Phys.* B **13** 3331
[24] Spaek J 2008 *Condens. Matter Phys.* **11** 455
[25] Su W P, Schrieffer J R and Heeger A J 1980 *Phys. Rev.* B **22** 2099–111
[26] Holstein T 1959 *Ann. Phys., NY* **8** 325–42
[27] Rycerz A 2003 Physical properties and quantum phase transitions in strongly correlated electron systems from a combined exact diagonalization–*ab initio* approach *PhD Thesis* Jagiellonian University
[28] Kochanski E, Roos B, Siegbahn P and Wood M 1973 *Theoret. Chim. Acta (Berl.)* **32** 151
[29] Hobza P, Zahradnĺk R and Čársky P 1979 *Theoret. Chim. Acta (Berl.)* **53** 1–7
[30] Martínez J I, Isla M and Alonso J A 2007 *Eur. Phys. J.* D **43** 61–64
[31] Ceperley D M and Alder B J 1980 *Phys. Rev. Lett.* **45** 566
[32] Traynor C A, Anderson J B and Boghosian B M 1991 *J. Chem. Phys.* **94** 3657
[33] Azadi S, Monserrat B, Foulkes W M C and Needs R J 2014 *Phys. Rev. Lett.* **112** 165501
[34] Lee J and Haule K 2014 arXiv:1403.2474
[35] Dickenson G D, Niu M L, Salumbides E J, Komasa J, Eikema K S E, Pachucki K and Ubachs W 2013 *Phys. Rev. Lett.* **110** 193601
[36] Calderini D, Cavalli S, Coletti C, Grossi G and Aquilanti V 2012 *J. Chem. Sci.* **124** 187–92

3.4 Paper A-4 – Combined shared and distributed memory *ab-initio* computations of molecular-hydrogen systems in the correlated state: process pool solution and two-level parallelism

In this paper we present the computational scheme of the **E**xact **D**iagonalization – **Ab** **I**nitio Approach (EDABI) when applied to realistic hydrogen systems. In particular, we focus on the two-level parallelization of the problem of parameterizing the Hamiltonian, employing both shared (by means of Open Multi-Processing - OMP) and distributed (by the Message Passing Interface - MPI) memory models. We also review why such elaborated scheme is required by comparing the results for H_2 chain with periodic boundary conditions, both for different Slater-type orbital Gaussian representation (STO-N_GG) resolution N_G, with the so-called background field size M (the neighborhood of the site, where electronic Coulomb repulsion, ion–ion interaction and electron–ion attraction are taken into account).

Firstly, we describe the **E**xact **D**iagonalization – **Ab** **I**nitio Approach (EDABI) for a general case, as well as present the procedure of orthogonalization of the single-particle basis via the corresponding bilinear form problem. This approach allows for error control for the case of infinite systems. Then we explain in detail the computational scheme, recognizing the calculation of microscopic parameters as the *bottleneck* of the problem solution and employing the two-level parallelism: *(i)* the *process–pool* or the *root–worker* solution, where the root process distributes the workload between the workers; this on the other hand allows, *(ii)* the second level parallelization of the integral calculations at each process (cf. Fig. 1 for the flowchart of the solution).

As a next step, we provide an exemplary physical system and analyze validity of the proposed numerical solution. We consider the $(H_2)_3$ chain with periodic boundary conditions within the extended Hubbard model, with the three nearest neighbor hoppings t_i (Fig. 2) and the intersite electron–electron Coulomb interaction K_{ij} included up to the interionic distance cut-off $r_{cut-off} = Ma$, where M is a parameter (the so-called background field size) and a is the intermolecular distance. We find the global minimum for $a = 4.12a_0$ and constant molecular bond length $R = R_{free} = 1.43042a_0$ (Figs. 3–5). The discussion of the system with optimized molecular size R is the subject of paper A-5. Here, we study the dependence of the global energy minimum on the background field size M (Fig. 6) and Gaussian basis resolution N_G (Fig. 7), as well as perform finite-size scaling to determine the effective values. We also perform the analysis of the proposed two-level parallelism by calculating the so-called speed-up (SU) as a function of the number of nodes P and compare it to the *Amdahl law* (Figs. 8–9). As we exchange only a small amount of data (the values of microscopic parameters) through the *Message Passing Interface*, we have an almost perfect scaling of speed-up with the increasing number of nodes and with 96.97% of the time spent in the parallelized part of the computations, allowing utilization of the vast amount of computational power on the TERA–ACMIN supercomputer.

As of August 3, 2015 the paper was accepted for publication in Computer Physics Communication and is in press.

Combined shared and distributed memory *ab-initio* computations of molecular-hydrogen systems in the correlated state: process pool solution and two-level parallelism

Andrzej Biborski,[1,*] Andrzej P. Kądzielawa,[2,†] and Józef Spałek[2,1,‡]

[1] *Academic Centre for Materials and Nanotechnology, AGH University of Science and Technology, al. A. Mickiewicza 30, 30-059 Krakow, Poland*

[2] *Marian Smoluchowski Institute of Physics, Jagiellonian University, ulica Łojasiewicza 11, PL-30-348 Kraków, Poland*

(Dated: August 4, 2015)

An efficient computational scheme devised for investigations of ground state properties of the electronically correlated systems is presented. As an example, $(H_2)_n$ chain is considered with the long-range electron-electron interactions taken into account. The implemented procedure covers: (*i*) single-particle Wannier wave-function basis construction in the correlated state, (*ii*) microscopic parameters calculation, and (*iii*) ground state energy optimization. The optimization loop is based on highly effective *process-pool* solution – specific *root–workers* approach. The hierarchical, two-level parallelism was applied: both shared (by use of Open Multi-Processing) and distributed (by use of Message Passing Interface) memory models were utilized. We discuss in detail the feature that such approach results in a substantial increase of the calculation speed reaching factor of 300 for the fully parallelized solution. The elaborated in detail scheme reflects the situation in which the most demanding task is the single-particle basis optimization.

PACS numbers: 31.15.A-, 03.67.Lx, 71.27.+a
Keywords: ab initio calculations, electronic correlations , quantum chemistry methods, parallelism

I. PHYSICAL MOTIVATION: EXACT DIAGONALIZATION + AB INITIO METHOD

Electronically correlated systems are important both from the point of view of their unique physical properties and from nontrivial computational methods developed to determine them. The latter cover methods based on the Density Functional Theory (DFT) with the energy functional enriched by the correlation terms – the on-site repulsion U in the Hubbard model [1] and the Hund's rule term in the case of orbital degeneracy. Often, they are incorporated into either DFT or the Dynamic Mean Field Theory (DMFT) approach supplemented with the LDA-type calculations (see e.g. [2]). On the other hand, the *Configuration-Interaction* (CI) method does not suffer from the well–known *double counting problem*[1, 2], inherent in the DFT+U or LDA+DMFT methods. Another approach, similar in its spirit to the CI method, formulated as a combination of *the first-* and *second quantization* (FQ, SQ respectively) formalisms was elaborated in our group in the last decade and termed the **E**xact **D**iagonalization **Ab I**ntito (EDABI) approach [3, 4]. This method allows for a natural incorporation of the correlation effects consistently by the advantages of using the SQ language so that the *double-counting problem* does not arise at all. Also, by construction, it includes the Pauli principle for the fermionic systems. In contrast to CI the EDABI approach avoids any direct dealing with the many–body wave function expressed via a linear combination of the Slater determinants [5]. Instead, it is based on the many–particle quantum states constructed in the occupation number representation [5] – standard procedure for the SQ formulated problems.

The application of EDABI was found promising in view of research devoted to the hydrogen molecular systems with inclusion of interelectronic correlations [6], nano-clusters [7], and to atomic hydrogen metallization [8]. As the many–particle state is explicitly written in the occupation-number representation (Fock space), the starting Hamiltonian is formulated in the SQ language. Electronic correlations are then automatically included in the modeled system. However, in the Hubbard–like starting Hamiltonians [9–12] the knowledge of microscopic parameters, such as the on-site energy, the intersite hoppings, and the Coulomb repulsion magnitudes are regarded as input information. These parameters are often estimated indirectly. With this limitation, specific *phase-diagrams* are constructed and the phase boundaries of interest are determined as a function of those microscopic parameters which are not directly measurable (cf. e.g. [13–15]). In EDABI we take a different route: relatively simple and small systems are to be described consistently in the sense that the microscopic parameters are obtained explicitly as an output of an appropriate ab-initio variational procedure. Therefore, the EDABI approach should be regarded as an *ab–initio* method but with the single-particle wave functions being determined self-consistently in the correlated state. In this manner, the problem solution is reversed with respect to that in either LDA+U or LDA+DMFT. Namely, we first formulate the Hamiltonian and diagonalize it in SQ formalism

* andrzej.biborski@agh.edu.pl
† kadzielawa@th.if.uj.edu.pl
‡ ufspalek@if.uj.edu.pl

and determine the single-particle wave function only as a second step. However realistic, such an approach to the electronically correlated systems implies a substantially greater computational complexity, since the variational optimization consists of (i) microscopic parameters calculation and (ii) concomitant Hamiltonian-matrix diagonalization. We address here the issue (i) presenting how the modern High Performance Computing (HPC) cluster architecture can be utilized in the context, where the number of microscopic parameters is substantial if not large, and their calculation is one of the potential *bottlenecks* in the whole computational procedure. We also provide an example how a many-body problem at hand may be supplemented with the two-level parallelism in an intuitive manner. We do not discuss either the methodology related to the point (ii) or to its algorithmic aspect or else, to technical opportunities provided by e.g. recent fast development of Graphic Processing Units (GPU) computational techniques that are also in the area of interest [16, 17]. Nonetheless, as it becomes clear below, heterogeneous solutions are also easily applicable in our scheme.

The structure of the paper is as follows. In Sec. II we describe briefly the EDABI method (cf. Appendix A for details) and emphasize the computational complexity aspects. Next, in Sec. III, we show how the *process–pool* concept enhanced by *the two-level parallelism* forms a natural solution. In Sec. IV we present the outcome of its implementation: results of calculations carried out for $(H_2)_n$ exemplary system and discuss the achieved speed–up when compared to the reference single CPU computations. In Appendix B we discuss the convergence of our model for the case of infinite systems.

II. COMPUTATIONAL METHOD - EDABI

As stated in the foregoing Section, the computational method considered here is based on the EDABI method, comprehensive description of which can be found e.g. in [3]. It allows for consideration of realistic, electronically–correlated nanosystems within the framework of the combined first– and second-quantization formalisms. Below we sketch this method (for details see Appendix A).

A. Second-quantization aspect

For the purpose of calculating the ground-state energy of given system we start with the second-quantization language [5, 18–20]. We introduce the fermonic *anihilator*$(creator)$ $\hat{c}^{(\dagger)}_{i\sigma}$ algebra by imposing the anticommutation relations among them, namely

$$\{\hat{c}^{\dagger}_{i\sigma}, \hat{c}^{\dagger}_{j\sigma'}\} \equiv \{\hat{c}_{i\sigma}, \hat{c}_{j\sigma'}\} \equiv 0 \quad \text{and} \quad \{\hat{c}^{\dagger}_{i\sigma}, \hat{c}_{j\sigma'}\} \equiv \delta_{ij}\delta_{\sigma\sigma'}, \tag{1}$$

where i and j denote sites (nodes) of a fixed lattice, $\sigma,\ \sigma' = \pm 1$ are the spin quantum number, and the anti-commutator is $\{A, B\} \equiv AB + BA$.

We represent the many-particle basis states $\{|\Phi_k\rangle\}$ on the lattice of Λ sites in the *Fock space* [19] in the following manner

$$|\Phi_k\rangle = \prod_{i\in\Omega_{\uparrow k}} \hat{c}^{\dagger}_{i\uparrow} \prod_{j\in\Omega_{\downarrow k}} \hat{c}^{\dagger}_{j\uparrow} |0\rangle\,, \tag{2}$$

where $\Omega_{\uparrow k}$ and $\Omega_{\downarrow k}$ are the subsets of sites occupied by fermions with $\Lambda_{\uparrow}$ and $\Lambda_{\downarrow}$ particles respectively, and $|0\rangle$ is the *vacuum* state (with no particles), with $\langle 0|\ 0\rangle \equiv 1$. Explicitly,

$$\begin{aligned} |\Phi\rangle =& \underbrace{|0, 1, \ldots, 1\rangle}_{\text{spin}\uparrow} \otimes \underbrace{|1, 0, \ldots, 1\rangle}_{\text{spin}\downarrow} = \\ =& \hat{c}^{\dagger}_{2\uparrow} \cdots \hat{c}^{\dagger}_{\Lambda\uparrow} \hat{c}^{\dagger}_{1\downarrow} \cdots \hat{c}^{\dagger}_{\Lambda\downarrow} |0\rangle\,. \end{aligned} \tag{3}$$

With this concrete (occupation-number) representation of an abstract Fock space we define next the microscopic Hamiltonian of our interacting system of fermions.

B. Definition of the physical problem

We take the real-space representation with the starting field operators in the form

$$\hat{\Psi}_{\sigma}(\mathbf{r}) = \sum_{i} w_i(\mathbf{r}) \chi_{\sigma} \hat{c}_{i\sigma}, \tag{4}$$

where $w_i(\mathbf{r})$ is the single-particle wave function for fermion (e.g. electron) located on i-th site, χ_{σ} is the spin wave function ($\sigma = \pm 1$) with global spin quantization axis (z-axis). In general, the many-particle Hamiltonian is defined in the form

$$\begin{aligned} \hat{\mathcal{H}} =& \sum_{\sigma} \int d^3r \hat{\Psi}^{\dagger}_{\sigma}(\mathbf{r}) \hat{\mathcal{H}}_1(\mathbf{r}) \hat{\Psi}_{\sigma}(\mathbf{r}) \\ &+ \frac{1}{2} \sum_{\sigma\sigma'} \iint d^3r d^3r' \hat{\Psi}^{\dagger}_{\sigma}(\mathbf{r}) \hat{\Psi}^{\dagger}_{\sigma'}(\mathbf{r}') \hat{V}(\mathbf{r} - \mathbf{r}') \hat{\Psi}_{\sigma'}(\mathbf{r}') \hat{\Psi}_{\sigma}(\mathbf{r}), \end{aligned} \tag{5}$$

where $\hat{\mathcal{H}}_1$ is the (spin-independent) Hamiltonian for a single particle in the milieu of all other particles and $\hat{V}(\mathbf{r} - \mathbf{r}')$ is the interaction energy for a single pair. For the modeling purposes we assume that $\hat{\mathcal{H}}_1$ is expressed in the atomic units ($\hbar = e^2/2 = 2m_e = 1$, where e is the charge of an electron and m_e is its mass) and expresses the particle kinetic energy and the attractive interaction with the protons located at $\{\mathbf{R}_i\}$, i.e.,

$$\hat{\mathcal{H}}_1(\mathbf{r}) \overset{a.u.}{=} -\nabla^2 - \sum_{i=1}^{N_S} \frac{2}{|\mathbf{R_i} - \mathbf{r}|}, \tag{6}$$

where N_S is the number of sites, whereas

$$\hat{V}(\mathbf{r} - \mathbf{r}') \overset{a.u.}{=} \frac{2}{|\mathbf{r} - \mathbf{r}'|}, \tag{7}$$

represents the Coulomb repulsive interaction between them. Substituting (4) into (5) we obtain the explicit second-quantized form of the Hamiltonian [5, 20] i.e.,

$$\mathcal{H} = \sum_{ij}\sum_{\sigma} t_{ij}\hat{c}^{\dagger}_{i\sigma}\hat{c}_{j\sigma} + \sum_{ijkl}\sum_{\sigma,\sigma'} V_{ijkl}\hat{c}^{\dagger}_{i\sigma}\hat{c}^{\dagger}_{j\sigma'}\hat{c}_{l\sigma'}\hat{c}_{k\sigma}, \quad (8)$$

where t_{ij} and V_{ijkl} are integrals associated with the one- and two-body operators respectively

$$t_{ij} \equiv \left\langle w_i(\mathbf{r}) \right| \hat{\mathcal{H}}_1 \left| w_j(\mathbf{r}) \right\rangle \quad (9a)$$
$$= \int d^3r \; w_i^*(\mathbf{r})\hat{\mathcal{H}}_1(\mathbf{r})w_j(\mathbf{r}),$$
$$V_{ijkl} \equiv \left\langle w_i(\mathbf{r})w_j(\mathbf{r}') \right| \hat{V} \left| w_k(\mathbf{r})w_l(\mathbf{r}') \right\rangle \quad (9b)$$
$$= \iint d^3r d^3r' \; w_i^*(\mathbf{r})w_j^*(\mathbf{r}')\hat{V}(\mathbf{r}-\mathbf{r}')w_k(\mathbf{r})w_l(\mathbf{r}').$$

The first term contains the single-particle part composed of the atomic energy $\epsilon_i \equiv t_{ii}$, as well as expresses the kinetic (hopping) part with t_{ij} $(i \neq j)$ being the so-called hopping integral. The second expression contains intraatomic (intrasite) part of the interaction between the particles ($U_i \equiv V_{iiii}$ – the so-called Hubbard interaction), and the intersite (interatomic) interaction ($K_{ij} \equiv V_{ijij}$ – the last important term for the purposes here). A remark is in place here: when the single-particle basis $\{w_i\}$ is assumed as real, the last two two-body interaction terms are the exchange-correlation energy ($J_{ij} \equiv V_{ijji}$) and the so-called correlated hopping ($V_{ij} \equiv V_{ijjj}$).

The Hamiltonian (5), with inclusion of all the two-site terms only, can be rewritten in the following form, with the microscopic parameters contained in an explicit manner, i.e.,

$$\hat{\mathcal{H}} = \sum_{i,\sigma}\epsilon_i\hat{n}_{i\sigma} + \frac{1}{2}\sum_{\sigma,i\neq j} t_{ij}\hat{c}^{\dagger}_{i\sigma}\hat{c}_{j\sigma} + \frac{1}{2}\sum_{i,\sigma} U_i\hat{n}_{i\sigma}\hat{n}_{i\bar{\sigma}} \quad (10)$$
$$- \sum_{i\neq j} J_{ij}\mathbf{S}_i\cdot\mathbf{S}_j + \frac{1}{2}\sum_{i\neq j}\left(K_{ij} - \frac{J_{ij}}{2}\right)\hat{n}_i\hat{n}_j$$
$$+ \sum_{i\neq j} J_{ij}\hat{c}^{\dagger}_{i\uparrow}\hat{c}^{\dagger}_{i\downarrow}\hat{c}_{j\downarrow}\hat{c}_{j\uparrow} + \sum_{\sigma,i\neq j} V_{ij}\hat{n}_{i\sigma}\left(\hat{c}^{\dagger}_{i\bar{\sigma}}\hat{c}_{j\bar{\sigma}} + \hat{c}^{\dagger}_{j\bar{\sigma}}\hat{c}_{i\bar{\sigma}}\right).$$

The basis $\left\{w_i(\mathbf{r})\right\}_{\alpha}$ in (4) needs to be orthonormal, i.e. orthogonal and normalized to unity. In the next Section, we describe how to construct the basis satisfying this condition. In summary, by solving (diagonalizing) $\hat{\mathcal{H}}$ we understand finding the optimal many-particle configuration with a simultaneous single-particle basis $\{w_i(\mathbf{r})\}$ determination. Typically [13–15, 21], the parameters $\epsilon_i = \epsilon$, t_{ij}, U, K_{ij} are regarded as extra parameters. Here we calculate them explicitly along with the diagonalization in the Fock space at the same time.

C. Basis orthogonalization as a bilinear problem

We require the orthonormality of the set of the single–particle wave functions $\{w_i(\mathbf{r},\alpha)\}$, i.e., set the conditions

$$\langle w_i(\mathbf{r})| \; w_j(\mathbf{r})\rangle \equiv \quad (11)$$
$$\int_{\mathbb{R}^3} d^3r \; w(\mathbf{r}-\mathbf{R}_i)w(\mathbf{r}-\mathbf{R}_j) = \delta_{ij},$$

where δ_{ij} is the Kronecker delta. Note that α will play a role of variational parameter specifying the way of constructing the basis (cf. Sec. II D). Namely, the single–particle wave functions (Wannier functions) are approximated by a finite linear combination in a selected set. These wave functions describe the single-electron states centered on every atomic/ionic site, i.e., at positions $\left\{\mathbf{R_i}\right\}$. Such approach is related to the *tight-binding* approximation (TBA [22]), where the atomic orbitals composing w_i are represented by e.g. the Slater-type orbitals (STO). For the purpose of the present model analysis, only the $1s$ Slater functions are taken into account, i.e.,

$$\psi_i(\mathbf{r}) \equiv \sqrt{\frac{\alpha^3}{\pi}}e^{-\alpha|\mathbf{r}-\mathbf{R}_i|}, \quad (12)$$

where α is the inverse wave-function size. Similarly to [23], for each position i we construct linear combination

$$w_i(\mathbf{r}) = \sum_{j=0}^{L}\beta_j\widetilde{\psi}_{\pi_i(j)}(\mathbf{r}), \quad (13)$$

where $\{\beta_j\}$ compose a set of $(L+1)$ mixing coefficients, and $\pi_i : \{0,\ldots,L\} \to \mathcal{N}_i$, is the function mapping indexes to the neighborhood $\mathcal{N}_i$ of the site (node) i located at $\mathbf{R}_i$.

Note that in general $\widetilde{\psi}_{\pi_i(j)}$ may be a sum over Slater functions in the neighborhood, which varies the number of β coefficients and the number of nodes in the neighborhood $\mathcal{N}_i$. This circumstance does not influence the discussion, but is of crucial importance when the scheme is implemented numerically. Also, the new basis $\{w_i(\mathbf{r})\}$ is orthogonal *in the neighborhood* $\mathcal{N}_i$.

We are looking for the set of $\{\beta_j\}$, orthonormalizing the basis $\{w_i(\mathbf{r})\}$ for given geometry (effectively described by set of ionic coordinates $\mathbf{R}_i$) and for the arbitrary inverse wave-function size α. In order to achieve this we replace the original problem $\forall j \in \left\{\pi_i(k)\middle| k \in \{0,1,\ldots,L\}\right\}$

$$\int_{\mathbb{R}^3} d^3r \; w_i(\mathbf{r})\, w_j(\mathbf{r}) = \delta_{ij} \quad (14)$$

with the equivalent set of bilinear equations

$$\underline{\beta}_i^T\mathbb{S}_{ij}\underline{\beta}_j = \delta_{ij}, \quad (15)$$

where

$$\underline{\beta}_i \equiv \begin{pmatrix} \beta_{\pi_i(0)} \\ \beta_{\pi_i(1)} \\ \vdots \\ \beta_{\pi_i(L)} \end{pmatrix}, \tag{16}$$

and the overlap integrals are

$$(\mathbb{S}_{ij})_{lm} \equiv \int_{\mathbb{R}^3} d^3r \; \widetilde{\psi}_{\pi_i(l)}(\mathbf{r}) \, \widetilde{\psi}_{\pi_j(m)}(\mathbf{r}), \tag{17}$$

with $(\mathbb{S}_{ii})_{ll} = 1$. For given geometry and the inverse wave-function size α we solve the system (15) numerically.

The computation of the two-body integrals (cf. Eq. (9b)) must be performed in a general case numerically (see e.g. [7] and citations therein). Therefore, STO are usually approximated by their expansion in the so-called Gaussian basis, namely

$$\psi_i(\mathbf{r}) \approx \alpha^{3/2} \sum_{a=1}^{N_G} \left(\frac{2\alpha^2 \Gamma_a^2}{\pi} \right)^{3/4} e^{-\alpha^2 \Gamma_a^2 |\mathbf{R_i} - \mathbf{a}|^2}, \tag{18}$$

with N_G being the parameter describing number of Gaussian functions taken into account and the adjustable set $\{\Gamma_a\}$ is obtained through a separate procedure [7]. Exact or approximate ground state properties (i.e. ground state energy, structural properties, electronic density, etc.) are obtained when the eigenstate corresponding to the lowest many-particle eigenvalue is determined with the diagonalization performed in the Fock space. In the context of EDABI, exact methods were successfully applied, e.g., the Lanczos [16] algorithm for the matrix diagonalization, executable for nanosystems [4, 6, 7].

Although originally EDABI was formulated for finite-size systems, the scheme can be regarded as a general variational procedure. According to its generic character, it is applicable in combination with another correlation oriented approach, dedicated to the approximate Hamiltonian diagonalization. As an example, the *bulk* systems with proper translational symmetries were analyzed [8, 24], based on the modified Gutzwiller Approximation (SGA). One may incorporate other diagonalization schemes applicable to the EDABI method. Here we consider only the scenario, according to which diagonalization in the Fock space is performed *exactly* – i.e., the Hamiltonian matrix is generated with the help of basis (2) and diagonalized in terms of iterative (e.g. Lanczos) numerical algorithm.

D. Optimization procedure and computational complexity

The set $\{w_i(\mathbf{r}, \alpha)\}$ describes the system in question: the interaction parameters $\{V_{ijkl}\}$ and intersite hoppings $\{t_{ij}\}$. On the other hand, there are independent parameters $\left\{\alpha, \{\mathbf{R_i}\}\right\}$, where $\{\mathbf{R_i}\}$ together with α form the multidimensional optimization space. The EDABI method is based on the variational principle within which the single-particle wave functions at given atomic configuration $\{\mathbf{R_i}\}$ are optimized to determine the ground-state energy of the correlated system. From the computational point of view, four main tasks are to be performed in a single iteration, i.e., for a given trial value of α:

1. Single particle basis ortonormalization - solution of $L+1$ dimensional bilinear set of equations.

2. Computation of the one-body microscopic parameters - scaling as $\mathcal{O}(L^2 N_G^2 N_S)$.

3. Computation of the two-body microscopic parameters - scaling as $\mathcal{O}(L^4 N_G^4)$.

4. Hamiltonian diagonalization - dependent on the selected approach (exact, mean-field, Gutzwiller Approximation, etc.).

The tasks corresponding to 2 and 3 are central to the subsequent considerations. While for relatively simple models, such as one band Hubbard model, there are only three integrals to compute (the nearest-neighbor hopping, the atomic reference site energy, and the on-site electrostatic repulsion), this is not the case in the situation, in which a more complicated Hamiltonian describes our system. The extended Hubbard model (see Sec. IV), where the non-local electron-electron interactions are taken up to some cut-off distance, is associated with the increasing number of the two–body integrals to be computed. However, also for the multiband Hubbard model case, the number of hopping integrals increases as $\mathcal{O}(N_b^2)$, where N_b is the number of bands. Therefore, an effective scheme allowing to obtain – possibly quite large – set of microscopic parameters in a run–time, is desired. In the following Section we propose an explicit solution of this last issue.

III. PROCESS-POOL SOLUTION AND TWO-LEVEL PARALLELISM

As we said above, the standard task is to diagonalize Hamiltonian (5) defined in the Fock space (occupation-number representation). This means, to determine the ground-state energy for given values of the microscopic parameters: ϵ_i, t_{ij}, U_i, and K_{ij} (in general, J_{ij} and V_{ij} as well). The principal work we would like to undertake here is to determine the renormalized wave functions $\{w_i(\mathbf{r})\}_{i=1,\ldots,N}$ in the resultant (correlated) ground state. The first aspect of the whole problem presents itself as an equally important part, as only then the ground state configuration of our system can be defined physically, i.e., as a (periodic) system with known lattice parameter (interionic distance). In the remaining part both aspects of the optimization problem are elaborated together with concomitant technical details provided.

A. Optimization loop

We focus our analysis according to the scenario that the computational time spent on the diagonalization in the Fock space is negligible when compared to the calculation of the two-body integrals appearing in the calculation of microscopic parameters. For the sake of clarity, let us rewrite Hamiltonian (8) in more compact form

$$\mathcal{H} = \sum_{m} \sum_{ij} \Xi_{m;ij} \hat{O}_{m;ij}, \tag{19}$$

where $\Xi_{m;ij} \in \{\epsilon_i, t_{ij}, U_i, K_{ij}, V_{ij}, J_{ij}\}$ and $\hat{O}_{m;ij}$ symbolizes the operator part, e.g., $\hat{O}_{t;ij} = \sum_\sigma \hat{c}^\dagger_{i\sigma} \hat{c}_{j\sigma}$. One should note that the parameter set $\Xi_{m;ij}$ must be calculated in each iteration step during the optimization procedure. Computation of the microscopic parameters can be performed independently which in turn provides an opportunity for its acceleration by means of the parallelism application.

Let us consider some generic optimization procedure $OP(\{\mathbf{R_i}\})$ returning the minimal energy at given accuracy, as a function of structural parameters. In OP the system energy is sampled as a function of α so we denote it as $E_G(\alpha)$. Taking into account that $\nabla_\alpha E_G(\alpha)$ is not obtainable in general case, the optimization scheme encoded in OP relates to a non-gradient method, e.g., *the golden–search* for the one-dimensional case. The computation of $E_G(\alpha)$ (sampled by OP) consists of calculation of $\{\Xi_{m;ij}\}$ combined with the Hamiltonian matrix diagonalization. Within our approach, the computation speed–up is achieved by implementing the *process-pool* or *the root–worker processes*. This solution might be regarded as *a thread–pool* pattern, but constructed within the framework of the distributed memory model. Working threads are replaced by the processes – let us call them *workers* – which may communicate by the utilizing the *Message Passing Interface* (MPI) – as it is done in our implementation. *Workers* remain in the infinite loop, monitoring signal from the *root* process which in turn is responsible for the job triggering and synchronization. It can also participate in the calculations – in our case it performs matrix diagonalization. Depending on what kind of signal is sent (in certain protocol established for the communication purposes between *workers* and *root*) workers: (*i*) wait, (*ii*) start to compute, (*iii*) break and exit from the loop. Since (*ii*) might be considered as a generic task, one can see that proposed approach is extendable to include diagonalization – e.g., if one deals with the big block–diagonal matrices, each block could be diagonalized independently by the worker processes. *Process–pool* is supposed to be efficient assuming that the following principal condition is fulfilled: the task performed by each of the *worker processes* (or at least by most of them) is computationally the most expensive part, particularly if it shadows the communication latency.

Each process in the *process-pool* may utilize – if there are available resources – *shared memory* model. Thus the solution benefits from *two-level parallelism*, where *worker–process* parent thread forks into working threads, allowing in turn to perform each task faster (integral computation in this context). In our case the elements from the set $\{\Xi_{m;ij}\}$ are distributed into the sub-sets $I_p = \{\Xi_{m;ij}\}_p$ where p denotes the processor *id*. The I_p relate to task stack assigned to p-th process. The sub-sets construction should be performed carefully to keep well-balanced workload on processor, e.g. providing equal distribution of the integrals calculation among I_p. The *process-pool* consists of $P+1$ processes, P of them are *workers* and one – as mentioned – is a *root*. As follows from the scheme (cf. Fig. 1), *process-pool* is applied to the EDABI optimization loop. The OP procedure performs α space sampling along non-gradient optimization scheme. Each trial–E_G computation demands parameters update and integrals calculations. The latter one exploits parallelism at two levels. Each of P processes computes integrals grouped in its assigned I_p subset and each of the two–body integral is calculated in the nested (fourth times) loops which are collapsed in terms of the utilization of the openMP framework. The whole computation originates from the need to determine the two-body integrals (9b) which are expressed as

$$\begin{aligned} V_{ijkl} &= \langle w_i w_j | \mathcal{V} | w_k w_l \rangle = \\ &= \sum_{pqrs} \beta_p \beta_q \beta_r \beta_s \langle \widetilde{\psi}_{\pi_i(p)} \widetilde{\psi}_{\pi_j(q)} | \mathcal{V} | \widetilde{\psi}_{\pi_k(r)} \widetilde{\psi}_{\pi_l(s)} \rangle = \\ &= \sum_{pqrs} V^{pqrs}_{ijkl}, \end{aligned} \tag{20}$$

where $\widetilde{\psi}$ represents the Gaussian contraction. Elements V^{pqrs}_{ijkl} are computable independently; therefore V_{ijkl} is obtained with the help of openMP *reduction* clause. Computed integrals are gathered in a single array in terms of MPI_Gather function or optionaly of $MPI\_Allgather$ if necessary (which potentially may increase communication latency). Then, Hamiltonian matrix is updated with the proper values and the diagonalization step starts. As an output of diagonalization, the trial E_G is computed and processed in OP. Our implementation bases on MPI and openMP, though its scheme is generic and might be implemented by means of any of known technologies or self–made implementations as well.

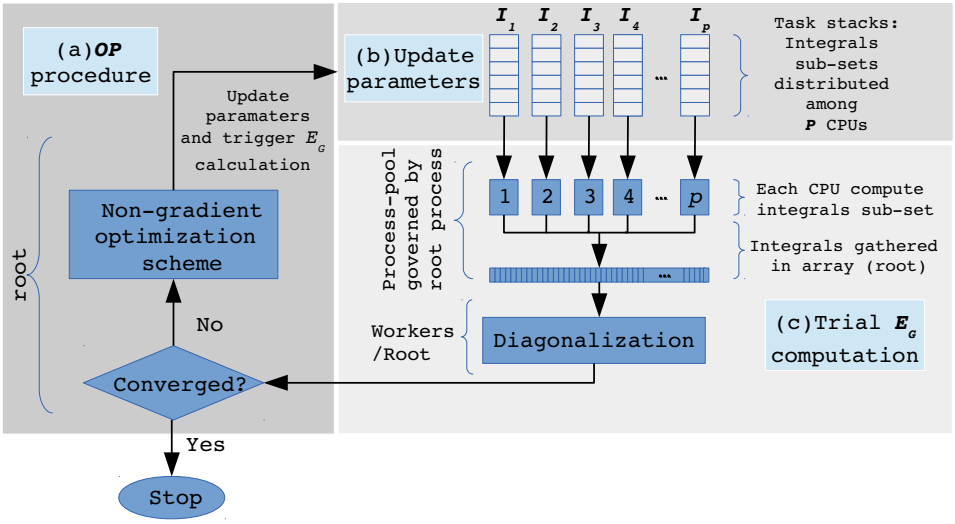

FIG. 1. Process-pool solution applied for the optimization procedure (OP) in the context EDABI method.

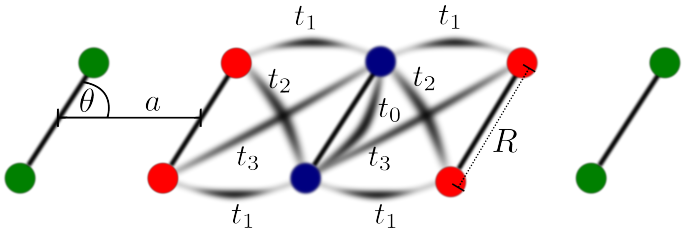

FIG. 2. $(H_2)_n$ molecular chain, its parametrization with possible hoppings from/to central (blue) molecule. Green molecules are included as *the background field* related to the system by the periodic boundary conditions.

IV. EXEMPLARY SOLUTION: MODEL OF $(H_2)_n$ CHAIN

We test our solution by means of analysis performed for the chain consisting of $n = 3$ hydrogen molecules stacked at intermolecular distance a, with the molecule bond-length R, and the tilt angle θ. We regard this configuration as a part of periodic system (cf. Fig. 2). Hydrogen molecular chains are interesting in view of the crucial role of electronic correlations in the molecules and related low-dimension systems [3, 6, 7]. The stability of the hydrogen molecular system was studied by means of variety of methods, e.g. DFT [25] or Self-Consistent Field (SCF) [26, 27], also in the context of the existence of superfluidity [28].

We discuss the molecular hydrogen chain within the so-called *extended Hubbard model*. This means that the interactions associated with the different atomic centers (K_{ij}) are taken into account. Eventually, the electronic

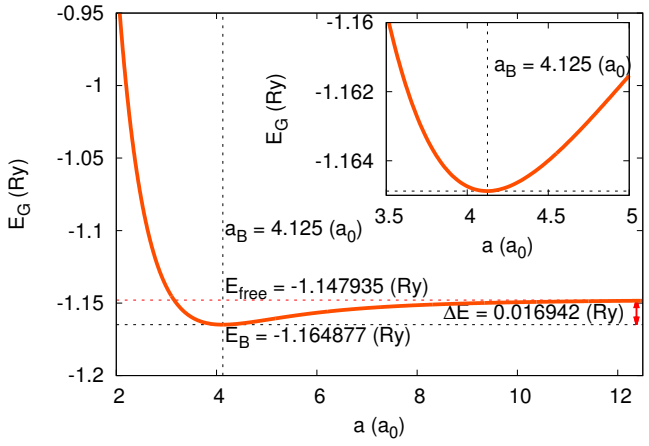

FIG. 3. Ground state energy (per atom) for $(H_2)_3$ molecular chain as a function of the intermolecular distance a. Note the convergence to analytical solution [6] for the separate free molecule limit when $a \to \infty$.

part of Hamiltonian, with the ion-ion interaction explicitly included, can be rewritten then as composed of the three parts:

$$\mathcal{H}_{Hubb} = \sum_i \epsilon_i \hat{n}_i + \sum_{ij\sigma} t_{ij} c^\dagger_{i\sigma} c_{j\sigma} + U \sum_i \hat{n}_{i\uparrow}\hat{n}_{i\downarrow}, \quad (21a)$$

$$\mathcal{H}_{ext} = \mathcal{H}_{Hubb} + \frac{1}{2}\sum_{ij} K_{ij}\hat{n}_i\hat{n}_j, \quad (21b)$$

$$\mathcal{H}_{tot} = \mathcal{H}_{ext} + \frac{1}{2}\sum_{ij} \frac{2}{|\mathbf{R_i} - \mathbf{R_j}|} = \mathcal{H}_{ext} + \mathcal{V}_{i-i}, \quad (21c)$$

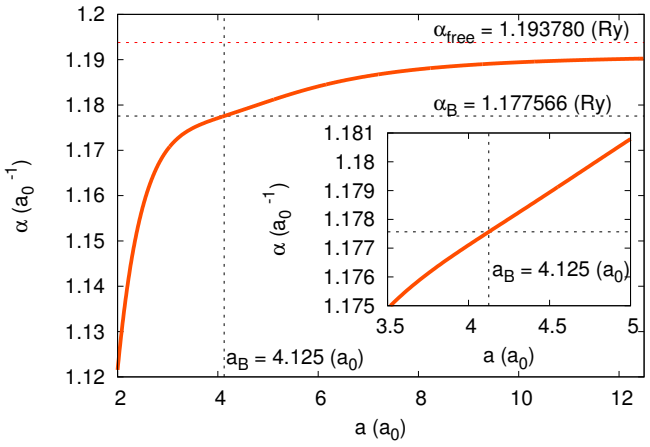

FIG. 4. Inverse atomic orbital size α versus the intermolecular distance a. Note the convergence to the analytical solution [6] for the separate free molecule limit when $a \to \infty$.

where the first two terms in (21a) represent the single-particle energy with all possible hoppings t_{ij} (to the fourth nearest neighbor, see Fig. 2) and are calculated with respect to *the background field* (see Sec. IV A for details), U is on-site Coulomb repulsion (Hubbard term), K_{ij} are intersite Coulomb repulsive interactions between supercell and the *background* sites (see [7] and Appendix B for details), $\mathcal{V}_{i-i}$ is the proton–proton repulsive interaction. Despite its relative simplicity, the system exhibits non–trivial properties. However, as we focus mainly on the computational aspects, we present here only the basic physical properties. Computational performance tests of our solution are undertaken for arbitrarily chosen molecular bond–length $R = 1.43042(a_0)$, corresponding to the equilibrium value obtained by us previously for a single H_2 molecule [6]; also $\theta = \pi/2$. The total number of electrons is equal to the number of atomic centres (6 for $n = 3$). We test E_G against the varying intermolecular distance a (as shown in Fig. 3) obtaining the van der Waals-like behavior of the total energy, as expected [3, 7, 26, 27]. The single (spatially separated) H_2-molecule ground-state energy is reproduced asymptotically for $a \to \infty$, as marked in Fig. 3. For the sake of completeness, we present in Fig. 4 the inverse atomic orbital size α. In Fig. 5 we plot the contours of the electronic density $n(\mathbf{r})$ as the cross–section on the $X - Y$ plane close to the configuration related to the minimal value of E_G. A very important feature of this solution worth mentioning is that as a diminishes and approaches R we observe a discontinuous phase transition from the molecular to the atomic states, but this feature of the results are discussed elsewhere [29]. Also, the minimum energy provides a stable configuration against the dissociation into separate molecules (cf. Fig. 3).

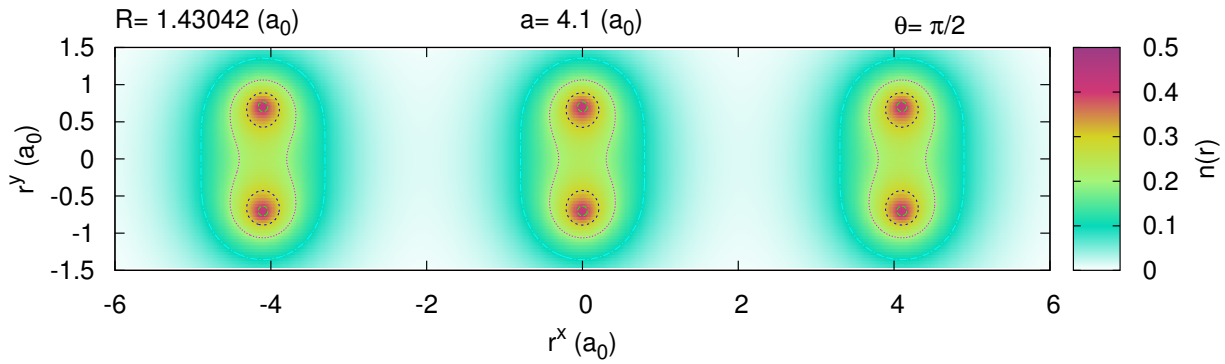

FIG. 5. Electronic density $n(\mathbf{r})$ projected on $X - Y$ plane of the aligned H_2 molecules for the intermolecular distance close to the equilibrium value (marked by the vertical dashed line in Fig. 3). The values of the structure parameters are specified.

A. Convergence study

We have performed the convergence study to obtain parameters suitable for the speed–up analysis of the implemented approach. There are two most important components playing crucial role: number of Gaussian functions N_G taken in contraction (18) and the size of periodic *background–field* of the super-cell. The former does not require additional comment; it is not the case for the latter. With the periodic boundary conditions being

imposed, a proper cut–off distance for the interactions must be also established. The atomic energy ϵ_0 becomes in general lower when a larger number of ionic centers are taken into account (i.e., the larger cut–off distance), then the contribution from *the electron–ion* becomes stronger. On the other hand, analogical in nature but opposite in sign effects originate from the Coulomb *ion–ion* and *the electron–electron* repulsions. In the limit $r_{cutoff} \to \infty$ both contributions cancel each other, as discussed in the context of EDABI in [30] and, for the sake of completeness, in Appendix B. One may note that the just described behavior is similar to the cancellation effect observed in *the jellium model* [31]. We define M as cut–off parameter, describing the size of background field as:

$$M = \frac{r_{cutoff}}{a} \tag{22}$$

In Fig. 6 we plot the system total energy as a function of intermolecular distance, close to the energy-minimum configuration. It is clear that if smaller cut–off distance is selected, the energy is underestimated. If cut–off was chosen to be $\geq 150a$, the consecutive energies differ by less than the assumed numerical error in Lanczos matrix diagonalization procedure (i.e. $10^{-4}Ry \sim 1meV$). Therefore, further calculations were carried out for $M = 250$, what results in 510 integrals to be calculated after reductions caused by the system symmetries. As it follows from Fig. 7, $N_G = 9$ is the number of Gaussians, when the energy becomes convergent, therefore the subsequent analysis corresponds to $N_G = 9$ and $M = 250$.

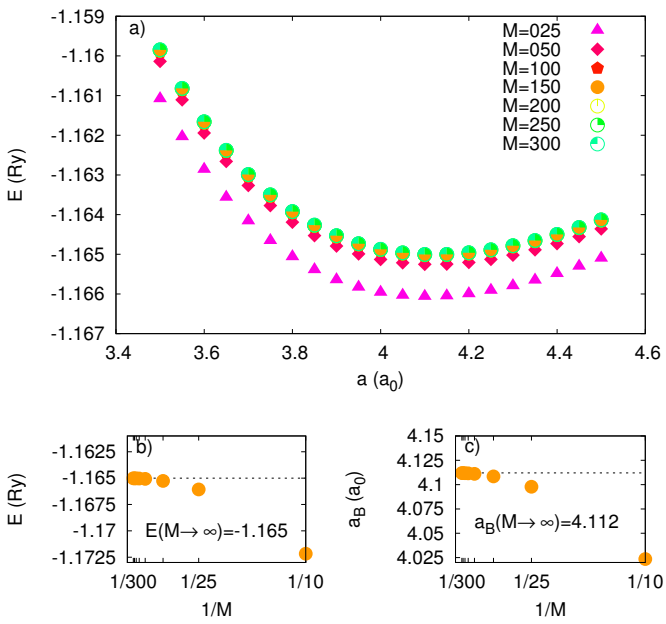

FIG. 6. Convergence study: a) ground-state energy E_G versus intermolecular parameter a close to the minimum for the different background field size M; b) limit of E_G for $M \to \infty$; c) limit of the optimal intermolecular parameter a_B (minimizing E_G) for $M \to \infty$. The plots in b) and c) represent the finite-size scaling analysis.

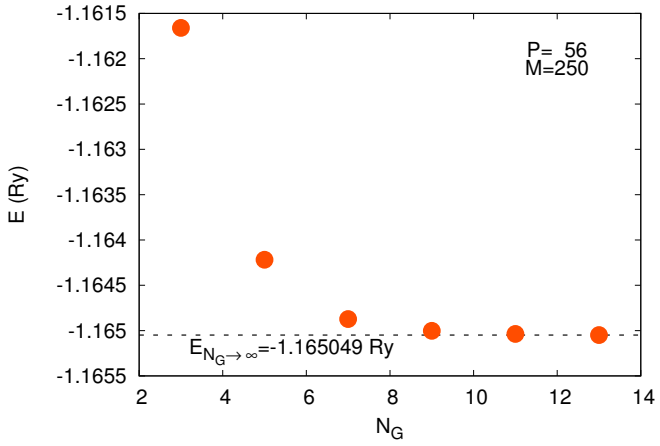

FIG. 7. Convergence study: Ground-state energy E_G versus number of Gaussians N_G taken to represent the atomic basis and for the background field size $M = 250$ and the number of SMP nodes $P = 56$.

B. Strong scaling for MPI+openMP solution

Taking into account that we have one electron per atomic center in a two band system (molecule consists of two hydrogen atoms), construction of the basis for three molecules leads to 924 basis states. The diagonalization in terms of the iterative algorithm – in this case Lanczos – is not a challenge, especially if only the lowest eigenvalue is desired. A remark is necessary here: system described by substantially larger Hamiltonian matrices can also be treated efficiently in the framework of the elaborated scheme. However, more sophisticated approaches (cf. Sec. III A) or approximate methods are then indispensable. Therefore, the example we provide, fulfills the requirement concerning the ratio of diagonalization to integration time. The latter is supposed to be the bottleneck during the execution of the optimization procedure. We investigate the speed-up (SU) defined as

$$SU(P, X, Y) = \frac{T_Y(P = 1)}{T_X(P)}, \tag{23}$$

with T denotes time spent on the computation and

$$X, Y \in \{I, II, \varnothing\}, \tag{24}$$

where first two symbols correspond to parallelism based on the application of openMP and openMP+MPI respectively and $\varnothing$ is associated with sequential solution. The calculations were performed for the energy optimization at given ion configuration, close to the energy minimum, allowing to collect CPU time consumed by OP. The measurement were covered on HP server consisting of 96 computational nodes each supplied with the two 8–cored Intel Xeon e5-2670 2.60GHz processors. The main board supported SMP exposing one logical 16–core processor per node thus P refers to the number of SMP

nodes. Physically, the communication among nodes was provided by the InfiniBand 4X QDR interface. The $SU(P, II, I)$ (Fig. 8) exhibits Amdahl law–like behaviour [32]. This law states that speed–up limit in the strong–scaling regime can be described in terms of the following formula

$$SU(P) = \frac{1}{1 - f + \frac{f}{P}}, \tag{25}$$

where f is the part of the program susceptible for the parallelization. The value of f was found by means of fit the Amdahl's law to the obtained data. Approximate value of f comes directly from the fit (see Fig. 8 for details) and maximal SU can also be estimated by

$$SU_{max} \approx \lim_{P \to \infty} SU(P). \tag{26}$$

We found $f \approx 0.97$ and $SU_{max} \approx 33$, which confirms suitability of the application of our scheme. However, for the sake of completeness, we investigated the Gaussian number threshold associated with the *process–pool* solution efficiency.

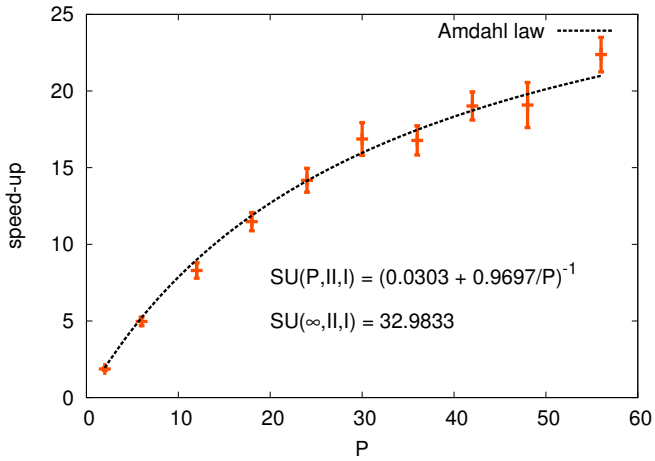

FIG. 8. Speed-up (SU) as a function of number of processes P. Amdahl law curve fited to data. Each point probed 50 times.

C. Number of Gaussians and Efficiency Threshold

As mentioned above, the efficiency of the *process-pool* solution depends on the workload assigned to each of the process in the pool. Notably, N_G and the total number of integrals (associated with M (22)) are the most important factors, influencing robustness of the proposed approach.

We have performed measurements of computation time as a function of N_G for a different number of P (see Fig. 10). For large number of Gaussians the optimization time has a universal scaling $T \sim N_G^p$, with $p \approx 4$, meaning that the two-particle integrals (20) are the most computationally expensive, as expected.

Following [33] we introduce the *extended-Amdahl law* to include potential communication overhead. In our case, the potentially most time-consuming (among MPI communication routines used) MPI_Gather routine scales lineraly with P. Taking this into account the speed–up can be approximated by the following formula

$$SU_{comm}(P, Y, X) = \frac{1}{1 - f - \delta + \frac{f}{P} + \delta P}, \tag{27}$$

where δ is constant to be determined. We performed fit of (27) to the speed–up as a function of P for $N_G \in \{3, 5, 7\}$ as we show in Fig. 9. As expected f decreases with decreasing N_G, but $\delta < 10^{-4}$ even for $N_G = 3$. This value is negligible for the reasonable P (the number of integrals is the upper bound) for any f. The lack of the communication overhead originates not only from the utilization of *InfiniBand* interface and linear scaling of the communication routine, but also from the small

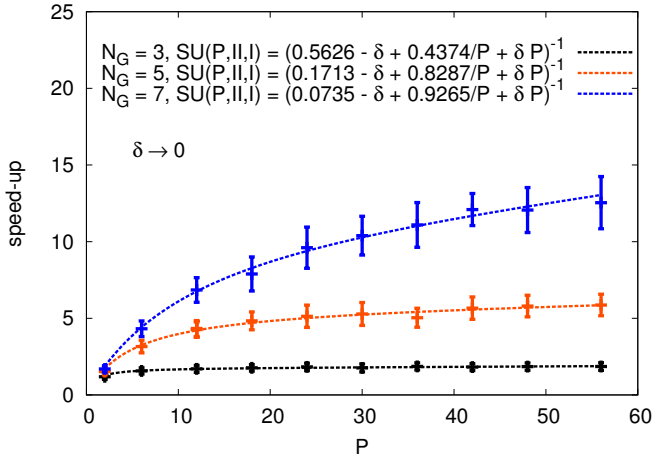

FIG. 9. The relative speed-up SU (23) versus number of nodes P for $N_G \in \{3, 5, 7\}$ measured 100 times. Note that when fitting the *so-called* extended Amdahl law, communication overhead factor $\delta \approx 0$. Note that for $N_G = 3$ only 44% of the program is performed parallelly.

amount of data sent by each process to the *root* (e.g. $\sim$ 80B for $P = 50$). Hence the deviation from linearity for higher values of P (see Fig. 10) comes from breaking the principal assumption:

For the lower numbers of Gaussians, the time of diagonalization (performed sequentially) becomes comparable or greater to that consumed by the integrals computations.

The analysis performed above allows to describe the boundaries where the proposed solution is effective. However, from the users perspective the most compelling feature is the absolute speed-up $SU(P, II, \varnothing)$, as it is the metric for the time save. In the next paragraph we present this result.

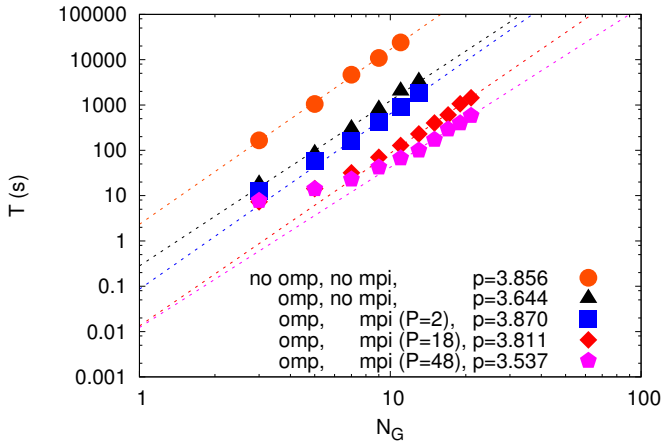

FIG. 10. Computation time as a function of N_G for sequential, only openMP, and MPI+openMP solutions. Note the linear behavior in the regime of large N_G on log–log scale, suggesting $T \sim N_G^p$. Values found from fit (see key) are consistent with ideal case $p = 4$, where whole time is spent on calculating two-body integrals (20). As one-body integrals have $p = 2$, values tend to drift from 4.

D. Absolute Speed-up

Whilst analysis of the speed–up in strong scaling regime allowed us to investigate the efficiency gain in terms of a number of processes engaged in computation it is interesting and important to answer what is the absolute acceleration $SU(P, II, \varnothing)$. Obviously, this quantity still depends on P. In Tab. I we show the values of the speed-up (23) for different number of nodes P. The extremal case ($P = 56$ with both levels of parallelization) the speed-up

$$SU\,(56, II, \varnothing) = 303.418. \tag{28}$$

However, even for the lower number of SMP nodes (P) the absolute speed–up is excellent. For the sake of completeness, we retrieved the acceleration associated with openMP utilization (fourth column in Tab. I). As each SMP node consisted of 16 cores the number of active threads was the same. We obtained $SU(P, II, I)$ by means of the identity

$$SU\,(P, II, I) = \frac{SU\,(P, II, \varnothing)}{SU\,(P, I, \varnothing)}. \tag{29}$$

We found good speed–up ratio $\sim$ 13 (while the upper bound is 16) coming from collapsing of nested loops (20).

V. CONCLUSIONS

We have presented an effective computational approach related to the EDABI method - quantum–mechanical approach allowing to treat the electronic correlations in a consistent manner. This means that we combine the second-quantization aspect (evaluation of energies for different many-particle configurations) with an explicit evaluation of the renormalized wave functions (first-quantization aspect) in the resultant correlated many-particle state. The number of microscopic parameters that are necessary for description of the physical system can be meaningful in many cases. Hence, their computations become challenging as an effect of numerical complexity caused by the vast number of integrations to be performed (9). Here we have addressed in detail the part of the whole problem that is associated with the single-particle basis optimization. We have proposed the scheme based on the *process–pool* concept enhanced by the *two–level* parallelism, and test it utilizing self–made generic implementation [34] configured for the specific computational problem – $(H_2)_n$ chain. The proposed approach is intuitive and has allowed us to speed up the calculations significantly (of the order of 10^2) while preserving its generic character. Employing *process–pool* solution to other systems is then straightforward.

TABLE I. Values of the speed-up (SU) for one– and two-level parallelism for the different number of nodes **P**.

P	**SU(P,I,∅)**	**SU(P,II,∅)**	**SU(P,II,I)**
2	1.866	25.304	13.561
6	4.969	67.382	13.561
12	8.288	112.391	13.561
18	11.479	155.656	13.561
24	14.174	192.207	13.561
30	16.870	228.763	13.561
36	16.779	227.531	13.561
42	19.026	258.007	13.561
48	19.085	258.811	13.561
56	22.375	303.418	13.561

Since the considered physical example serves as an illustration of the elaborated scheme capability, one may consider engaging it to a wide class of computationally advanced physical problems tractable within the framework of EDABI or similar methods. Such problems cover:

- **lattice vibration (phonon) spectrum** via the so-called direct method (where all but few symmetries are lost, increasing the number of integrals dramatically – from 510 to over 10 000 for $(H_2)_n$ chain);
- calculation of **the electron–lattice coupling** parameters in direct space;
- electronic structure calculations of the **realistic two– and three-dimensional** atomic and molecular crystals (e.g. hydrogen, lithium hydride), where both the number of atomic orbitals and *the background field* increase essentially.

Neither form of the starting Hamiltonian nor the diagonalization scheme choice is essential for the applicability of the method, allowing us to incorporate other approaches such as the Gutzwiller approximation [8, 15, 21] or Gutzwiller Wave Function - Diagramatic Expansion [35] to study molecular and extended spatially systems. In this manner, one can address e.g. the fundamental question of metallization in correlated systems [36, 37] with the explicit evaluation of an model parameters. So far we have been able to solve exactly the chain with $N = 3$, 4, 5, and 6 molecules and the results are of similar type [29]. The finite-size type of scaling on the basis of these results requires additional analysis.

VI. ACKNOWLEDGMENTS

The authors are grateful to the Foundation for Polish Science (FNP) for financial support within the Project TEAM and to the National Science Center (NCN) for the support within the Grant MAESTRO, No. DEC-2012/04/A/ST3/00342. We are also grateful to dr hab. Adam Rycerz from the Jagiellonian University for helpful comments.

Appendix A: EDABI method: A brief overview

The **E**xact **D**iagonalization **Ab I**nitio (EDABI) approach combines first- and second-quantization aspects when solving the many-particle problem as expressed formally by its Hamiltonian.

The starting Hamiltonian (8) contains all possible dynamical processes starting from two-body interaction $V(r-r')$ in the coordinate (Schrödinger) representation. Its version (10) is already truncated and limited to two-state (here two-site) terms, i.e., the three- and four-site terms have been neglected. The rationale behind this omission is that, as shown elsewhere [3, 4], already the two-site terms (matrix elements) $\sim J_{ij}$ and V_{ij} are much smaller than those $\sim U$ and K_{ij}. Parenthetically, all the terms are taken into account in the starting atomic basis composing the Wannier function. Nonetheless, there is no principal obstacle in including all those terms in the case of the small systems considered here.

The second characteristic feature of EDABI is the single-particle basis optimization which composes the main topic of this paper. If the basis defining the starting Wannier-function basis were complete (i.e., $L \to \infty$ in Eq. (13)), then no basis optimization is required and an exact solution is achieved. However, as our basis $\{w_i\}$ is incomplete one, in our view, we are forced to readjust the basis so that the system dynamics (correlations) are properly accounted for. This introduces a variational aspect to our solution, since we introduce a variable wave function size, adjustable in the interacting (correlated) state. This very feature represents one of the factors defining the method. Such adjustment is also reasonable from a physical point of view, as the single-particle orbital adapts then itself to the presence of other particles (electrons). In other words, the correlations induced by the predominant interaction terms ($\sim U$ and K_{ij}) influence the size and shape of the states $\{w_i(\mathbf{r})\}$. This means that the orbitals get renormalized in the process of the correlated state formation. Nonetheless, it is not a priori determined that negligence of the higher virtually excited states in the expansion (13) is minimized is such a manner. This should be tested and is one of the subjects of our current research. This is not the primary topic of this paper so we shall not dwell upon it any further here.

Note also that by selecting the diagonalization of many-particle Hamiltonian in the second-quantized form, one avoids writing the many-determinantal expansion of the multiparticle wave function, as is the case in the CI methods. However, out of our formulation one can obtain the function $\Psi(\mathbf{r}_1, \ldots, \mathbf{r}_N)$ and in particular, define many-particle covalency [4]. This transition from the Fock space back to the Hilbert space is possible as the two languages of description are equivalent in the non-relativistic situation (for a lucid and didactic exposition of the first- and second-quantization schemes and their equivalence see e.g. [38]). The principal limitation of our method is the circumstance that it can be applied directly only to relatively small systems when the exact diagonalization is utilized.

Appendix B: Convergence of the single-particle energy for infinite system

In (21a) we have the microscopic parameter contained in the single-particle energy expression, namely

$$\epsilon_i = \left\langle \psi_i \middle| \left(-\bigtriangledown^2 - \sum_j \frac{2}{|\mathbf{r} - \mathbf{R}_j|} \right) \middle| \psi_i \right\rangle, \tag{B1}$$

where i labels lattice site (node) at which we calculate this single-particle energy, and j goes over the whole system. Also, ψ_i is the $1s$ Slater-type orbital centered on that site. For the sake of clarity, we disregard the orthogonalization procedure, as the one-body parameters contain, strictly speaking, a linear combination of integrals in STO basis.

For an infinite system, the sum $\sum_j$ constitutes a series of the form [39]

$$\begin{aligned} \epsilon_i =& - \left\langle \psi_i \right| \bigtriangledown^2 \left| \psi_i \right\rangle - \sum_j \left\langle \psi_i \middle| \frac{2}{|\mathbf{r} - \mathbf{R}_j|} \middle| \psi_i \right\rangle \\ =& \alpha^2 - 2\alpha - \sum_j \frac{2}{|\mathbf{R}_{ij}|} + 2\left(\alpha + \frac{1}{|\mathbf{R}_{ij}|} \right) e^{-2\alpha|\mathbf{R}_{ij}|}, \end{aligned} \tag{B2}$$

which diverges to $-\infty$. In this Appendix we show that there is an *effective* single-particle energy with no divergence for the infinite systems (case more general than those discussed in [7, 30]).

We start from Hamiltonian (21c)

$$\mathcal{H}_{tot} = \mathcal{H}_{ext} + \mathcal{V}_{i-i}, \tag{B3}$$

where *ion–ion* interaction is defined in the classical limit, i.e.,

$$\mathcal{V}_{i-i} \equiv \frac{1}{2}\sum_{i\neq j}\frac{2}{|\mathbf{R}_{ij}|}, \tag{B4}$$

and $|\mathbf{R}_{ij}|$ is the distance between sites i and j. We analyze next the remaining contributions, term by term.

1. Intersite Coulomb term

The intersite Coulomb term from (21b) cab be rewritten in the form

$$\frac{1}{2}\sum_{ij} K_{ij}\hat{n}_i\hat{n}_j = \overbrace{\frac{1}{2}\sum_{i\neq j} K_{ij}\delta\hat{n}_i\delta\hat{n}_j}^{K^{(0)}} + \overbrace{\frac{1}{2}\sum_i\sum_j (1-\delta_{ij})\,K_{ij}\hat{n}_i}^{K^{(1)}} + \overbrace{\frac{1}{2}\sum_i\sum_j (1-\delta_{ij})\,K_{ij}\hat{n}_j}^{K^{(2)}} - \overbrace{\frac{1}{2}\sum_{i\neq j} K_{ij}}^{K^{(3)}}, \tag{B5}$$

where $\delta\hat{n}_i \equiv (\hat{n}_i - 1)$ and δ_{ij} is Kronecker's delta.

We observe that when all sites are taken into account, the terms $K^{(1)}$ and $K^{(2)}$ are equivalent. We can rewrite them as follows

$$\begin{aligned}\mathcal{H}_{\rm K} =& K^{(0)} - K^{(3)} + 2\,\frac{1}{2}\sum_i\sum_j (1-\delta_{ij})\,K_{ij}\hat{n}_i = \\ \approx& K^{(0)} - K^{(3)} + 2\,\frac{1}{2}\sum_i \hat{n}_i\sum_{j(i)} K_{ij},\end{aligned} \tag{B6}$$

where $j(i)$ denotes the neighborhood of site i. Likewise,

$$K^{(3)} = \frac{1}{2}\sum_{i\neq j} K_{ij} = \frac{1}{2}\sum_i\sum_{j(i)} K_{ij}. \tag{B7}$$

We can write finally that

$$\begin{aligned}\mathcal{H}_{\rm K} =& K^{(0)} + \frac{1}{2}\sum_i \hat{n}_i\sum_{j(i)} K_{ij} \\ &+\frac{1}{2}\sum_i \delta\hat{n}_i\sum_{j(i)} K_{ij}.\end{aligned} \tag{B8}$$

Note that for half-filling $\langle\hat{n}_i\rangle = 1$ and the last part and $\left\langle K^{(0)}\right\rangle$ disappears.

2. Ion-ion repulsion

Similarly, we can rewrite (B4) to the form

$$\begin{aligned}\mathcal{V}_{i-i} =& \frac{1}{2}\sum_{i\neq j}\frac{2}{|\mathbf{R}_{ij}|} \approx \frac{1}{2}\sum_i\sum_{j(i)}\frac{2}{|\mathbf{R}_{ij}|} = \frac{1}{2}N\sum_{j(i_0)}\frac{2}{|\mathbf{R}_{i_0 j}|} \\ =& \frac{1}{2}\sum_i \hat{n}_i\sum_{j(i)}\frac{2}{|\mathbf{R}_{ij}|} - \frac{1}{2}\sum_i \delta\hat{n}_i\sum_{j(i)}\frac{2}{|\mathbf{R}_{ij}|}.\end{aligned} \tag{B9}$$

Again, the average of the latter term disappears for one particle per site.

3. Total Hamiltonian

We rearrange (21c) obtaining so that the new form of Hamiltonian is

$$\mathcal{H}_{\mathcal{N}} = \mathcal{H}_{\epsilon^{\rm eff}} + \mathcal{H}_{\rm Hubbard} + \mathcal{H}_{\delta n}. \tag{B10}$$

The new terms are

$$\mathcal{H}_{\epsilon^{\rm eff}} = \sum_i \epsilon_i^{\rm eff}\hat{n}_i, \tag{B11}$$

with $\epsilon_i^{\rm eff} = \epsilon_i + 1/2\sum_{j(i)}(2/|\mathbf{R}_{ij}| + K_{ij})$,

$$\mathcal{H}_{\rm Hubbard} = \sum_{ij}\sum_\sigma t_{ij}c_{i\sigma}^\dagger c_{j\sigma} + U\sum_i \hat{n}_{i\uparrow}\hat{n}_{i\downarrow}, \tag{B12}$$

$$\begin{aligned}\mathcal{H}_{\delta n} =& \frac{1}{2}\sum_{i\neq j} K_{ij}\delta\hat{n}_i\delta\hat{n}_j + \\ &+ \frac{1}{2}\sum_i \delta\hat{n}_i\sum_{j(i)}\left(K_{ij} - \frac{2}{|\mathbf{R}_{ij}|}\right).\end{aligned} \tag{B13}$$

The last question is whether the effective single-particle energy is now convergent.

4. Convergence of the single-particle energy

We can take ϵ_i^{eff} from eqs. (B2) and (B11) and rearrange it in a following manner

$$\begin{aligned}\epsilon_i^{\text{eff}} =&\epsilon_i + \frac{1}{2}\sum_j \left(\frac{2}{|\mathbf{R}_{ij}|} + K_{ij}\right) \\ =&\alpha^2 - 2\alpha + \sum_j -\frac{2}{|\mathbf{R}_{ij}|} + 2\left(\alpha + \frac{1}{|\mathbf{R}_{ij}|}\right)e^{-2\alpha|\mathbf{R}_{ij}|} \\ &+ \frac{1}{2}\sum_j \left(\frac{2}{|\mathbf{R}_{ij}|} + K_{ij}\right) \\ =&\alpha^2 - 2\alpha + \sum_j 2\left(\alpha + \frac{1}{|\mathbf{R}_{ij}|}\right)e^{-2\alpha|\mathbf{R}_{ij}|} \\ &+ \sum_j \left(\frac{1}{|\mathbf{R}_{ij}|} + \frac{1}{2}K_{ij} - \frac{2}{|\mathbf{R}_{ij}|}\right).\end{aligned} \tag{B14}$$

The latter part disappears in the classical limit $|\mathbf{R}_{ij}| \gg \alpha^{-1}$, where

$$K_{ij} \to \frac{2}{|\mathbf{R}_{ij}|}, \tag{B15}$$

and the remaining part $\sum_j 2\left(\alpha + |\mathbf{R}_{ij}|^{-1}\right)e^{-2\alpha|\mathbf{R}_{ij}|}$ is convergent.

[1] B. Himmetoglu, A. Floris, S. de Gironcoli, and M. Cococcioni, Int. J. Quant. Chem. **114**, 14 (2014).
[2] M. Karolak, G. Ulm, T. Wehling, V. Mazurenko, A. Poteryaev, and A. Lichtenstein, J. Electron. Spectrosc. Relat. Phenom. **181**, 11 (2010).
[3] J. Spałek, R. Podsiadły, W. Wójcik, and A. Rycerz, Phys. Rev. B **61**, 15676 (2000).
[4] J. Spałek, E. Görlich, A. Rycerz, and R. Zahorbeński, J. Phys.: Condens. Matter **19**, 255212 (2007), pp. 1-43.
[5] P. Surjan, *Second Quantizied Approach to Quantum Chemistry* (Springer, Berlin, 1989).
[6] A. P. Kądzielawa, A. Bielas, M. Acquarone, A. Biborski, M. M. Maśka, and J. Spałek, New J. Phys. **16**, 123022 (2014).
[7] A. Rycerz, *Physical properties and quantum phase transitions in strongly correlated electron systems from a combined exact diagonalization – ab initio approach*, Ph.D. thesis, Jagiellonian University (2003).
[8] A. P. Kądzielawa, J. Spałek, J. Kurzyk, and W. Wójcik, Eur. Phys. J. B **86**, 252 (2013).
[9] J. Hubbard, Proc. Roy. Soc. (London) **276**, 238 (1963).
[10] M. C. Gutzwiller, Phys. Rev. Lett. **10**, 159 (1963).
[11] M. C. Gutzwiller, Phys. Rev. **137**, A1726 (1965).
[12] J. Kanamori, Prog. Theor. Phys. **30**, 275 (1963).
[13] M. Zegrodnik and J. Spałek, Phys. Rev. B **86**, 014505 (2012).
[14] M. Zegrodnik, J. Bünemann, and J. Spałek, New J. Phys. **16**, 033001 (2014).
[15] M. M. Wysokiński, M. Abram, and J. Spałek, Phys. Rev. B **90**, 081114(R) (2014).
[16] T. Siro and A. Harju, Comput. Phys. Commun. **183**, 1884 (2012).
[17] K. A. Wendt, J. E. Drut, and T. A. Lähde, Comput. Phys. Commun. **182**, 1651 (2011).
[18] P. A. M. Dirac, Proc. Roy. Soc. (London) A **114**, 243 (1927).
[19] V. Fock, Z. Phys. **75**, 622 (1932).
[20] A. L. Fetter and J. D. Walecka, *Quantum Theory of Many-Particle Systems* (Dover, 2003).
[21] M. M. Wysokiński, M. Abram, and J. Spałek, Phys. Rev. B **91**, 081108 (2015).
[22] N. Ashcroft and N. Mermin, *Solid State Physics* (Saunders College, Philadelphia, 1976).
[23] R. S. Mulliken, J. Chem. Phys. **3**, 375 (1935).
[24] J. Kurzyk, W. Wójcik, and J. Spałek, Eur. Phys. J. B **66**, 385 (2008).
[25] J. I. Martínez, M. Isla, and J. A. Alonso, Eur. Phys. J. D **43**, 61 (2007).
[26] E. Kochanski, B. Roos, P. Siegbahn, and M. Wood, Theoret. Chim. Acta (Berl.) **32**, 151 (1973).
[27] E. Kochanski, Theoret. Chim. Acta (Berl.) **39**, 339 (1975).
[28] F. Mezzacapo and M. Boninsegni, Phys. Rev. Lett. **97**, 045301 (2006).
[29] A. P. Kądzielawa, A. Biborski, and J. Spałek, arXiv: 1506.3356 (2015).

[30] J. Kurzyk, *Układy skorelowanych elektronów o różnej wymiarowości z uwzględnieniem optymalizacji jednocząstkowej funkcji falowej*, Ph.D. thesis, Jagiellonian University (2007), in Polish.
[31] G. F. Giuliani and G. Vignale, *Quantum Theory of the Electron Liquid* (Cambridge, 2005).
[32] G. M. Amdahl, in *Proceedings of the April 18-20, 1967, Spring Joint Computer Conference*, AFIPS '67 (Spring) (ACM, New York, 1967) pp. 483–485.
[33] J. Schneider and S. Kirkpatrick, *Stochastic Optimization* (Springer, Berlin, 2006).
[34] A. Biborski and A. Kądzielawa, "`QMT: Quantum Metallization Tools Library`," (2014).
[35] J. Kaczmarczyk, J. Bünemann, and J. Spałek, New J. Phys. **16**, 073018 (2014).
[36] F. Gebhard, *The Mott Metal-Insulator Transition: Models and Methods* (Springer, Berlin, 1997).
[37] E. Koch, O. Gunnarsson, and R. M. Martin, Comput. Phys. Commun. **127**, 137 (2000).
[38] B. Robertson, Am. J. Phys. **41**, 678 (1973).
[39] J. C. Slater, *Quantum Theory of Molecules and Solids*, Vol. 1 (McGraw-Hill, New York, 1963).

3.5 Paper A-5 – Discontinuous transition of molecular-hydrogen chain to the quasi-atomic state: Exact diagonalization – ab initio approach

This paper represents the first implementation of the methods developed for the purpose of this Thesis, to the solid molecular hydrogen metallization. Namely, we apply the **E**xact **D**iagonalization – **Ab I**nitio Approach (EDABI) to the case of one-dimensional H_2 chain under external pressure (applied force). We optimize not only the single-particle basis wave functions, but also the molecular size (H_2 bond length) R. We start with the extended Hubbard model with the single-particle energy ϵ, the hopping integrals t_i (up to the third-nearest neighbor), the Hubbard interaction U, and the intersite electron–electron Coulomb interaction K_{ij} included up to the distance of $r_{cut-off} = 250a$, where a is the intermolecular distance (selected based on the analysis performed in paper A-4).

We find, that although there is only one minimum in the thermodynamic potential, connected to the molecular chain, when no force is applied, there are two minima in enthalpy when a sufficiently large force ($\sim 5nN$) is applied to the molecules which stabilizes the system. Additional stable phase appearing under pressure has a quasiatomic structure (a comparison of electronic densities is available in Fig. 3). Evolution of enthalpy of both minima is presented in Fig. 2, meaning in the regime of low applied force the molecular phase is stable, whereas for large forces quasiatomic chain has the lowest enthalpy. The transition comes with discontinuous change of lattice parameters, including intermolecular distance a (whole evolution is showed in Fig. 4) and effective (optimized) molecular size R_{eff} (inset in Fig. 2). As of the nature of transition, we calculated the Hubbard ratio U/W (inset in Fig. 3) that discontinuously drops below 1 at the transition, as well as the averages C_0 and C_1 connected respectively with intramolecular and intermolecular hopping. These averages exhibit an interesting property: they change from the molecular phase case $C_0 \approx 1$ and $C_1 \approx 0$ to $C_1 \approx C_0$ in the quasiatomic phase. The principal conclusion of the paper is that the molecular $\rightarrow$atomic-solid transition is concomitant with the Mott-Hubbard transition. The evolution from the molecular to the quasiatomic phase has also been illustrated on the computer animation enclosed to the Thesis (cf. `http://th-www.if.uj.edu.pl/ztms/download/supplementary_material/molecular_to_quasiatomic_transition-hydrogen_chain.avi`)

The paper has been submitted to the Physical Review B.

Discontinuous transition of molecular-hydrogen chain to the quasi-atomic state: Exact diagonalization – ab initio approach

Andrzej P. Kądzielawa,[1,*] Andrzej Biborski,[2,†] and Józef Spałek[1,2,‡]

[1] *Marian Smoluchowski Institute of Physics, Jagiellonian University, ulica Łojasiewicza 11, PL-30-348 Kraków, Poland*

[2] *Academic Centre for Materials and Nanotechnology, AGH University of Science and Technology, al. Mickiewicza 30, PL-30-059 Kraków, Poland*

(Dated: June 11, 2015)

We obtain in a direct and rigorous manner a transition from a stable molecular hydrogen nH_2 single chain to the quasiatomic two-chain $2nH$ state. We devise an original method composed of an exact diagonalization in the Fock space combined with an ab initio adjustment of the single-particle wave function in the correlated state. In this approach the well-known problem of double-counting the interparticle interaction does not arise at all. The transition is strongly discontinuous, and appears even for relatively short chains possible to tackle, $n = 3 \div 6$. The signature of the transition as a function of applied force is a discontinuous change of the equilibrium intramolecular distance. The corresponding change of the Hubbard ratio U/W reflects the Mott–Hubbard-transition aspect of the atomization. Universal feature of the transition relation to the Mott criterion for the insulator–metal transition is also noted. The role of the electron correlations is thus shown to be of fundamental significance.

PACS numbers: 31.15.A-, 71.27.+a, 67.80.F-, 67.63.Gh

1. Motivation The metallization of solid hydrogen is one of the central problems in physics [1–4], as well as in astrophysics of Jupiter, Saturn and exoplanets [5]. The building block, the H_2 molecule, is relatively simple, since the electrons are in the spin-singlet state in the ground state composed mainly of $1s$ states of atoms. Those molecular states with the experimental value of bond length $R \approx 1.401a_0$ [6] form at ambient pressure a molecular crystal with the lattice constant $a \sim 7a_0 \gg R$ [7]. Thus, to achieve atomic structure and metallicity one has to break the molecular bond, e.g., by achieving a more typical atomic solid configuration with $a \sim R$, what amounts in practice to applying an enormous pressure, as demonstrated repeatedly over the decades [2, 8]. But even then one may not achieve metallicity, as due to the relatively large atomic separation the system may compose a Mott (or Mott-Hubbard) insulator [9, 10], as the original interelectronic correlation effects may still be sufficiently strong. The fundamental aspect of this paper is to address this issue in a rigorous manner, albeit still in model situation, as detailed below.

The related and probably more intriguing question related to the hydrogen metallization is the conjecture that the system may exhibit a room-temperature superconductivity. The line of reasoning [11, 12] is based on the Bardeen-Cooper-Schrieffer (BCS) theory that as the critical temperature T_s is proportional to $M^{-1/2}$, where M is the ionic mass, then the hydrogen metal should have T_s at least one order of magnitude higher than that of a typical metal. However, here again the correlation effects must be carefully taken into account as they should not be too strong to destroy the metallicity, but essential, as they can lead by themselves also to the high-temperature superconductivity when the starting point is the atomic solid with half-filled Mott-Hubbard metal [13]. A marriage of strong electron–lattice and correlation effects should be possible to be accounted for at the starting stage. In this respect, here we determine rigorously the magnitude of the local correlation effects as described by the effective extended Hubbard model at the molecular → quasiatomic solid transition.

Recently, the molecular–atomic hydrogen transition has been discussed by a number of methods [14–17]. In this respect, the present results can be regarded as a basis for testing the approximate methods applicable to realistic calculations (see also discussion below).

2. Model and method We start with the extended Hubbard model with additional term $V_{\text{ion–ion}}$ expressing ion–ion repulsion namely,

$$\hat{\mathcal{H}} = \sum_i \epsilon_i \hat{n}_i + \sum_{\sigma, i \neq j} t_{ij} \hat{c}^{\dagger}_{i\sigma} \hat{c}_{j\sigma} + U \sum_i \hat{n}_{i\uparrow} \hat{n}_{i\downarrow} + \frac{1}{2} \sum_{i \neq j} K_{ij} \hat{n}_i \hat{n}_j + V_{\text{ion–ion}}, \quad (1)$$

where ϵ_i is the single-particle energy, t_{ij} are the so-called hopping integrals (all of them: t_0 (intramolecular) and t_1, t_2, and t_3 (intermolecular) have been marked explicitly in Fig. 1), U is the on-site Coulomb repulsion, and K_{ij} is the amplitude of intersite Coulomb repulsion, here taken into account for the interaction radius up to $250a$ in the starting atomic representation, where a is the intermolecular distance (see [18] for details). The configuration of the

* kadzielawa@th.if.uj.edu.pl
† andrzej.biborski@agh.edu.pl
‡ ufspalek@if.uj.edu.pl

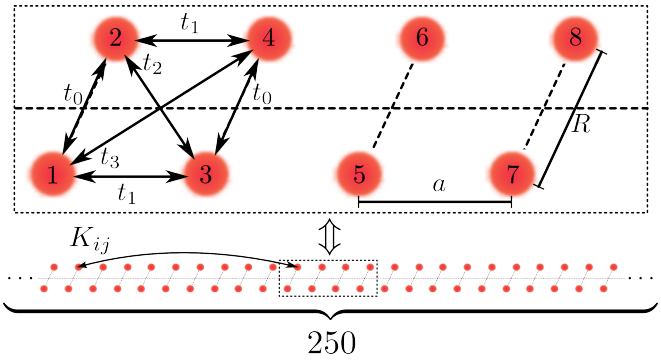

FIG. 1. Schematic representation of H_2 molecular chain with possible nearest-neighbor and next nearest neighbor hoppings $\{t_i\}_{i=0,1,2,3}$ marked. The labeling of the sites $i = 1, 2, 3, \ldots$ is specified, as well as the bond length R at intermolecular distance a. The radius of included intersite Coulomb interaction is equal to $250a$ in the atomic representation.

molecules and related microscopic parameters are shown in Fig. 1.

Explicitly, those parameters can be defined in the following manner

$$\begin{aligned}\langle w_i|\, H_1\, |w_j\rangle &\equiv \int d^3r\ w_i^*(\mathbf{r}) H_1(\mathbf{r}) w_j(\mathbf{r}) \\ &\equiv \epsilon_i\delta_{ij} + t_{ij}(1-\delta_{ij},) \qquad (2)\\ \langle w_i w_j|\, V_{12}\, |w_i w_j\rangle &\equiv \int d^3r d^3r'\ |w_i(\mathbf{r})|^2 V_{12}(\mathbf{r}-\mathbf{r}')|w_j(\mathbf{r}')|^2 \\ &\equiv U\delta_{ij} + K_{ij}(1-\delta_{ij}), \qquad (3)\end{aligned}$$

where H_1 is the Hamiltonian of single electron in the medium and V_{12} is the Coulomb repulsive interaction for a single pair of them. Furthermore, the Wannier functions are defined in terms of atomic (Slater) functions, i.e.,

$$w_i(\mathbf{r}) = \sum_j \beta_{ij}\psi_j(\mathbf{r}), \qquad (4)$$

where the $1s$-type Slater function in defined as $\psi_i(\mathbf{r}) \equiv \psi(\mathbf{r} - \mathbf{R}_i) = (\alpha^3/\pi)^{1/2}\exp(-\alpha|\mathbf{r}-\mathbf{R}_i|)$, with α being its inverse size in the medium, here taken as a variational parameter for given intermolecular distance a and determined in the correlated state ($i \equiv \mathbf{R}_i$ is the i-th proton position). Each Slater function is approximated by its expansion in the Gaussian basis

$$\psi_i(\mathbf{r}) \approx \alpha^{\frac{3}{2}} \sum_{q=1}^{p} \left(\frac{2\alpha^2\Gamma_q^2}{\pi}\right)^{\frac{3}{4}} e^{-\alpha^2\Gamma_q^2|\mathbf{r}-\mathbf{R}_i|^2}, \qquad (5)$$

with p being the number of Gaussian functions taken into account to express accurately the functions $\{\psi_i(\mathbf{r})\}$ and $\{\Gamma_q\}$ is the set of adjustable parameters obtained from a separate procedure (for details see [19]). In effect, all the parameters: ϵ_i, t_{ij}, U, K_{ij} can be expressed in terms of α and are determined in the correlated state (after the exact diagonalization in the Fock space has also been carried out simultaneously). Strictly speaking, to obtain proper atomic limit we have to take: $\epsilon_i \to \epsilon_i^{eff} = \epsilon_i + (1/2)\sum_j(2/R_{ij} + K_{ij})$ [18].

First, we determine values of hopping integrals t_0, t_1, t_2 and t_3, Hubbard (intraatomic) and intersite interactions U and K_{ij}, by determining the Wannier functions defining them. The Wannier functions are expressed in terms of (atomic) Slater functions of adjustable size α^{-1}, each of which is expressed in turn via $p = 9$ Gaussian functions [18]. In the next step, we determine the lowest eigenvalue of the Hamiltonian (1) with periodic boundary conditions, by diagonalizing it by means of Lanczos algorithm. By finding the ground state energy in the Fock space and subsequently, by optimizing the energy also with respect to the size α^{-1}, we obtain a true physical ground state energy in the correlated state for given intermolecular distance a. Such extended calculations make the results not limited to the parametrized-model considerations, as U, t_{ij}, and K_{ij} are evaluated explicitly, as is also the ground state energy, for fixed a. One should note that in the procedure the bond length is also optimized ($R \to R_{eff}$). All this is carried out first for the zero-applied force to obtain the system equilibrium configuration, i.e., the energy and the effective bond length R_{eff} in the multimolecular configuration. In the second step, we apply the external compressing force f to the end molecules and determine the enthalpy minimum to trace the system evolution as a function of a. The part of the procedure connected with the optimization of the single-particle wave functions has been discussed in detail elsewhere [18]. The code used for the computation is also available [20].

Typical numerical procedure starts with fixing a and R, and selecting input value for the variational parameter α. Next, we vary the inverse wave function size α to find the physical ground-state energy employing, at every step, the so-called *process–pool solution* for the computationally expensive problem of obtaining the microscopic parameters. We include all the intersite interactions for the sites with a relative distance smaller than $250a$. The accuracy of the numerical results is set to be of the order of $10^{-4}Ry$. Impact of these parameters was examined carefully in [18] and achieving the values above proved to be sufficient. The long range of the interactions in the atomic representation is expected to emulate correctly a longer-chain behavior.

3. Results In Fig. 2 we display the system enthalpy as a function of force f exerted on the edge molecules. Typically, two solutions appear which we call respectively as the molecular and the quasi-atomic, each of which is characterized below. The solid points mark the transition points for $4H_2$ (left) and $3H_2$ (right). In the Inset we show the effective bond length R_{eff} vs a. Note two specific features. First, the lattice contracts in a discon-

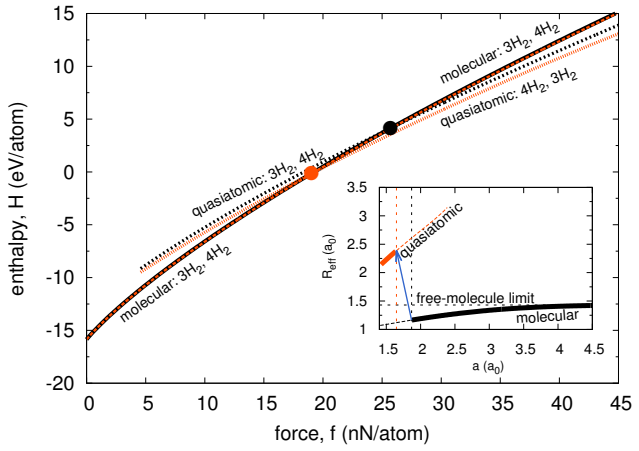

FIG. 2. Phase diagram encompassing quasiatomic and molecular states for nH_2 chain as a function of exerted force along the chain. Inset: Effective bond length R_{eff} vs. the intermolecular distance a.

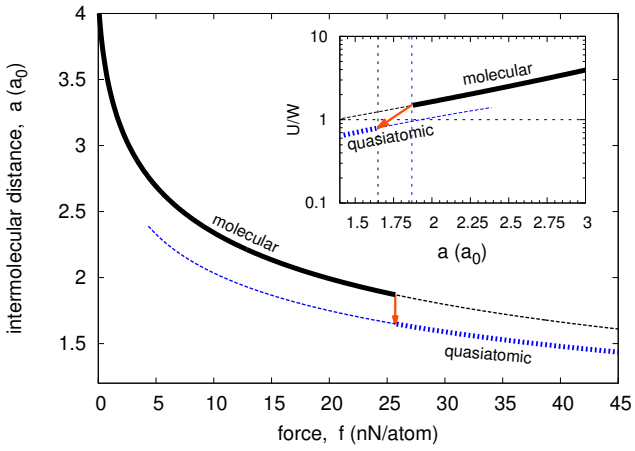

FIG. 4. Equilibrium intermolecular distance a versus exerted force f for the case of $3H_2$ system. The transition is of the first order as marked. Inset: U/W ratio vs. a showing that in the quasiatomic state $U/W \sim 0.8$ signaling the onset of a correlated metallic state.

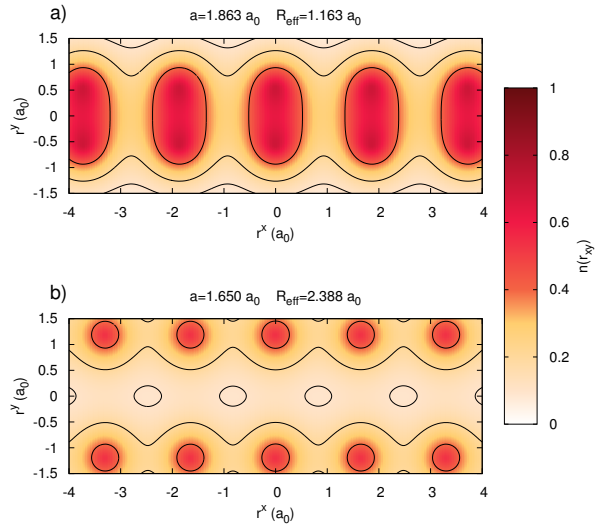

FIG. 3. Electron density projected onto the plane of H_2 molecules near the molecular $\rightarrow$ atomic transition: a) for the molecular state; b) for the quasiatomic state. In case a) the density is very small in the space in between molecules (vertical line joining the atoms). The critical intermolecular distance a and the effective bond length R_{eff} are also specified in each of the states. The corresponding critical force is $f_C = 25.705nN$ for $3H_2$ system.

tinuous manner at the transition and second, the bond length jumps then from an almost single-molecule value $R_{eff} \ll a$ to the limit $R_{eff} \sim a$ signaling their separation into a quasi-atomic configuration. The last feature of the transition is explicitly illustrated in Fig. 3, where the projected electron density onto the plane composed of molecules is shown both on the molecular (top) and the quasi-atomic (bottom) sides of transition. The parameters a and R_{eff} are listed also in each case. As said above, due to the supercell (nH_2) construction and the use of periodic boundary conditions, the system emulates an extended-system behavior.

In Fig. 4 the interdependence of the intermolecular distance versus force is provided. As shown also in the inset to Fig. 2, this figure demonstrates the first-order transition, since the cell volume a changes discontinuously at this mol. $\rightarrow$ quasiat. transition from $1.869a_0$ to $1.647a_0$. In the inset to Fig. 4 we provide the ratio of the Hubbard interaction U to the bandwidth defined (for perpendicular orientation of molecules, when $t_2 \equiv t_3$) as $W = -4t_1 + |t_0 + 2t_2| - |t_0 - 2t_2|$, as a function of f. Note the fundamental characteristic: this ratio jumps from the value $U/W \sim 1.49$ to 0.8. So, the system is indeed strongly correlated at the transition with the effective gap near the transition from the molecular side estimated as $\epsilon_g/W = U/W - 1 \approx 0.49$. Furthermore, the value $U/W \sim 1$ is the typical value for the Mott-Hubbard transition, weakly dependent on the system structure [21]. It is also interesting to note that here the Mott-Hubbard transition takes place from a non-magnetic (spin-singlet) molecular configuration to a correlated atomic solid, with strong suggestion for metallicity of such system with one electron per atom in predominantly $1s$ state. The possibility of magnetic (antiferromagnetic) and/or superconducting quasiatomic state should be analyzed separately.

In Fig. 5 we present a dependence of the intramolecular (t_0) and intermolecular (t_1) hopping parameters. At the transition the parameters t_0 and t_1 roughly equalize showing again that the solid at small a is of quasiatomic nature. In the inset we present the intramolecular ($C_0 \equiv \left\langle \hat{c}^\dagger_{1\sigma}\hat{c}_{2\sigma} \right\rangle$) and intermolecular ($C_1 \equiv \left\langle \hat{c}^\dagger_{1\sigma}\hat{c}_{3\sigma} \right\rangle$) hopping probabilities. In the molecular state $C_0 \approx 1$ and $C_1 \approx 0$ (a strong molecular bond is formed), whereas in the quasiatomic state $C_0 \sim C_1$. These two quan-

TABLE I. Microscopic parameters at the molecular → quasiatomic transition. The values are in eV if not specified otherwise.

	a (a_0)	R (a_0)	W	t_0	t_1	t_2	U	K_0	K_1	K_2	$\alpha(a_0^{-1})$
molecular	1.869	1.164	17.881	−15.487	−6.161	1.691	26.472	15.238	13.516	10.551	1.194
quasiatomic	1.647	2.386	33.124	−5.270	−8.445	0.164	26.404	10.825	14.701	8.976	1.251

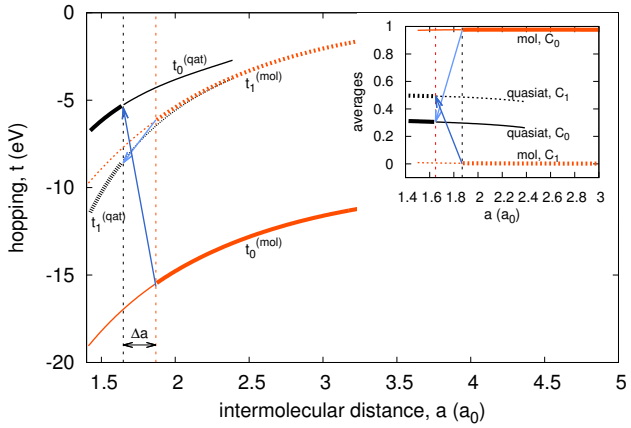

FIG. 5. Evolution of the intra- and inter-molecular hopping parameters, t_0 and t_1 respectively, versus intermolecular distance a. Note the jump of a at the transition molecular → quasiatomic configurations as marked by the arrows. Inset: hopping probabilities: intra- and inter-molecular, C_0 and C_1, respectively. For discussion see main text.

tities illustrate thus in a direct manner the nature of the states and in particular, the metallic type of the bonding in the quasiatomic solid state. For the sake of completeness, in Table I we list all the principal microscopic parameters in the correlated state for intermolecular distances at transition. The values of K_{ij} converge towards the asymptotic value $K_{ij} \to 0$ slowly. Such behavior is in accordance with the view [22] that the long-range part of the Coulomb interaction is not screened efficiently in low-dimensional systems. This is the reason why we have taken their long-range character, at least in the atomic representation. Parenthetically, note that we have neglected the direct exchange interaction and the so-called correlated-hopping terms [23], as they are of much smaller amplitude at these distances. Note also that the Mott criterion at the transition [24, 25] takes in the present situation the form $a_B n_C^{1/d} \equiv (\alpha a)^{-1} \approx 0.45$ at the transition, not too far from the value 0.25 for 3-dimensional ($d = 3$) systems.

4. Outlook We have described in a direct and rigorous manner the behavior of electrons in the short H_2 chains by a proper choice of the supercell and including the long-range Coulomb interactions, as well as utilizing the periodic boundary conditions, emulating together an extended-chain behavior. Amazingly, the results obtained meet some of the features one can expect for a three-dimensional hydrogen molecular → quasiatomic transformation. Obviously, no detailed realistic phase diagram can be obtained, as both the structural details and the effect of zero-point motion are still missing. However, a unique character of the Mott-Hubbard transition is already established. The model formulated here may form a basis for quantitative approach to solid hydrogen with a proper account of electronic correlations. In such approach a three-dimensional realistic model must be constructed. We think that tackling of this problem is possible on a small scale within our **E**xact **D**iagonalization **Ab I**nitio (EDABI) approach employed here and to other problems [26] involving electronic correlations as an essential aspect of their physical properties. For $3d$ system, approximate second-quantization diagonalization schemes such as the statistically-consistent Gutzwiller approximation may be used with concomitant single-particle wave-function optimization [25]. These methods can be tested in the present exact limit.

One should also note that the principal assumption made at this point is that the protons form a lattice even in the metallic phase, not a proton-electron quantum-liquid plasma [15, 27–29]. Such problem is possible to tackle within the present model by assessing the optimal ground-state energy for a random choice of the proton positions. But first, an accurate estimate of the zero-point motion amplitude and the corresponding energy [30] must be carried out for an extended system with correlations [31]. Finally, the estimate of the superconducting gap magnitude by incorporating correlations for the extended Hubbard model [13] and realistic values of the local electron-proton coupling [30] may be possible in not too distant future.

5. Acknowledgments We are grateful to Drs. Adam Rycerz and Marcello Acquarone, and to Prof. Maciek M. Maśka for helpful discussions. The work was supported by the National Science Centre (NCN), Grant No. DEC-2012/04/A/ST3/00342. The computations were carried out on supercomputer TERA-ACMIN located at the AGH University of Science and Technology in Kraków.

[1] E. Wigner and H. B. Huntington, "On the possibility of a metallic modification of hydrogen," J. Chem. Phys. **3**, 764 (1935).

[2] H. K. Mao and R. J. Hemley, "Ultrahigh-pressure transitions in solid hydrogen," Rev. Mod. Phys. **66**, 671–692 (1994).

[3] I. Silvera, "The insulator-metal transition in hydrogen," Proc. Natl. Acad. Sci. U.S.A. **107**, 12743 (2010).

[4] J. M. McMahon, M. A. Morales, C. Pierleoni, and D. M. Ceperley, "The properties of hydrogen and helium under extreme conditions," Rev. Mod. Phys. **84**, 1607–1653 (2012).

[5] I. Baraffe, G. Chabrier, and T. Barman, "The physical properties of extra-solar planets," Rep. Prog. Phys. **73**, 016901 (2010).

[6] W. Kołos and L. Wolniewicz, "Improved theoretical ground-state energy of the hydrogen molecule," J. Chem. Phys. **49**, 404 (1968).

[7] A. E. Curzon and A. J. Mascall, "The crystal structures of solid hydrogen and solid deuterium in thin films," British Journal of Applied Physics **16**, 1301 (1965).

[8] R. T. Howie, Ch. L. Guillaume, T. Scheler, A. F. Goncharov, and E. Gregoryanz, "Mixed molecular and atomic phase of dense hydrogen," Phys. Rev. Lett. **108**, 125501 (2012).

[9] F. Gebhard, *The Mott Metal-Insulator Transition: Models and Methods* (Springer, Berlin, 1997).

[10] A. P. Kądzielawa, J. Spałek, J. Kurzyk, and W. Wójcik, "Extended hubbard model with renormalized Wannier wave functions in the correlated state III," Eur. Phys. J. B **86**, 252 (2013).

[11] N. W. Ashcroft, "Metallic hydrogen: A high-temperature superconductor?" Phys. Rev. Lett. **21**, 1748–1749 (1968).

[12] E. Babaev, A. Sudbo, and N. W. Ashcroft, "A superconductor to superfluid phase transition in liquid metallic hydrogen," Nature **431**, 668 (2004).

[13] J. Kaczmarczyk, J. Spałek, T. Schickling, and J. Bünemann, "Superconductivity in the two-dimensional Hubbard model: Gutzwiller wave function solution," Phys. Rev. B **88**, 115127 (2013).

[14] S. Azadi, W. M. C. Foulkes, and T. D. Kühne, "Quantum monte carlo study of high pressure solid molecular hydrogen," New J. Phys. **15**, 113005 (2013).

[15] G. Mazzola, S. Yunoki, and S. Sorella, "Unexpectedly high pressure for molecular dissociation in liquid hydrogen by electronic simulation," Nat. Commun. **5** (2014), http://dx.doi.org/10.1038/ncomms4487.

[16] I. Errea, M. Calandra, Ch. J. Pickard, J. Nelson, R. J. Needs, Y. Li, H. Liu, Y. Zhang, Y. Ma, and F. Mauri, "High-pressure hydrogen sulfide from first principles: A strongly anharmonic phonon-mediated superconductor," Phys. Rev. Lett. **114**, 157004 (2015).

[17] S. Azadi and W. M. C. Foulkes, "Fate of density functional theory in the study of high-pressure solid hydrogen," Phys. Rev. B **88**, 014115 (2013).

[18] A. Biborski, A. P. Kądzielawa, and J. Spałek, "Combined shared and distributed memory ab-initio computations of molecular-hydrogen systems in the correlated state: process pool solution and two-level parallelism," arXiv:1504.00500 (2015).

[19] A. Rycerz, *Physical properties and quantum phase transitions in strongly correlated electron systems from a combined exact diagonalization – ab initio approach*, Ph.D. thesis, Jagiellonian University (2003), `th-www.if.uj.edu.pl/ztms/download/phdTheses/Adam_Rycerz_doktorat.pdf`.

[20] A. Biborski and A. Kądzielawa, "`QMT: Quantum Metallization Tools Library`," (2014), `https://bitbucket.org/azja/qmt`.

[21] A. Datta, J. M. Honig, and J. Spałek, "Discontinuous metal-insulator transitions of correlated electrons at nonzero temperature: Effect of the shape of the density of states," Phys. Rev. B **44**, 8459–8466 (1991).

[22] J. Hubbard, "Generalized Wigner lattices in one dimension and some applications to tetracyanoquinodimethane (TCNQ) salts," Phys. Rev. B **17**, 494 (1978).

[23] J. Spałek, R. Podsiadły, W. Wójcik, and A. Rycerz, "Optimization of single-particle basis for exactly soluble models of correlated electrons," Phys. Rev. B **61**, 15676 (2000).

[24] N. F. Mott, *Metal-insulator transitions* (Taylor & Francis, London, 1991).

[25] J. Spałek, J. Kurzyk, R. Podsiadły, and W. Wójcik, "Extended Hubbard model with the renormalized Wannier wave functions in the correlated state II: quantum critical scaling of the wave function near the Mott-Hubbard transition," Eur. Phys. J. B **74**, 63 (2010).

[26] J. Spałek, E.M. Görlich, A. Rycerz, and R. Zahorbeński, "The combined exact diagonalization–ab initio approach and its application to correlated electronic states and Mott–Hubbard localization in nanoscopic systems," J. Phys.: Condens. Matter **19**, 255212 (2007), pp. 1-43.

[27] M. A. Morales, C. Pierleoni, E. Schwegler, and D. M. Ceperley, "Evidence for a first-order liquid-liquid transition in high-pressure hydrogen from ab initio simulations," Proc. Natl. Acad. Sci. U.S.A. **107**, 12799 (2010).

[28] S. A. Bonev, E. Schwegler, T. Ogitsu, and G. Galli, "A quantum fluid of metallic hydrogen suggested by first-principles calculations," Nature **431**, 672 (2004).

[29] W.J. Nellis, "Discovery of metallic fluid hydrogen at 140 gpa and ten-fold compressed liquid density," The Review of High Pressure Science and Technology **17**, 328–333 (2007).

[30] A. Kądzielawa, A. Bielas, M. Acquarone, A. Biborski, M. M. Maśka, and J. Spałek, "H_2 and $(H_2)_2$ molecules with an ab initio optimization of wave functions in correlated state: electron–proton couplings and intermolecular microscopic parameters," New J. Phys. **16**, 123022 (2014).

[31] J. Spałek and A. Rycerz, "Electron localization in a one-dimensional nanoscopic system: A combined exact diagonalization - an *ab initio* approach," Phys. Rev. B **64**, 161105 (2001).

Chapter 4

Summary and Conclusions

The principal aim of this Thesis is to develop and implement a reliable method of calculating the physical properties of solid hydrogen system, both in terms of its insulator-to-metal and molecular-to-atomic transition. In order to do so we have successfully employed the **E**xact **D**iagonalization – **Ab I**nitio Approach (EDABI), both in its original *exact-method-of-diagonalization* based version and the modified, using the so-called the **S**tatistically-Consistent **G**utzwiller **A**pproximation (SGA). We have also created the open access, computational `C++`-based library: **Q**uantum **M**etallization **T**ools (*QMT* [44]), that provides a generic description of quantum-mechanical system in terms of EDABI method.

We have used EDABI in combination with SGA to model the metallization of atomic hydrogen (cf. papers A-1 and A-2). Rather than including the electron–electron Coulomb interaction explicitly, we have used an effective approximation, working only close to the half-filling. As a final result, we obtained the metallization pressure $\sim 100GPa$. This is still a rather simplistic model and it requires a more involved approach to make realistic estimate of the critical pressure. This means explicitly to *(i)* describe the hydrogen as a molecular crystal (in all of phases I, II, III and IV discussed in the introductory Chapters), modify EDABI with a Hamiltonian diagonalization scheme that include *(ii)* long-range (Coulomb) interactions and *(iii)* a multi-orbital picture, *(iv)* find the proper thermodynamic potential to describe the system under high pressure, *(v)* assess the zero-point motion energy and calculate the electron–lattice coupling, and finally *(vi)* use the outcome of steps *(i)*–*(v)* to study whether, and under which conditions, the system manifests superconducting properties. This path led us to the creation of *QMT* and results presented in papers A-3, A-4, and A-5.

We started *(i)* with the simplest building-block of three-dimensional molecular crystals - a H_2 molecule (cf. paper A-3). This case was already well described in a static situation [107], which gave us a point of reference for further development. We used the full Hamiltonian with all two-site interaction terms, which in turn led to the results differing by $\sim 2\%$, even when omitting in the single-particle basis wave functions different from $1s$. For

the purpose of *(v)*, we devised an approach to asses the zero-point motion amplitude and energy, as well as electron–proton couplings, resulting in the value close to that observed experimentally. We expanded *(i)* and tested our computational approach in paper A-4, where we also made first attempts to deal with the problem *(ii)*. This requires a separate study, as the standard Gutzwiller approximation increases the numerical complexity exponentially when the intersite interactions are included. For this purpose, we plan to employ modified SGA or the so-called diagrammatic expansion for the Gutzwiller wave function (DE-GWF) [68]. When the long-range interactions are included, the most time-consuming element of EDABI is the Hamiltonian parametrization, the part of the problem that can be efficiently parallelized, thus allowing to use the modern supercomputer infrastructure. We proceeded with *(i)* by modeling the one-dimensional H_2 crystal (cf. papers A-4 and A-5). It has been completed with semi-realistic description of H_2 chain including optimization of molecular size and renormalization of the single-particle basis. Treating *(iv)*, we chose enthalpy, a thermodynamic potential allowing for description with pressure as a proper variable to analyze the system behavior. We have found two classes of enthalpy minima – one connected to the H_2 molecular crystal and one connected to $2H$ quasiatomic phase. Moreover, we determine a critical applied force causing the system transition from molecular to quasiatomic structure in a discontinuous (first-order) manner. This is what we expect to happen when describing the hydrogenic systems. Up to this moment, we used Lanczos algorithm for the diagonalization of parameterized Hamiltonian in the Fock space. The next step will be to use modified SGA in a way that it includes: *(ii)* long-range both Coulomb and exchange interaction. As of *(iii)*, we have prepared computational methods for incorporating higher s– and p–type orbitals. This is not included in any of the papers here, but the reader may refer to Sec. 2.2.3 with the results concerning the ground-state and the ionization energies of first ten elements of the Periodic Table.

Only when steps *(i)*–*(v)* are completed, we can approach the superconducting state of these systems. This topic is the final goal of the whole project on the metal hydrogen. It is still a long way to go. Nonetheless, few decisive results towards this final goal have been accomplished. First of all, that the metallization can be understood in the terms of Mott-Hubbard localization. In this respect, a successful model has been formulated. Second, the zero-point motion energy has been estimated in realistic terms. Third, local electron–lattice interaction coefficients have been evaluated. The knowledge of these parameters is indispensable to estimate the value of the superconducting transition temperature. However, a simple BCS-like estimate will not work, as we have shown that even in the metallic state the electrons are moderately to strongly correlated ($U/W \lesssim 1$), so there may appear an essential contribution to the pairing coming from the correlations. It would be very interesting to see if the electron–phonon interaction alone can account for the superconductivity with such a high transition temperature. The future will tell.

Chapter 5

Bibliography

Bibliography

[1] F. Gebhard, *The Mott Metal-Insulator Transition: Models and Methods* (Springer, Berlin, 1997).

[2] F. Bloch, "Bemerkung zur Elektronentheorie des Ferromagnetismus und der elektrischen Leitfähigheit," Z. Physik **57**, 545 (1929).

[3] A. H. Wilson, "The theory of electronic semi-conductors," Proc. Roy. Soc. London A **133**, 458 (1931).

[4] A. H. Wilson, "The theory of electronic semi-conductors II," Proc. Roy. Soc. London A **134**, 277 (1931).

[5] R. E. Peierls, *Quantum Theory of Solids* (Clarendon Press, Oxford, 2001).

[6] H. Frohlich, "On the Theory of Superconductivity: The One-Dimensional Case," Proc. Roy. Soc. London A **223**, 296 (1954).

[7] P. W. Anderson, "Absence of diffusion in certain random lattices," Phys. Rev. **109**, 1492 (1958).

[8] N. F. Mott, "The basis of the electron theory of metals, with special reference to the transition metals," Proc. Phys. Soc. A **62**, 416 (1949).

[9] N. F. Mott, "Metal-Insulator Transition," Rev. Mod. Phys. **40**, 677 (1968).

[10] N. F. Mott, *Metal-Insulator Transitions*, 2nd ed. (Taylor and Francis, London, 1990).

[11] A. Klejnberg and J. Spałek, "Simple treatment of the metal-insulator transition: Effects of degeneracy, temperature, and applied magnetic field," Phys. Rev. B **57**, 12041 (1998).

[12] J. Spałek, "Fermi liquid behavior and the metal-insulator transition of almost localized electrons: A brief theoretical review and an application to V_2O_3 system," J. Solid State Chem. **88**, 70 (1990).

[13] J.-M. Carter, V. Shankar V., and H.-Y. Kee, "Theory of metal-insulator transition in the family of perovskite iridium oxides," Phys. Rev. B **88**, 035111 (2013).

[14] B. J. Kim, H. Jin, S. J. Moon, J.-Y. Kim, B.-G. Park, C. S. Leem, J. Yu, T. W. Noh, C. Kim, S.-J. Oh, J.-H. Park, V. Durairaj, G. Cao, and E. Rotenberg, "Novel $J_{\text{eff}} = 1/2$ Mott State Induced by Relativistic Spin-Orbit Coupling in Sr_2IrO_4," Phys. Rev. Lett. **101**, 076402 (2008).

[15] S. J. Moon, H. Jin, K. W. Kim, W. S. Choi, Y. S. Lee, J. Yu, G. Cao, A. Sumi, H. Funakubo, C. Bernhard, and T. W. Noh, "Dimensionality-Controlled Insulator-Metal Transition and Correlated Metallic State in $5d$ Transition Metal Oxides $Sr_{n+1}Ir_nO_{3n+1}$ ($n = 1$, 2, and ∞)," Phys. Rev. Lett. **101**, 226402 (2008).

[16] A. K. Raychaudhuri, K. P. Rajeev, H. Srikanth, and N. Gayathri, "Metal-insulator transition in perovskite oxides: Tunneling experiments," Phys. Rev. B **51**, 7421–7428 (1995).

[17] H. T. Dang, A. J. Millis, and C. A. Marianetti, "Covalency and the metal-insulator transition in titanate and vanadate perovskites," Phys. Rev. B **89**, 161113 (2014).

[18] M. Kamada, N. Mori, and T. Mitsui, "Electrical resistivity near the critical boundary of antiferromagnet in $NiS_{2-x}Se_x$," J. Phys. C: Solid State Phys. **10**, L643 (1977).

[19] J. M. Honig and J. Spałek, "Electronic Properties of $NiS_{2-x}Se_x$ Single Crystals: From Magnetic Mott-Hubbard Insulators to Normal Metals," Chem. Mater. **10**, 2910 (1998).

[20] S. Miyasaka, H. Takagi, Y. Sekine, H. Takahashi, N. Môri, and R. Cava, "Metal-Insulator Transition and Itinerant Antiferromagnetism in $NiS_{2-x}Se_x$ Pyrite," J. Phys. Soc. Jpn. **69**, 3166 (2000).

[21] C. Marini, B. Joseph, S. Caramazza, F. Capitani, M. Bendele, M. Mitrano, D. Chermisi, S. Mangialardo, B. Pal, M. Goyal, A. Iadecola, O. Mathon, S. Pascarelli, D. D. Sarma, and P. Postorino, "Local disorder investigation in $NiS_{2-x}Se_x$ using Raman and Ni K-edge x-ray absorption spectroscopies," J. Phys. Condens. Matter **26**, 452201 (2014).

[22] F. J. Morin, "Oxides of the 3d Transition Metals*," Bell Syst. Tech. J. **37**, 1047 (1958).

[23] C. Weber, D. D. O'Regan, N. D. M. Hine, M. C. Payne, G. Kotliar, and P. B. Littlewood, "Vanadium Dioxide: A Peierls-Mott Insulator Stable against Disorder," Phys. Rev. Lett. **108**, 256402 (2012).

[24] J. Wei, Z. Wang, W. Chen, and D. H. Cobden, "New aspects of the metal-insulator transition in single-domain vanadium dioxide nanobeams," Nat. Nano. **4**, 420 (2009).

[25] M. M. Qazilbash, A. A. Schafgans, K. S. Burch, S. J. Yun, B. G. Chae, B. J. Kim, H. T. Kim, and D. N. Basov, "Electrodynamics of the vanadium oxides VO_2 and V_2O_3," Phys. Rev. B **77**, 115121 (2008).

[26] N. Ashcroft and N. Mermin, *Solid State Physics* (Saunders College, Philadelphia, 1976).

[27] J. Spałek, *Wstęp do fizyki materii skondensowanej* (Wydawnictwo Naukowe PWN, Warszawa, 2015) in Polish.

[28] J. Kurzyk, *Układy skorelowanych elektronów o różnej wymiarowości z uwzględnieniem optymalizacji jednocząstkowej funkcji falowej*, Ph.D. thesis, Jagiellonian University (2007), in Polish, `th-www.if.uj.edu.pl/ztms/download/phdTheses/Jan_Kurzyk_doktorat.pdf`.

[29] J. Kurzyk, W. Wójcik, and J. Spałek, "Lieb-Wu solution, Gutzwiller-wave-function, and Gutzwiller-ansatz approximation with adjustable single-particle wave function for the Hubbard chain," Acta Phys. Polon. A **111**, 603 (2007).

[30] J. Kurzyk, W. Wójcik, and J. Spałek, "Extended hubbard model with renormalized wannier wave functions in the correlated state: beyond the parametrized models," Eur. Phys. J. B **66**, 385–398 (2008).

[31] J. Spałek, J. Kurzyk, R. Podsiadły, and W. Wójcik, "Extended Hubbard model with the renormalized Wannier wave functions in the correlated state II: quantum critical scaling of the wave function near the Mott-Hubbard transition," Eur. Phys. J. B **74**, 63 (2010).

[32] A. P. Kądzielawa, J. Spałek, J. Kurzyk, and W. Wójcik, "Extended hubbard model with renormalized Wannier wave functions in the correlated state III," Eur. Phys. J. B **86**, 252 (2013).

[33] G. Mazzola, S. Yunoki, and S. Sorella, "Unexpectedly high pressure for molecular dissociation in liquid hydrogen by electronic simulation," Nat. Commun. **5** (2014), 10.1038/ncomms4487.

[34] J. McMinis, R. C. Clay, D. Lee, and M. A. Morales, "Molecular to Atomic Phase Transition in Hydrogen under High Pressure," Phys. Rev. Lett. **114**, 105305 (2015).

[35] W. L. Mao, "High pressure: Compressed hydrogen heats up," Nat. Mater. **14**, 466–468 (2015).

[36] R. T. Howie, P. Dalladay-Simpson, and E. Gregoryanz, "Raman spectroscopy of hot hydrogen above 200 GPa," Nat. Mater. **14**, 495–499 (2015).

[37] C.-S. Zha, Z. Liu, and R. J. Hemley, "Synchrotron Infrared Measurements of Dense Hydrogen to 360 GPa," Phys. Rev. Lett. **108**, 146402 (2012).

[38] S. Azadi and W. M. C. Foulkes, "Fate of density functional theory in the study of high-pressure solid hydrogen," Phys. Rev. B **88**, 014115 (2013).

[39] C. J. Pickard and R. J. Needs, "Structure of phase III of solid hydrogen," Nature Phys. **3**, 473–476 (2007).

[40] M. I. Eremets and I. A. Troyan, "Conductive dense hydrogen," Nat. Mater. **10**, 927–931 (2011).

[41] A. F. Goncharov, J. S. Tse, H. Wang, J. Yang, V. V. Struzhkin, R. T. Howie, and E. Gregoryanz, "Bonding, structures, and band gap closure of hydrogen at high pressures," Phys. Rev. B **87**, 024101 (2013).

[42] C.-s. Zha, Z. Liu, M. Ahart, R. Boehler, and R. J. Hemley, "High-Pressure Measurements of Hydrogen Phase IV Using Synchrotron Infrared Spectroscopy," Phys. Rev. Lett. **110**, 217402 (2013).

[43] I. Amato, "Metallic hydrogen: Hard pressed," Nature **486**, 174–176 (2012).

[44] A. Biborski and A. Kądzielawa, "`QMT: Quantum Metallization Tools Library`," (2014), `https://bitbucket.org/azja/qmt`.

[45] N. W. Ashcroft, "The hydrogen liquids," J. Phys.: Condens. Matter **12**, A129 (2000).

[46] A. Kądzielawa, A. Bielas, M. Acquarone, A. Biborski, M. M. Maśka, and J. Spałek, "H_2 and $(H_2)_2$ molecules with an ab initio optimization of wave functions in correlated state: electron–proton couplings and intermolecular microscopic parameters," New J. Phys. **16**, 123022 (2014).

[47] S. Scandolo, "Liquid–liquid phase transition in compressed hydrogen from first-principles simulations," Proc. Natl Acad. Sci. **100**, 3051–3053 (2003).

[48] S. A. Bonev, B. Militzer, and G. Galli, "*Ab initio* simulations of dense liquid deuterium: Comparison with gas-gun shock-wave experiments," Phys. Rev. B **69**, 014101 (2004).

[49] I. Tamblyn and S. A. Bonev, "Structure and Phase Boundaries of Compressed Liquid Hydrogen," Phys. Rev. Lett. **104**, 065702 (2010).

[50] S. Azadi, W. M. C. Foulkes, and T. D. Kühne, "Quantum Monte Carlo study of high pressure solid molecular hydrogen," New J. Phys. **15**, 113005 (2013).

[51] C. Pierleoni, D. M. Ceperley, and M. Holzmann, "Coupled Electron-Ion Monte Carlo Calculations of Dense Metallic Hydrogen," Phys. Rev. Lett. **93**, 146402 (2004).

[52] L. Stella, C. Attaccalite, S. Sorella, and A. Rubio, "Strong electronic correlation in the hydrogen chain: A variational Monte Carlo study," Phys. Rev. B **84**, 245117 (2011).

[53] E. Kochanski, B. Roos, P. Siegbahn, and M. H. Wood, "Ab initio SCF-CI studies of the intermolecular interaction between two hydrogen molecules near the Van der Waals minimum," Theoret. Chim. Acta (Berl.) **32**, 151–159 (1973).

[54] M. Urban and P. Hobza, "Weak intermolecular interaction," Theoret. Chim. Acta (Berl.) **36**, 207–214 (1975).

[55] P. Hobza, R. Zahradník, and P. Čársky, "Clusters of hydrogen molecules: Ab initio SCF calculations corrected semiempirically for correlation energies," Theoret. Chim. Acta (Berl.) **53**, 1–7 (1979).

[56] P. Bokes, I. Štich, and L. Mitas, "Electron correlation effects in ionic hydrogen clusters," Int. J. Quant. Chem. **83**, 86–95 (2001).

[57] V. I. Anisimov, J. Zaanen, and O. K. Andersen, "Band theory and Mott insulators: Hubbard U instead of Stoner I," Phys. Rev. B **44**, 943–954 (1991).

[58] V. I. Anisimov, F. Aryasetiawan, and A. I. Lichtenstein, "First-principles calculations of the electronic structure and spectra of strongly correlated systems: the LDA + U method," J. Phys.: Condens. Matter **9**, 767 (1997).

[59] W. Metzner and D. Vollhardt, "Correlated Lattice Fermions in $d = \infty$ Dimensions," Phys. Rev. Lett. **62**, 324–327 (1989).

[60] E. Müller-Hartmann, "Correlated fermions on a lattice in high dimensions," Z. Phys. B: Condens. Matter **74**, 507–512 (1989).

[61] U. Brandt and C. Mielsch, "Thermodynamics and correlation functions of the Falicov-Kimball model in large dimensions," Z. Phys. B: Condens. Matter **75**, 365–370 (1989).

[62] A. Georges and G. Kotliar, "Hubbard model in infinite dimensions," Phys. Rev. B **45**, 6479–6483 (1992).

[63] A. Georges, G. Kotliar, W. Krauth, and M. J. Rozenberg, "Dynamical mean-field theory of strongly correlated fermion systems and the limit of infinite dimensions," Rev. Mod. Phys. **68**, 13–125 (1996).

[64] A. Biborski, A. P. Kądzielawa, and J. Spałek, "Combined shared and distributed memory ab-initio computations of molecular-hydrogen systems in the correlated state: process pool solution and two-level parallelism," arXiv:1504.00500 (2015).

[65] A. P. Kądzielawa, A. Biborski, and J. Spałek, "Discontinuous transition of molecular-hydrogen chain to the quasi-atomic state: Exact diagonalization - ab initio approach," arXiv:1506.03356 (2015).

[66] A. Kądzielawa, "Metallization of Atomic Solid Hydrogen within the Extended Hubbard Model with Renormalized Wannier Wave Functions ," Acta Phys. Polon. A **126**, A–58 (2014).

[67] J. Kaczmarczyk, J. Spałek, T. Schickling, and J. Bünemann, "Superconductivity in the two-dimensional Hubbard model: Gutzwiller wave function solution," Phys. Rev. B **88**, 115127 (2013).

[68] J. Bünemann, T. Schickling, and F. Gebhard, "Variational study of Fermi surface deformation in Hubbard models," Eur. Phys. Lett. **98**, 27006 (2012).

[69] J. Kaczmarczyk, J. Bünemann, and J. Spałek, "High-temperature superconductivity in the two-dimensional t – J model: Gutzwiller wavefunction solution," New J. Phys. **16**, 073018 (2014).

[70] J. Kaczmarczyk, "Comparison of two approaches for the treatment of Gutzwiller variational wave functions," Phil. Mag. **95**, 563 (2015).

[71] J. Kaczmarczyk, T. Schickling, and J. Bünemann, "Evaluation techniques for Gutzwiller wave functions in finite dimensions," Phys. Status Solidi B. **1–13** (2015), 10.1002/pssb.201552082.

[72] M. M. Wysokiński, J. Kaczmarczyk, and J. Spałek, "Univeral regimes of heavy fermions: Gutzwiller wave function solution to ALM," arXiv:1505.07003 (2015).

[73] M. Born and R. Oppenheimer, "Zur Quantentheorie der Molekeln," Ann. Phys. **389**, 457 (1927).

[74] P. Hohenberg and W. Kohn, "Inhomogeneous Electron Gas," Phys. Rev. **136**, B864–B871 (1964).

[75] W. Kohn, "Nobel lecture: Electronic structure of matter—wave functions and density functionals," Rev. Mod. Phys. **71**, 1253–1266 (1999).

[76] V. Fock, "Näherungsmethode zur Lösung des quantenmechanischen Mehrkörperproblems," Zeitschrift für Physik **61**, 126–148 (1930), in German.

[77] D. R. Hartree, Proc. Cambridge Phil. Soc **24**, 89 (1928).

[78] D. R. Hartree and W. Hartree, "Self-Consistent Field, with Exchange, for Beryllium," Proc. R. Soc. Lond. A **150**, 9–33 (1935).

[79] J. A. Pople and R. K. Nesbet, "Self-Consistent Orbitals for Radicals," J. Chem. Phys. **22**, 571–572 (1954).

[80] C. C. J. Roothaan, "Self-Consistent Field Theory for Open Shells of Electronic Systems," Rev. Mod. Phys. **32**, 179–185 (1960).

[81] C. Møller and M. S. Plesset, "Note on an Approximation Treatment for Many-Electron Systems," Phys. Rev. **46**, 618–622 (1934).

[82] C. D. Sherrill and H. F. Schaefer III., "The Configuration Interaction Method: Advances in Highly Correlated Approaches," (Academic Press, 1999) pp. 143 – 269.

[83] J. Spałek, R. Podsiadły, W. Wójcik, and A. Rycerz, "Optimization of single-particle basis for exactly soluble models of correlated electrons," Phys. Rev. B **61**, 15676 (2000).

[84] J. Spałek, E. Görlich, A. Rycerz, and R. Zahorbeński, "The combined exact diagonalization–ab initio approach and its application to correlated electronic states and Mott–Hubbard localization in nanoscopic systems," J. Phys.: Condens. Matter **19**, 255212 (2007), pp. 1-43.

[85] A. Rycerz, *Physical properties and quantum phase transitions in strongly correlated electron systems from a combined exact diagonalization – ab initio approach*, Ph.D. thesis, Jagiellonian University (2003), `th-www.if.uj.edu.pl/ztms/download/phdTheses/Adam_Rycerz_doktorat.pdf`.

[86] A. L. Fetter and J. D. Walecka, *Quantum Theory of Many-Particle Systems* (Dover, 2003).

[87] P. Surjan, *Second Quantizied Approach to Quantum Chemistry* (Springer, Berlin, 1989).

[88] J. C. Slater, "Atomic shielding constants," Phys. Rev. **36**, 57–64 (1930).

[89] R. S. Mulliken, "Electronic structures of polyatomic molecules and valence vi. on the method of molecular orbitals," J. Chem. Phys. **3**, 375–378 (1935).

[90] P. O. Löwdin, "On the non-orthogonality problem connected with the use of atomic wave functions in the theory of molecules and crystals," J. Chem. Phys. **18**, 365 (1950).

[91] D. R. Lide, ed., *CRC Handbook of Chemistry and Physics, 84th Edition* (CRC Press, Boca Raton, Florida, 2003).

[92] M. C. Gutzwiller, "Effect of Correlation on the Ferromagnetism of Transition Metals," Phys. Rev. Lett. **10**, 159 (1963).

[93] M. C. Gutzwiller, "Effect of Correlation on the Ferromagnetism of Transition Metals," Phys. Rev. **134**, A923 (1964).

[94] M. C. Gutzwiller, "Correlation of Electrons in a Narrow s Band," Phys. Rev. **137**, A1726–A1735 (1965).

[95] J. Bünemann and W. Weber, "Generalized Gutzwiller method for n$\geqslant$2 correlated bands: First-order metal-insulator transitions," Phys. Rev. B **55**, 4011–4014 (1997).

[96] J. Bünemann, W. Weber, and F. Gebhard, "Multiband Gutzwiller wave functions for general on-site interactions," Phys. Rev. B **57**, 6896–6916 (1998).

[97] M. Schiró and M. Fabrizio, "Time-Dependent Mean Field Theory for Quench Dynamics in Correlated Electron Systems," Phys. Rev. Lett. **105**, 076401 (2010).

[98] F. C. Zhang, C. Gros, T. M. Rice, and H. Shiba, "A renormalised hamiltonian approach to a resonant valence bond wavefunction," Supercond. Sci. Technol. **1**, 36 (1988).

[99] F. C. Zhang, "Gossamer Superconductor, Mott Insulator, and Resonating Valence Bond State in Correlated Electron Systems," Phys. Rev. Lett. **90**, 207002 (2003).

[100] S. Guertler, Q.-H. Wang, and F.-C. Zhang, "Variational Monte Carlo studies of gossamer superconductivity," Phys. Rev. B **79**, 144526 (2009).

[101] M. Abram, J. Kaczmarczyk, J. Jędrak, and J. Spałek, "d-wave superconductivity and its coexistence with antiferromagnetism in the t–J–U model: Statistically consistent Gutzwiller approach," Phys. Rev. B **88**, 094502 (2013).

[102] O. Howczak and J. Spałek, "Anderson lattice with explicit Kondo coupling revisited: metamagnetism and the field-induced suppression of the heavy fermion state," J. Phys.: Condens. Matter **24**, 205602 (2012).

[103] O. Howczak, J. Kaczmarczyk, and J. Spałek, "Pairing by Kondo interaction and magnetic phases in the Anderson-Kondo lattice model: Statistically consistent renormalized mean-field theory," Phys. Status Solidi (b) **250**, 609–614 (2013).

[104] M. M. Wysokiński, M. Abram, and J. Spałek, "Ferromagnetism in UGe_2: A microscopic model," Phys. Rev. B **90**, 081114(R) (2014).

[105] M. M. Wysokiński, M. Abram, and J. Spałek, "Criticalities in the itinerant ferromagnet UGe_2," Phys. Rev. B **91**, 081108 (2015).

[106] J. Jędrak, J. Kaczmarczyk, and J. Spałek, "Statistically-consistent Gutzwiller approach and its equivalence with the mean-field slave-boson method for correlated systems," (2010), arXiv:1008.0021 [cond-mat.str-el].

[107] W. Kołos and L. Wolniewicz, "Improved Theoretical Ground-State Energy of the Hydrogen Molecule," J. Chem. Phys. **49**, 404 (1968).